

T-cell surface modification with synthetic nanomaterials for cell-mediated delivery to the central nervous system

THÈSE N° 7986 (2017)

PRÉSENTÉE LE 1 SEPTEMBRE 2017
À LA FACULTÉ DES SCIENCES ET TECHNIQUES DE L'INGÉNIEUR
LABORATOIRE DES POLYMÈRES
PROGRAMME DOCTORAL EN SCIENCE ET GÉNIE DES MATÉRIAUX

ÉCOLE POLYTECHNIQUE FÉDÉRALE DE LAUSANNE

POUR L'OBTENTION DU GRADE DE DOCTEUR ÈS SCIENCES

PAR

Maxime AYER

acceptée sur proposition du jury:

Prof. P. Murali, président du jury
Prof. H.-A. Klok, directeur de thèse
Prof. B. Engelhardt, rapporteuse
Prof. M. A. Gauthier, rapporteur
Prof. L. Tang, rapporteur



ÉCOLE POLYTECHNIQUE
FÉDÉRALE DE LAUSANNE

Suisse
2017

The work described in this Thesis was performed at the École Polytechnique Fédérale de Lausanne (EPFL) from August 2012 until July 2017 under the supervision of Prof. Harm-Anton Klok.

This work was financially supported by the Swiss National Science Foundation

Acknowledgments

First of all I would like to thank Prof. Harm-Anton Klok for his support, for believing in my (sometimes crazy) ideas and helping me to reach my goals. I am extremely grateful that our relation has been consistently excellent over the years, and I am very thankful for your guidance and your precious advice. Thanks HAK!

Second, I would like to thank our collaborators in Bern, Prof. Britta Engelhardt from Theodor Kocher Institute for all her help, her advice and for the nice discussions. Besides, I would like to thank two members of her group, Isabelle Gruber and Claudia Blatti, who were kind enough to teach me almost everything I know in experimental biology and especially Isabelle for your patience during the many hours in front of the microscope together. I always felt welcome in Bern and I really enjoyed my time there very much. I also would like to greatly acknowledge the Bioimaging and Optics Platform (BIOP); especially Olivier Burri and Romain Guet for their help in developing tools to process our images. Miguel Garcia from the Flow Cytometry Core Facility (FCCF) is also greatly acknowledged for his help. Finally, I take a few lines to thank the members of my jury, Prof Marc A. Gauthier, Prof. Li Tang and Prof. Paul Muralt, for the time they invested in reading and evaluating this thesis and for their extremely valuable feedback.

I had five memorable years at the Polymers Laboratory (LP). Arda and Nariye from the Turkish diaspora, I have been missing you guys so much for the last one year. Claudia, you were here from the beginning to the last minute and you were a kind and comforting support. You, all three, have great hearts and I am so grateful for our priceless friendship and for the nice moments and memories we had together and that I will never forget. Cindy, sometimes I feel like we could have gone to high school together instead of meeting each other here, anyways I can only agree with Claudia, that Tuesdays and Thursdays have always been the best days of the week! Ana and Solenne, you guys both welcomed me warmly in your lab and your office when I first got here and I have always been happy to hang out with you two! Finally, thanks to all present and past LP members: especially to Jacques for your kindness and your effectiveness in solving problems, to Tanja for always being keen on sharing a few moments after work and for your nice smile, to Cristiana, Markus, Piotr, Jian, Julian, Alexandre, Philippe, Béatrice, Cindy Känel, Chie, Raoul and Eloise, Justin, Ioana, Yasushi, Li, Nicolas, Caroline, Tugba, Sorin, Vitaliy as well as the newcomers.

Egalement, un immense merci à mes très chers amis pour votre soutien et votre amitié inconditionnelle, tout particulièrement à Antoine et Aniko, Jonathan Q. et Maxime S., Jonathan V. et Céline, Alain, Christophe, Valeska, Christina, Jean-Baptiste et Valentine, Guillaume, Damien, Gédéon et Myriam, Patrick ainsi que Mathilde et Julien, Emilie Z., Audrey et Benoit, Emilie C. et Adrien.

Mes remerciements les plus sincères et mes sentiments les plus profonds vont à ma famille pour leur soutien indéfectible au cours de ces innombrables années d'études : à mon père, Nicolas et à ma mère, Eliane, pour les valeurs que vous m'avez transmises et pour tout votre amour ; à mes deux frères Antoine et Christian et leurs compagnes, Louise (tak) et Nicole ainsi qu'à ma nièce Luna et mon filleul Emil ; à ma chère marraine Antoinette, mon oncle René ainsi qu'à la famille Faustino, Manuel, Olga et Pedro, merci de tout cœur.

Pour terminer, mes mots les plus doux sont pour ma belle Ana ! Sans ton précieux et unique soutien durant les cinq dernières années, je ne serais pas arrivé là où je suis aujourd'hui. Je te serai à jamais infiniment reconnaissant et te remercie du plus profond de mon cœur et avec mon amour le plus fort et le plus sincère d'avoir toujours été présente, surtout pendant les moments plus difficiles.

Une pensée émue pour mon cher ami de toujours, Marc Andres, qui a dû filer plus vite que prévu et à qui je dédie cette thèse en souvenir des inoubliables années passées ensemble à partager notre intérêt grandissant pour les sciences.

Table of contents

Summary.....	1
Résumé.....	3
1. Cell-mediated delivery of synthetic nano- and microparticles	5
1.1. Introduction.....	5
1.2. Cells used for cell-mediated drug delivery	6
1.2.1. Red blood cells.....	6
1.2.2. Leukocytes	7
1.2.3. Stem cells	9
1.3. Chemical modification of cell surfaces.....	11
1.3.1. Non-covalent cell surface modification	14
1.3.2. Covalent cell surface modification.....	27
1.4. Conclusions and outlook.....	33
1.5. References.....	34
2. T cell-mediated delivery of polymer nanoparticles across the blood brain barrier.....	45
2.1. Introduction.....	45
2.2. Experimental Section	48
2.2.1. Materials	48
2.2.2. Methods.....	48
2.2.3. Procedures.....	49
2.3. Results and Discussion	54
2.3.1. Particle synthesis.....	54
2.3.2. T-cell surface modification and characterization	55
2.3.3. Functional assays	59
2.4. Conclusions.....	66
2.5. References and Notes.....	67
2.6. Supporting information.....	71
3. Biotin-NeutrAvidin mediated immobilization of polymer nanoparticles on T lymphocytes.....	79
3.1. Introduction.....	79
3.2. Experimental Section	80
3.2.1. Materials	80
3.2.2. Methods.....	81
3.2.3. Procedures.....	81
3.3. Results and Discussion	84
3.3.1. T-cell surface modification and characterization	84
3.3.2. Binding assay	93

Table of Contents

3.4. Conclusions	94
3.5. References	94
3.6. Supporting Information	97
4. Conclusions and Perspectives	99
Curriculum vitae.....	a

Summary

The future of medicine lies in therapeutic approaches that can specifically target sites of disease and induce a localized effective and precise therapeutic effect. Cell-mediated delivery, especially using cells of the circulatory repertoire such as T lymphocytes, represents an extremely attractive opportunity to transport and deliver synthetic therapeutic materials across endothelial barriers to sites of inflammation and is also an elegant way to escape nanoparticle clearance from the reticuloendothelial system. The work presented in this Thesis explores the feasibility of using a T cell carrier to transport model nanoparticles to the central nervous system. The use of non-phagocytic cells as carriers, such as T lymphocytes, for the transport of nanomaterials essentially relies on the attachment of the therapeutic cargo on their surface. Cell-surface modification is an emerging field of research with many opportunities for therapy. This work has also tried to address a more fundamental question encountered in this field and describes a novel methodology to precisely and quantitatively determine the localization of nanomaterials on the cell carrier after surface-conjugation.

Chapter 1 presents a comprehensive review of the scientific literature that covers the different approaches used for the attachment of synthetic nano- and microparticles to a variety of cells, spanning from erythrocytes, monocytes and macrophages to T lymphocytes and adult stem cells. This Chapter highlights the (bio)chemical tools that are available to modify cell surfaces with synthetic materials. To name a few, non-covalent approaches using for example non-specific interactions (i.e. electrostatic), ligand-receptor mediated interactions, as well as covalent conjugation approaches based on several well-known ligation chemistries used in bioconjugation i.e. maleimide-thiol coupling, or disulfide bond formation as well as strain promoted alkyne-azide cycloaddition are described in this first section. These methods have been used for the attachment of a variety of synthetic materials such as polymer micron-size patches also named cellular backpacks, polymer nano- and microparticles as well as lipid-based nanomaterials. A strong emphasis was given to therapeutic applications of the surface modified cells, which can be used to enhance systemic circulation time of nanoparticles or to mediate the transport of nanomaterials to a site of disease or in combination with cell therapy.

Chapter 2 explores the actual use of a cell carrier to mediate the transport of nanoparticles to the central nervous system. Here CD4⁺ T_{EM} cells were used as vehicles to deliver polymer nanoparticles across the blood-brain barrier (BBB). In fact, effective

delivery of central nervous system (CNS) active compounds across the BBB remains as one of the biggest challenges in drug delivery due to the very restrictive nature of the BBB. Polymer model nanoparticles were attached on the surface of T cells using a maleimide-thiol covalent ligation which yielded on average approx. 100 nanoparticles per T cell. The T-cell surface modification was shown to be stable and non-toxic for the T cells over a period of 24h. Nanoparticle decorated T cells were then subjected to a series of functional assays to determine the influence of surface-conjugation. In particular, their ability to cross the BBB was assessed and it was demonstrated that surface-modified T cells remained functional and that they were able to transport partially their nanoparticle cargo across the BBB *in vitro*. The multi-step extravasation of nanoparticle modified T cells across the BBB was observed for the first by means of time-lapse live cell imaging techniques.

Chapter 3 capitalizes on a method that was initially developed in Chapter 2 for the determination of the localization and distribution of nanoparticles on T lymphocytes after surface-conjugation. The method is based on a staining protocol that allows to visualize the entire cell as well as the membrane by confocal microscopy. 3D-reconstruction of confocal micrograph z-stacks followed by image processing provided the distance of fluorescently labelled nanoparticles from the cell surface as function of time. The method developed previously was here challenged with a range of different nanoparticles sizes and across two different cell lines and was validated for semi-quantitative estimation of surface-conjugated versus internalized nanoparticles.

Keywords: Cell-mediated drug delivery, cell-surface conjugation, nano- and microparticles, PEGylation, blood-brain barrier, CD4⁺ T_{EM} cell, neuroinflammation, transendothelial migration, time-lapse live cell imaging.

Résumé

Le futur de la médecine repose en partie sur de nouvelles approches thérapeutiques capables de cibler précisément un site atteint d'une affection et d'y déclencher un effet thérapeutique localisé et efficace. L'administration ciblée d'agents thérapeutiques utilisant des véhicules cellulaires, en particulier en ayant recours aux cellules du répertoire circulatoire, représente une opportunité extrêmement attrayante pour le transport des matériaux thérapeutiques à travers les barrières endothéliales vers des sites inflammatoires et est également une manière élégante d'esquiver l'élimination par le système réticulo-endothélial. Le travail décrit dans cette Thèse explore l'utilisation de lymphocytes T pour le transport de nanoparticules vers le système nerveux central. L'utilisation pour le transport de nanomatériaux de cellules dépourvues de compétences phagocytaires, comme c'est le cas pour les lymphocytes T, repose essentiellement sur l'attachement du chargement thérapeutique à la surface de ces véhicules cellulaires. La modification de surfaces cellulaires avec des nanomatériaux est un domaine de recherche émergent et prometteur pour la médecine. Ce travail s'intéressera également à une question plus fondamentale liée à ce domaine de recherche particulier, et tentera d'aborder la question de la localisation précise des nanomatériaux après leur conjugaison à la surface d'un transporteur cellulaire de type lymphocyte T.

Le **1^{er} chapitre** présente une revue de la littérature scientifique traitant des différentes approches existantes pour la fonctionnalisation de cellules, telles que les érythrocytes, les monocytes et les macrophages, ainsi que les lymphocytes T ou encore les cellules souches adultes avec des nano- et microparticules. Cette section décrit en particulier les différentes méthodes (bio)chimiques utilisées pour la modification de surfaces cellulaires avec des matériaux synthétiques. Les approches de modifications non-covalentes ayant recours à des interactions non-spécifiques (i.e. électrostatiques), ou des interactions entre un ligand et son récepteur, ou encore des approches covalentes basées sur des méthodes de ligations utilisées en bioconjugaison telles que le couplage maléimide-thiol ou la formation de liaison disulfure ou encore la cycloaddition 1,3-dipolaire entre un alcyne et un azoture, sont décrites dans cette première section. Ces méthodes ont été utilisées pour la fixation d'une variété de matériaux synthétiques tels que les patches polymères micrométriques aussi appelés sac-à-dos cellulaires, des nano- et microparticules polymères ainsi que des nanomatériaux lipidiques. Un accent important a été mis sur les utilisations thérapeutiques de ces cellules modifiées avec des matériaux synthétiques.

Celles-ci peuvent être aussi bien utilisées pour augmenter le temps de circulation des nanoparticules dans le flux sanguin ou pour diriger le transport de nanomatériaux thérapeutiques vers des sites d'inflammation ou alors encore en complément d'une thérapie cellulaire.

Le 2^{ème} **chapitre** explore l'utilisation d'un véhicule cellulaire pour le transport de nanoparticules vers le système nerveux central. Ici, l'utilisation de lymphocytes T_{EM} CD4⁺ est envisagée pour véhiculer le transport de nanoparticules à travers la barrière hémato-encéphalique. En effet, l'administration de composés actifs dans le système nerveux central représente encore un enjeu majeur en médecine. Ceci est principalement dû à la nature extrêmement restrictive de la barrière hémato-encéphalique. Pour ce faire, des nanoparticules polymères ont été attachées à la surface de lymphocytes T de manière covalente grâce au couplage maléimide-thiol, ce qui a permis de produire des véhicules cellulaires équipés d'environ 100 nanoparticules chacun. La modification de ces lymphocytes avec ces nanoparticules s'est révélée stable et non-toxique durant au moins 24h. Les véhicules cellulaires ainsi décorés de nanoparticules ont passé une série de tests fonctionnels afin de déterminer en particulier l'influence des nanoparticules accrochées à leur surface sur leur capacité à traverser un modèle *in vitro* de barrière hémato-encéphalique. L'extravasation par étape des lymphocytes T décorés de nanoparticules polymères à travers la barrière hémato-encéphalique a été pour la première fois observée *in vitro* par des techniques de microscopie en temps réel.

Enfin, le **chapitre 3** s'est intéressé à la validation d'une méthode développée dans le chapitre précédent pour la détermination de la localisation et la distribution des nanoparticules sur les lymphocytes T. Cette méthode est basée sur des protocoles de coloration permettant de visualiser la cellule dans son entier ainsi que la membrane plasmique par microscopie confocale. La reconstruction 3D à partir d'images prises en coupe ainsi que le traitement de celles-ci par des outils informatiques a permis d'obtenir la distance des nanoparticules marquées d'un fluorophore de la surface de la cellule en fonction du temps. Cette méthode a été validée à travers l'utilisation d'une gamme de nanoparticules de différentes tailles ainsi que sur différentes lignées cellulaires et permet de discriminer les nanoparticules associées à la surface des lymphocytes de celles internalisées.

Keywords: Véhicule cellulaire, nano- et microparticules, PEGylation, barrière hémato-encéphalique, lymphocyte T_{EM} CD4⁺, neuroinflammation, migration transendothéliale, techniques d'imagerie en temps réel.

1. Cell-mediated delivery of synthetic nano- and microparticles

1.1. Introduction

Small molecule drugs are lacking tissue and organ specificity, suffer from rapid body clearance and are often associated with numerous side effects, especially chemotherapeutic agents, which are usually highly toxic [1]. The use of polymer conjugates or lipid or polymer nanoparticles to encapsulate, transport and release an active substance has allowed to enhance tissue and organ specificity, either in a passive fashion taking advantage of the so-called enhanced permeation and retention (EPR) effect or by exploring active targeting strategies by incorporating ligands that target receptors that are overexpressed at the cancer cell surface [1-3]. While the EPR effect and active targeting strategies allow to modulate the biodistribution to some extent, still only a fraction of all nanocarriers reaches the tumor while the vast majority of drug loaded nanocarriers are cleared by the reticuloendothelial system (RES). Additionally, the clinical translation of the EPR effect from animal models to humans has proven to be challenging [4]. Moreover, whereas the EPR effect may be relatively efficient in some cancer models due to the leaky nature of blood vessels in angiogenic tumors, there is a range of indications to which it does not apply. In several instances, for example, the active substances need to be transported across tight endothelial cell barriers. Finally, targeting circulating or disseminated tumor cells after primary tumor resection is extremely challenging and is unmet with current nanocarrier approaches.

A strategy that potentially allows to overcome many of the challenges listed above and to control biodistribution in a highly specific manner involves the use of cells to mediate the transport of drug loaded nanocarriers [5-7]. Cells have unique properties e.g. to circulate in the blood stream for extended periods of time, to target (cancer) cells or to pass challenging biological barriers. Attaching polymer-drug conjugates or drug-loaded nanocarriers to the cell surface or incorporating them in the cell could provide unique possibilities to enhance the cell or tissue specificity or circulation time of those nanomedicines. While this article will focus exclusively on the decoration of cell surfaces

with synthetic nano- and microparticles, cells are also explored as Trojan horses [5]. There are a number of limitations associated with the internalization of drug-loaded particles and polymer conjugates in cell carriers. A first one is the risk of premature degradation of the nanoparticle and its payload inside the cell carrier. A second is the need for the cell carrier to release its cargo at the target site, which adds an additional step to the whole process. Finally, internalization of a cargo is essentially limited to cells with an efficient phagocytic system such as monocytes or macrophages whereas surface functionalization is in principle possible with the entire repertoire of circulating cells, opening doors to long circulating delivery approaches based on red blood cell functionalization or highly specific targeting strategies based on modification of cells from the adaptive immune system such as B and T lymphocytes [8,9] or based on the pathotropism of stem cells [10].

The aim of this article is to provide an overview of the state-of-the art in the use of surface-modified cells to mediate the delivery of synthetic nano- and microparticles. The first part of this article will present and discuss the different types of cells that have been explored for cell mediated drug delivery. The second part of this review will discuss the various chemical strategies that have been elaborated for the conjugation or immobilization of nano- and microparticles on the surface of these cells.

1.2. Cells used for cell-mediated drug delivery

This section will give an overview of the different types of cells that have been used as vehicles for the cell surface attachment and transport of synthetic nano- and microparticles.

1.2.1. Red blood cells

Red blood cells (RBCs) are biconcave disk-shaped cells lacking organelles and a nucleus, measuring approx. 7 μm in diameter. They constitute > 99% of the blood and are long-circulating, up to approx. 120 days in humans [11]. They are specialized in oxygen transport, which is mediated by hemoglobin, encapsulated in large amounts inside RBCs. RBCs are highly deformable and flexible to allow them to reach capillary venules. RBCs do not normally extravasate from the circulation into tissues except within the spleen and liver where senescent RBCs are removed from the circulation by the phagocytic system [11]. The plasma membrane of a RBC is slightly negatively charged and comprised of > 300 different membrane proteins [12], which offer many opportunities for

cell surface modification. RBCs intrinsically play an important role in altering the biodistribution and pharmacokinetics of many drugs, increasing their circulation times [11]. The ability to prolong the circulation time of drugs, together with a high biocompatibility, especially in the case of autologous transfer, are very attractive features in the context of drug delivery. RBCs have been intensively investigated as carriers for the vascular delivery of a variety of surface bound molecules and more recently for the transport of nanoparticulate carriers as will be discussed in the next section [11,13].

1.2.2. Leukocytes

Leukocytes form the innate and adaptive immune system and respond, for example, against infection, inflammation and tumor growth [14]. Both the innate and adaptive immune system play a crucial role in detecting and killing cancer cells. The unique features of leukocytes, such as their ability to travel to a specific site of disease as well as to transmigrate across endothelial barriers [15] and penetrate into hypoxic tumor regions [16] provide unique opportunities for delivery to areas that are otherwise difficult or impossible to reach by traditional drug delivery approaches. Particularly interesting cells for cell-mediated delivery are monocytes, which are long lived white blood cells deriving from the bone marrow and which can differentiate into tissue-resident macrophages or dendritic cells (DC) [17], as well as B cells, T cells, especially of the CD4⁺ (helper) and CD8⁺ (cytotoxic) subtypes and natural killer (NK) cells. The T lymphocytes used in adoptive cell therapy could potentially concomitantly serve as drug carrier. The decorated adoptively transferred lymphocytes are then not only a carrier but also directly exert a therapeutic activity.

The primary mission of monocytes is to replenish the pool of tissue-resident immune cells [18]. Furthermore, they are also involved in the innate immune response against bacterial, fungal, parasitic and viral infection [19]. In humans, 3 classes of monocytes coexist in the peripheral blood circulation, which are characterized by their relative expression of CD14 and CD16 surface markers. The largest subpopulation, consisting of approx. 80 to 90% of all monocytes, is the CD14⁺ CD16⁻ subset, which shows the highest phagocytic activity and also produces IL-10. In contrast, the others subpopulations are expressing CD16 and express CD14 at high or low level. These are divided in two classes (i) the CD14⁺ CD16⁺ subset, which is entirely responsible for the production of TNF- α and IL-1 and which also has a phagocytic activity and (ii) the CD14^{dim}CD16⁺ subset, whose actual function is not well understood. Monocytes of this last subset express low

level of the CD14 markers. They are poorly phagocytic and do not express cytokines such as TNF- α and IL-1 [20].

Tissue differentiated macrophages are present in a broad spectrum of pathological conditions including cancers and several inflammatory diseases [18]. Monocytes and macrophages along with DCs, neutrophils and mast cells are ‘professional’ phagocytic cells, which express specialized membrane receptors and are able to detect apoptotic/necrotic cells, opsonized pathogens or cell debris [18]. The phagocytic competence of macrophages and monocytes represents a major challenge in attaching and immobilizing a cargo on their surface for delivery purposes [21]. The few successful examples of stable and long-lasting surface functionalization required the use of very large synthetic particles, which have a disk-like shape, thus avoiding internalization (see Doshi et al. [22]). These examples will be discussed in more detail in the following section.

B and T lymphocytes are part of the adaptive immune system and immunological memory. B lymphocytes originate from the bone marrow and are the central player of the humoral immunity [23]. Upon antigen exposure, mature naïve B cells, which trafficked to secondary lymphoid organs, differentiate via a series of fast evolutionary selection steps to antibody-secreting B cells also called plasma cells [24]. These plasma cells can subsequently reenter the blood circulation via the lymphatic system to reach distant sites of infection/inflammation. T lymphocytes derive from the thymus and are classified in two important subsets, which mediate the adaptive cellular response through (i) activation of other immune cells (CD4⁺ Helper T cells) or (ii) via killing target/infected cells (CD8⁺ Cytotoxic T cells) [25]. Lymphocyte trafficking depends on their activation status. While blood-borne naïve T cells, similarly to naïve B cells, possess surface markers that enable them to home to secondary lymphoid organs, antigen-experienced lymphocytes migrate towards sites of inflammation [26]. This duality in homing properties, i.e. secondary lymphoid organs vs inflamed tissues is very attractive for cell-mediated drug delivery, especially in the context of cancer therapy, in which these distinct trafficking patterns allow targeting either the primary tumor or disseminated tumor cells in the lymph nodes. T lymphocytes are activated by DCs in the lymph nodes via interaction with the MHC class II complexes. The migration and accumulation of lymphocytes into diseased tissues is general to all subsets of circulating leukocytes [27]. It is triggered by an adhesion cascade, consisting of a series of interactions between endothelial recruiting molecules called selectins and activation of lymphocyte chemoattractant receptors. This

activation induces the expression of integrins on the lymphocytes, which mediate firm binding to intercellular and vascular endothelial adhesion molecules. Finally, lymphocytes diapedese through the endothelial barrier to reach their target area [25].

CD8⁺ T cells elicit their cytotoxic effect essentially by secreting perforin together with a variety of granzymes or via activation of the tumor-necrosis factor receptor Fas of target cells and to a lesser extent via production of cytokines such as tumor-necrosis factor (TNF) and interferon- γ (IFN- γ) that have cytotoxic action when secreted nearby target cells [28]. CD4⁺ T cells mediate the immune response via the release of cytokines of two different classes, T helper 1 (Th1) type and T helper 2 (Th2) type, which activate different cells of the innate and adaptive immune system [29].

Natural killer (NK) cells represent about 10–20% of all peripheral blood mononuclear cells [30]. Human NK cells are subdivided into 5 categories depending on the relative expression of the surface markers CD56 (an adhesion molecule) and CD16 (a low affinity Fc receptor) [31]. NK cells are not only localized in peripheral blood but are also present in lymph nodes, spleen and bone marrow where they exert different functions based on their phenotype [30]. NK cells are mainly involved in innate immunity [32] but also influence and shape adaptive immune responses [31]. Their role in immunoregulation is also important and predominantly mediated through secretion of cytokines of the Th1 type [32]. NK cells are activated by a variety of stimuli, in particular by contact with DCs, MHC-I-negative cells, IgG of the immune complexes or via direct activation by tumor-associated markers present on tumor cells or pathogen-derived products as well as a myriad of interleukins and type I interferons [30]. NK cells represent the first line of defense against tumor and infected cells, recognizing stressed cells with low MHC class I expression and elicit a cytotoxic and necrotic effect via liberation of perforin and granzymes [30]. Additionally, NK cells are eliciting an apoptotic effect on targeted cells, induced by exposition of surface ligand of the TNF family such as the Fas Ligand, TNF- α and the tumor necrosis factor-related apoptosis-inducing ligand (TRAIL), the latter having gained some clinical interest as a drug and whose effective delivery will be discussed in greater detail later on in this review.

1.2.3. Stem cells

Stem cells, in particular adult stem cells such as hematopoietic stem cells and mesenchymal stem cells, which can be directly obtained from patients, cultured and expanded in vitro and used in subsequent autologous transplant, have attracted

considerable interest in recent years [33]. Adult stem cells, as opposed to embryonic stem cells, which originate from the inner cell mass of a blastocyst, are tissue specific cells, which can in principle only differentiate to a limited set of specialized cells [34]. Although not as pluripotent and as self-renewing as embryonic stem cells, adult stem cells have the important advantage that they are much less likely to give rise to tumors after transplantation [33]. Moreover, many accounts also suggest that most adult stem cells from a tissue specific lineage are able to be converted to tissues types of another lineage through mechanism such as transdifferentiation or dedifferentiation [35,36].

While the main focus in stem cell therapy has been on cell replacement or tissue regeneration, the pathotropic nature of stem cells, and more specifically their ability to migrate towards tumor tissues, also makes them ideal delivery vectors in cancer therapy [33]. Stem cells are used as carriers to efficiently deliver genetically encoded apoptotic proteins [37], immunomodulators [38], oncolytic viruses [39] or nanoparticle encapsulated chemotherapeutic agents (as will be discussed in detail below) [40], with high precision and enhanced tracking of tumor metastases.

Principally, two different stem cell lineages have been utilized for their tumor-tropic properties, mesenchymal stem cells (MSCs), which are primarily derived from bone marrow and neural stem cells (NSCs) deriving from specific neurogenic regions of the brain. MSCs can spread into many tissues after being systemically injected and, similar to immune cells, can extravasate from the blood vessels due to the expression of adhesion molecules on their surface [41]. MSCs have been used as a delivery vector in various types of cancers, such as melanoma [42] but have also been shown to be effective in targeting glioma [43] or disseminated metastases [44]. Although MSCs are readily isolated clinically and as such represent an important source of adult stem cells, they have also been associated with promoting primary and metastatic tumor growth and development via an immunosuppressive mechanism, which may restrict their use in specific clinical settings [45-47]. NSCs are well-characterized non-tumorigenic and minimally immunogenic adult stem cells, showing extensive tropism to a multitude of tumors types. NSCs have been used as delivery vectors in particular for gene therapy [48]. One major drawback linked to clinical harnessing of NSCs lies in the accessibility of its source for autologous transfer, which is the brain, and the complications associated with an invasive procedure to withdraw these cells. However, some reports have shown that autologous neural stem-like cells could potentially be

accessible from bone marrow, which represents a very attractive opportunity for future clinical uses [49,50].

The use of stem cells is, of course, not limited to tumor targeting. Stem cells show tropism to a variety of other lesions as well as to neurodegenerative areas and as such represent a unique delivery vector with a very broad scope for therapy [10,48].

1.3. Chemical modification of cell surfaces

This section will provide an overview of the various strategies that have been used to decorate cell surfaces with synthetic nano- and microparticles and discuss the properties and uses of the resulting surface modified cells. Table 1 provides an overview of the different cell surface modification strategies that have been used so far. Cell surface modification strategies can be subdivided in two main classes, viz. non-covalent and covalent. The remainder of this section will first discuss non-covalent cell surface modification approaches and the properties of the resulting cells and then present covalent cell surface modification strategies. Whereas covalent approaches are usually considered as more stable, their principal disadvantage lies in the fact that the site of modification is not controlled. Non-covalent approaches that use ligand-receptor interactions can be highly specific, yet pose the risk of triggering undesired cellular responses. These two examples already illustrate that selecting the appropriate cell surface modification strategy is a challenging task that depends on many factors including but not restricted to the cell type, cell surface biochemistry, the need for a robust particle conjugation or for release strategies, to name a few. In either way, a common feature of any cell surface modification strategy is that it should not affect the viability and function of the cell.

Table 1. Overview of different strategies that have been used for the conjugation or immobilization of synthetic nano- or microparticles to cell surfaces.

Method	Mechanism	Cell type	Type of cargo (payload)	Application	Ref.
Non-Covalent	Nonspecific adsorption (Van der Waals, electrostatic, hydrogen bonds, hydrophobic interactions)	Murine and human red blood cells (RBCs)	Polystyrene based nano- and microparticles (range between ~ 100nm – 1000 nm)	Long circulating delivery vehicles	[51-53]
	Nonspecific adsorption	Mouse red blood cells (RBCs)	(Anti-ICAM-1 coated) polystyrene based nanoparticles and nanorods	Nanoparticle delivery to the lungs	[54, 55]
	Cell adhesive polyelectrolyte	Human chronic myeloid leukemia derived K562 cell, mouse embryonic stem cells (mESCs) and human mesenchymal stem cells (hMSCs)	Disc-shaped microdevices	Drug delivery	[56-59]
	Hyaluronic acid mediated adhesion	Human T lymphocytes and mouse B lymphocytes	Superparamagnetic nanoparticles loaded polyelectrolyte multilayer (PEM) patches	Spatial migration of cells towards a magnetic field	[60]
	Chitosan / hyaluronic acid mediated adhesion	Mouse B lymphocytes	PEM patches / polymeric backpacks	Cell aggregation induced by freely suspended backpacks	[61]
	Chitosan / hyaluronic acid mediated adhesion	Mouse B lymphocytes	PEM patches / polymeric backpacks	Mechanistic studies of B cell immobilization by PEM patches	[64]
	Chitosan / hyaluronic acid mediated adhesion	Mouse macrophages	PEM patches / polymeric backpacks	Cell-based drug delivery	[22]
	Chitosan / hyaluronic acid mediated adhesion	Mouse B lymphocytes	Polymeric microtubes	Selective orientation of microtubes on cell surface	[65]
	Antibody targeted (normal mouse IgG)	Mouse monocytes	PEM patches / polymeric backpacks (DOX loaded liposomes)	Targeted drug delivery	[62, 63]
	Antibody targeted (mouse IgG)	Mouse monocytes	Polymeric backpacks	<i>In vivo</i> targeted delivery	[67]
	Antibody targeted (anti CD73, CD90)	Human mesenchymal stem cells (hMSCs)	Silica nanorattles (Dox loaded)	Tumor-targeted drug delivery	[68]
	Biotin-avidin	Human embryonic kidney (HEK293) and murine T lymphoma EL4 cells	PLA-PEG ⁽¹⁾ microparticles (average diameter of 1.4 μ m)		[74]
	Biotin-Neutravidin	Human neural stem cells (NSCs)	PEG-PDPAEMA ⁽²⁾ nanoparticles	Brain tumor targeting	[40, 75]
	Biotin-Neutravidin	Human mesenchymal stem cells (hMSCs)	40 nm diameter polystyrene based nanoparticles	Tumor-tropic delivery	[73]
	E-selectin - mediated, anti-CD57 antibody and anti-NK1.1 antibody - mediated	Human leukocytes, murine natural killer cells	Liposomes	Circulating tumor cells tracking and killing	[76-79]

Covalent	Biomimetic polymer or dendrimer – agglutinin or lectin	Chinese hamster ovary (CHO), Jurkat T cells	Carbon nanotubes (CNTs)	Model system for non-toxic CNTs binding	[80, 81]
	Biomimetic dendrimer - agglutinin	Chinese hamster ovary	Boron nitride nanotubes (BNNTs)	Biosensing and bioimaging	[82]
	Coupling to amine groups (via NHS ester, isocyanate or cyanuric chloride end-functionalized polymers)	Langerhans islets and red blood cells	Synthetic branched or linear polymers	Graft and cytoprotection	[86-89]
	Maleimide - thiol	Mouse CD8 ⁺ T lymphocyte and hematopoietic stem cells (HSCs)	Lipid nanoparticles (immunomodulator)	Adoptive cell therapy	[92, 93]
	Maleimide - thiol	Mouse CD4 ⁺ and CD8 ⁺ T cells	Lipid nanoparticles (Chemotherapeutic agent SN-38)	Disseminated tumor targeted chemotherapy	[94]
	Disulfide	Mouse CD8 ⁺ T cells	Lipid based nanoparticles	Reversible attachment of nanoparticles	[96]
	Schiff base	Mouse macrophages	Quantum dots and stealth dendrimer nanoparticles	Hypoxia-targeted drug delivery	[97]
	SPAAC	Mouse macrophages	PAMAM dendrimers		[98]
	(1) Poly(lactic acid)-poly(ethylene glycol) (2) poly(ethylene glycol)-poly((diisopropyl amino) ethyl methacrylate)				

1.3.1. Non-covalent cell surface modification

Non-covalent attachment of synthetic polymer nano- or microparticles to cell surfaces can be achieved using both non-specific (e.g. hydrophobic, electrostatic) interactions as well as specific ligand-receptor interactions. The remainder of this section will present several examples that highlight the use of these different approaches.

1.3.1.1. Non-specific interactions

Mitragotri and coworkers, in a series of studies, have extensively explored adsorption of model polystyrene nanoparticles onto RBCs as a means to avoid clearance by the reticuloendothelial system (RES). It was found that circulation times can be dramatically altered, by several orders of magnitude, if the nanoparticles are adsorbed onto RBCs. The adsorption of the polystyrene nanoparticles was proposed to involve a combination of van der Waals, electrostatic, hydrogen bonding and hydrophobic forces [51]. This hypothesis was supported by the observation that nanoparticle adsorption was inhibited in the presence of serum or albumin [52]. When nanoparticles and RBCs were mixed at a ratio of 100:1, approximately 25 nanoparticles were adsorbed to each cell. This was found to be the maximum loading capacity, since higher nanoparticles loadings tend to cause cell aggregation. The RBC morphology and integrity is not adversely affected by the nanoparticle adhesion also under osmotic, mechanical, oxidative or complement stress that are typically encountered in the systemic circulation [53]. The conjugation is stable in vitro for many hours [51] and circulation times of RBC-bound nanoparticles are increased approximately 100-fold in vivo as compared to free nanoparticles [52]. Circulation times are maximal for nanoparticles in the middle-size range (200–500 nm) and are dependent of nanoparticle surface chemistry [52]. The prolonged circulation times are due to a decrease in uptake and clearance by the spleen and liver. Interestingly, this lowered clearance was accompanied by accumulation in the lung. This effect was even more pronounced when (i) surface bound nanoparticles were coated with anti-ICAM-antibody and (ii) when nanorods were used instead of spherical nanoparticles (Fig. 1) [54]. The combination of both i.e. adsorption of nanorods onto RBCs with subsequent anti-ICAM coating of the exposed surface of nanorods, led to the best performance in terms of immune system avoidance and lung targeting for a RBC-hitchhiked nanomaterial [54,55]. Nanoparticles are eventually detached from RBC surface over time, essentially due to shear stress, cell-cell and cell-vessel wall interactions that become increasingly challenging in capillaries [52].

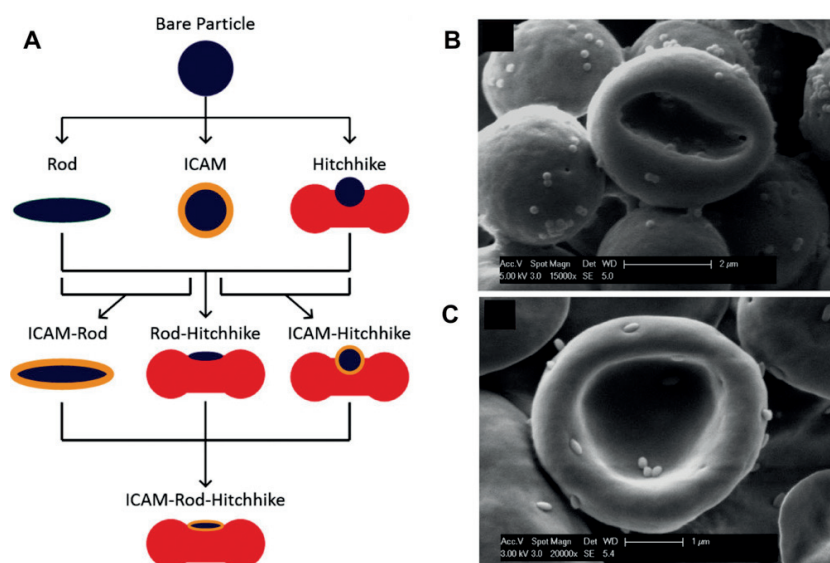


Figure 1. (A) Schematic overview of the preparation of spherical or rod-shaped nanoparticle decorated RBCs. Scanning electron micrographs of nanoparticle formulations: (B) 200 nm spheres attached to red blood cells and (C) rods stretched from 200 nm spheres attached to red blood cells. Reprinted from Biomaterials, 68, A.C. Anselmo, S. Kumar, V. Gupta, A.M. Pearce, A. Ragusa, V. Muzykantov, S. Mitragotri, Exploiting shape, cellular-hitchhiking and antibodies to target nanoparticles to lung endothelium: Synergy between physical, chemical and biological approaches, 1-8, Copyright (2015), with permission from Elsevier. [54]

A second example of the application of non-specific, non-covalent interactions to modify cell surfaces with synthetic nano- and microparticles involves the use of cell adherent polyelectrolytes. This approach has been explored by Guan et al. to decorate a variety of cells, including human leukemic cells, mouse embryonic stem cells and human mesenchymal stem cells, with a range of microcontact-printed biomaterials [56,57]. Fig. 2 schematically outlines the process developed by the Guan lab to prepare cell adhesive microparticles. Microcontact printed particles are disk-like multilayered particles ranging in the size of several micrometers (7 μm particles are typically used for cell surface modification), which can be prepared from a large variety of cationic and anionic polymers such as poly(allylamine hydrochloride) (PAH), poly(diallyl dimethyl ammonium chloride) (PDAC), poly(ethylene imine) (PEI), poly(L-Lysine) (PLL), chitosan, poly(acrylic acid) (PAA), poly(sodium 4-styrene sulfonate) (PSS) as well as biodegradable and biocompatible polymers such as PLGA or poly(lactic acid) (PLA) and poly(ε-caprolactone) (PCL), which are particularly interesting for drug delivery purposes. The microparticles are fabricated by soaking a poly(dimethyl siloxane) (PDMS) stamp

with a micropillar surface structure into a polymer solution. Additional layers are subsequently adsorbed on the stamp via a layer-by-layer (LbL) assembly process. Finally, the multilayer film on the stamp is transferred via microcontact printing onto a substrate coated with a polymer sacrificial layer which will be subsequently used to release of the microparticles [56]. The sacrificial layer, which is composed of poly(vinyl alcohol) (PVA) or poly(*N*-isopropylacrylamide) (PNIPAM) is deposited onto the glass substrate via spin-coating. The PVA sacrificial layers are primarily used for the preparation of a suspension of the microdevices. In this case, the release of the microdevices is simply triggered by dissolution of the PVA film in an aqueous medium. PNIPAM is used as a thermoresponsive sacrificial layer when cells are first bound to the printed materials directly on the array and subsequently the cell-microdevice complexes are released from the substrate upon decreasing the temperature below the lower critical solution temperature (LCST) of PNIPAM as illustrated in Fig. 2 [57]. This second approach yields well-defined cell-microdevice complexes in which each cell is bearing a single microdisk. Cell binding is mediated through electrostatic interactions with a cell-adhesive polyelectrolyte such as PAH, PLL or PEI. This fabrication process can in principle also be used for the preparation of ligand functionalized microdevices for receptor-mediated cell-attachment [58]. Interestingly, asymmetric PLGA/(3-aminopropyl)triethoxysilane/glutaraldehyde/PAH microdevices, with covalent bonding between the (3-aminopropyl)triethoxysilane-coated PLGA region and PAH systems, prepared via LbL assembly and microcontact printing showed no cell aggregation upon functionalization of cells with a microdevices suspension [58]. Single cell bearing multiple microdevices were also detected, especially at high microdevice-to-cell ratio. No evidence of internalization of the microdevices was observed. Viability and proliferation of these cells were not affected over a period of seven days [58]. This technique was also used to modify cells with 2-naphtalenethiol coated gold nanoparticles packed microdisks. These microdisks could be used as non-invasive in vivo tracking system for therapeutic cells [59].

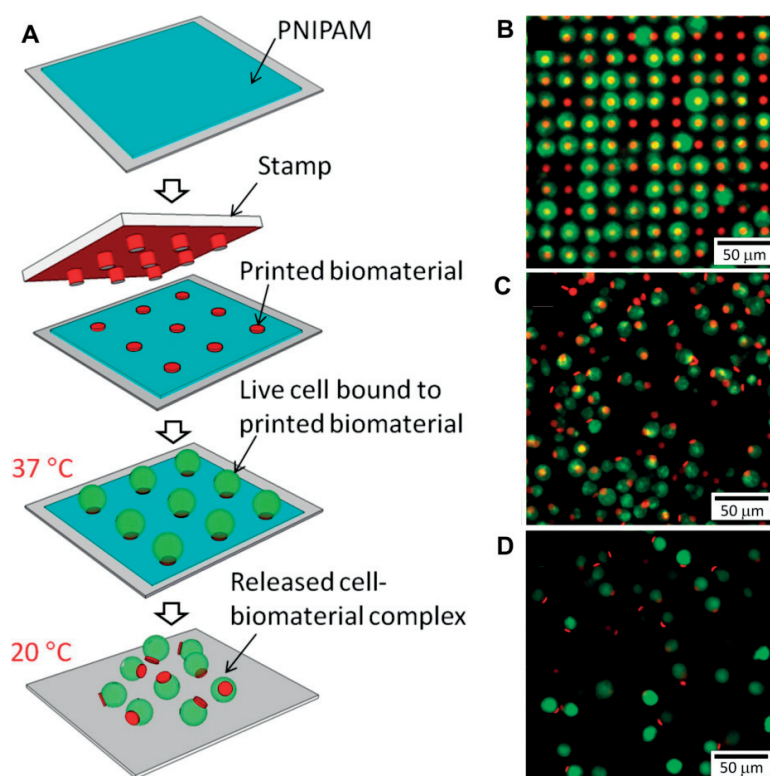


Figure 2. Functionalization of live cells with microcontact printed biomaterials using spin-coated PNIPAM as the sacrificial layer. (B) Fluorescence micrograph of K562 cells (green) immobilized on an array of circular microparticles of polyelectrolyte multilayer (red) before being released, (C) immediately after being released and (D) cell-microparticle complexes after being cultured for 24 h. Reprinted from *Acta Biomater.*, 11, Z. Wang, J. Xia, Y. Yan, A.-C. Tsai, Y. Li, T. Ma, J. Guan, Facile functionalization and assembly of live cells with microcontact-printed polymeric biomaterials, 80-87, Copyright (2015), with permission from Elsevier. [57]

1.3.1.2. Ligand-receptor mediated cell surface conjugation

As an alternative to the non-specific interactions discussed above, another approach that has been successfully and extensively explored to non-covalently conjugate synthetic nano- and microparticles to cell surfaces involves the use of specific ligand-receptor interactions. This approach has been pioneered by Rubner and coworkers who have used CD44-hyaluronic acid and Fc receptor-Fc interactions to conjugate polyelectrolyte multilayer (PEM) patches to cells [60]. Cell surface conjugation of PEM patches is a three step process in which first a patterned array of cell-adhesive functionalized heterostructured patches is prepared via a photolithographic lift-off process combined with a multilayer assembly of ultrathin polymer films (LbL assembly). Cells are then

sedimented onto the patterned array and binding is promoted by incubation at 37 °C. Finally, the cell-patch complexes are released from the substrate by a pH and/or temperature or an enzyme-mediated triggering mechanism (Fig. 3). This approach ensures the production of well-defined cell-patch complexes bearing a single patch per cell whereas the use of freely suspended backpacks prepared by this method tends to lead to cell aggregation during cell functionalization [61]. Using pre-released backpacks, however, is attractive from a clinical perspective as they could be used to modify cells *ex vivo* before reinjection or as a direct injectable formulation. Cell-patch complexes could nevertheless be prepared in suspension if the ratio of cells-to-backpacks as well as the size of the backpacks are carefully adjusted. Large aggregates could partially be avoided by moderate agitation [61] and/or are removed using a cell strainer [62].

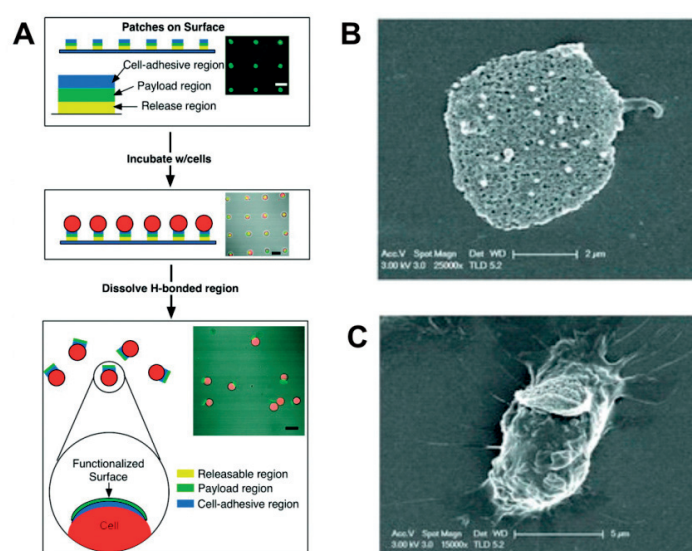


Figure 3. (A) Schematic overview of the fabrication and cell surface attachment of polymer patches. Scanning electron micrograph of (B) PEM backpack and (C) a macrophage modified with a HA/CHI coated backpack. Adapted with permission from Nano Lett., 8, A.J. Swiston, C. Cheng, S.H. Um, D.J. Irvine, R.E. Cohen, M.F. Rubner, Surface Functionalization of Living Cells with Multilayer Patches, 4446-4453, Copyright (2008) American Chemical Society. [60] Adapted with permission from Adv. Mater., 23, N. Doshi, A.J. Swiston, J.B. Gilbert, M.L. Alcaraz, R.E. Cohen, M.F. Rubner, S. Mitragotri, Cell-Based Drug Delivery Devices Using Phagocytosis-Resistant Backpacks, H105-H109, Copyright (2011) John Wiley and Sons [22].

As illustrated in Fig. 3, cellular backpacks are 3-layer heterostructured assemblies that are composed of (i) a releasable region that deconstructs and releases the patches from the

substrates (in microcontact printed patches, the release region is replaced by a spin-coated sacrificial layer) (ii) a payload region that encapsulates a cargo and (iii) a cell-adhesive region to anchor the patch to the cell membrane (Fig. 3). The release region of the patch is designed to dissolve upon exposure to a stimulus such as pH, temperature, enzymatic or a combination of those. The stimulus needs to be noncytotoxic if the attachment of cells is performed prior to the release of cell-patch complexes. One example of a release region that has been used are hydrogen-bonded, poly(methacrylic acid)-poly(*N*-isopropylacrylamide) (PMAA-PNIPAM) multilayers, which are both pH and thermally responsive. The release only occurs at a pH higher than approx. 6.2 and below the LCST of PNIPAAm (approx. 32 °C). Sacrificial thin film systems based on bovine submaxillary mucin (BSM) and the lectin jacalin (JAC) were also used for post-cell attachment release. These films are stable over a wide range of pH (pH 3–9) and ionic strengths, allowing LbL assembly of additional films in a variety of conditions. The (BSM/JAC) film disintegrates at physiological pH in presence of melibiose [63] and a mucinase enzyme [62]. When patches are first to be released and used as a suspension to modify cells, the release region is designed as simple pH responsive region and is made of a poly(methacrylic acid) (PMAA) and poly(vinylpyrrolidone) (PVPON) hydrogen-bonded multilayer system, which dissolves at a pH value of approx. 6.4. The second region of the heterostructured patch is the payload region, which can encapsulate drugs, proteins, nanoparticles or even liposomes. This region is usually composed of structural multilayers and a cargo containing region. The structural rigidity is required to withstand sonication during patch fabrication. For example, anionic superparamagnetic nanoparticles can be alternately deposited with a poly(allylamine hydrochloride) (PAH) to create magnetically responsive patches conferring magnetic properties to the patched cells [60]. The advantage of this ‘magnetic region’ is two-fold, as it facilitates purification of the complexes and adds additional structural rigidity. Proteins, such as bovine serum albumin (BSA) can be entrapped in the payload region with poly(lactic-*co*-glycolic acid) (PLGA) using an airbrush spraying method to form a biodegradable film, which is usually deposited in between rigid PEM films such as the one above or alternatively poly(diallyl dimethyl ammonium chloride) (PDAC) and poly(styrene sulfonate) (PSS) or (PAH/PSS) based films [22]. Direct loading of small molecules such as doxorubicin (DOX) into PEM films can be challenging as they may rapidly elute from the polymer films. This can be overcome by loading DOX into liposomes, which are then subsequently incorporated in the payload region. Maintaining liposomal integrity is not

trivial during adsorption at a solid-fluid interface and may result in vesicle disruption or fusion into a lipid bilayer. It was possible to incorporate intact DOX loaded liposomes in a sandwich-like structure with (PDAC/PSS). These constructs showed up to a nine-fold increase in DOX loading within the payload region as compared to the free DOX [62]. The third region of the patch is the cell-adhesive region and is composed of a biocompatible and biodegradable hyaluronic acid/chitosan multilayer (HA/CHI). The binding affinity of the HA/CHI layer can be tuned by and depends on the deposition conditions as well as on the nature of the last deposited layer (HA or CHI) [64]. HA binds specifically to CD44 cell-surface receptors and the positively charged CHI chains contribute to the overall binding through electrostatic interactions with the negatively charged cell membrane [64]. By controlling the presentation of the cell adhesive HA/CHI domains, polymer microtubes could be attached to B-cells either in an end-on or side-on fashion [65]. In addition to the HA-CD44 binding motif, Rubner et al. have also used mouse IgG antibodies to bind to the Fc receptors of immune cells to decorate cell surfaces with backpacks. The antibodies are introduced onto a final PEM film through biotinylation [62]. Patch attachment is normally non-toxic and does not impair key cellular functions. Proliferation inhibition was, however, observed when monocytes were functionalized with patches containing DOX loaded liposomes, likely due to the close proximity of DOX release from the carrying cells [62]. Remarkably, functionalized T cells retain their ability to migrate on intercellular adhesion molecule-1 (ICAM-1), a common inflammatory marker, coated substrates. The patch only blocked a fraction of all CD44 receptors and was found at the trailing end of the polarized lymphocytes during migration when CD44 are clustering at the uropod [66]. Micron-scale patches are also particularly suitable for delivery with monocytes and macrophages. Most approaches for monocyte/macrophage-mediated drug delivery use ex vivo nanoparticle internalization followed by re-injection to the systemic circulation or target site [5]. This approach is potentially deleterious for the payload, which can be degraded along the endosomal pathway before its release. Disk-like PEM patches efficiently avoid phagocytic internalization while remaining on the monocyte or macrophage surface. Backpack attachment does not adversely alter normal phagocytosis, nor reduces the mobility of these patched cells, making them particularly suitable for cell-mediated drug delivery [22]. Monocytes modified with backpacks that were attached via mouse IgG-Fc interaction also retained key cellular functions [67]. Differentiation of backpack modified monocytes to macrophages was unaltered. Patched monocytes were also able to

transmigrate through a confluent HUVEC monolayer and approx. 60% of monocyte-hitchhiked backpacks were transported through the endothelial monolayer after 48 h whereas their free counterparts were not transported at all. In vivo, monocyte-hitchhiked backpacks showed a 9-fold higher accumulation in a skin inflammation model and a 2-fold higher accumulation in a lung inflammation model as compared to the free backpacks in those two models. This selective accumulation of monocytes into inflamed tissues is mediated by ICAM and VCAM which are overexpressed on inflamed endothelial barriers [67].

In addition to CD44-hyaluronic acid and Fc receptor-Fc interaction, a third example of a specific non-covalent interaction that has been used for cell surface modification with synthetic nano- and microparticles is that between the CD73 and CD90 membrane proteins of mesenchymal stem cells (MSCs) and the respective monoclonal antibodies. Using this strategy, Li et al. conjugated anti-CD73/CD90 monoclonal antibody coated silica nanorattles to mesenchymal stem cells for tumor-tropic delivery of doxorubicin (DOX) (Fig. 4) [68]. Silica nanorattles are biocompatible, mesoporous and hollow structures with very high drug loading capacity and sustained drug release properties. Exposing MSCs to antibody coated silica nanorattles was found to lead both to cell surface conjugation as well as internalization of the nanoparticles. DOX loaded silica nanorattles had negligible adverse effects on MSC viability. Modified cells showed slightly decreased migratory capacities in chemotaxis assay as compared to unmodified cells. In mice, MSC mediated delivery of DOX loaded silica nanorattles was found to result in increased accumulation and broader distribution in tumor tissues and consequently resulted in enhanced tumor cell apoptosis compare to free DOX or silica nanorattles encapsulated DOX.

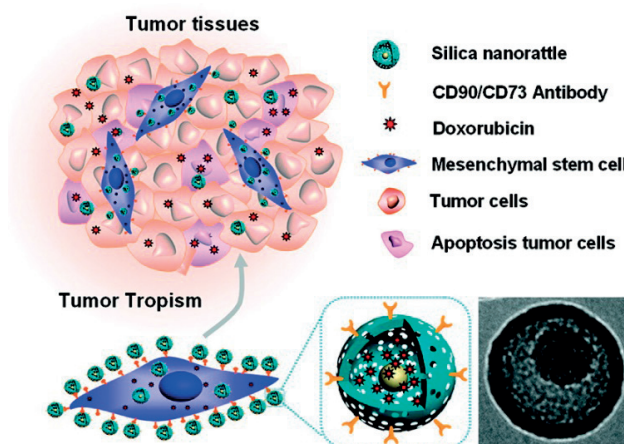


Figure 4. MSC mediated tumor tropic delivery of cell-surface anchored Doxorubicin-loaded silica nanorattles. Reprinted with permission from *Acs Nano*, 5, L. Li, Y. Guan, H. Liu, N. Hao, T. Liu, X. Meng, C. Fu, Y. Li, Q. Qu, Y. Zhang, S. Ji, L. Chen, D. Chen, F. Tang, Silica Nanorattle-Doxorubicin-Anchored Mesenchymal Stem Cells for Tumor-Tropic Therapy, 7462-7470. Copyright (2011) American Chemical Society [68].

Another example of specific, non-covalent interactions that has been extensively used for cell surface conjugation is that between biotin and (strept)avidin. The biotin-(strept)avidin interaction is among the strongest interactions known [69,70] and biotinylation has been widely used in biotechnology for decades e.g. in immunological assays and as an affinity system for biomolecule purification [71]. While concerns about the potential immunogenicity of the biotin-(strept)avidin link have been cited [72], which may require the use of alternative cell-surface conjugation approaches in further translational work, this interaction has been successfully used in several reports [40]. Attachment of synthetic materials to cell surfaces via biotin-avidin mediated conjugation requires pre-treating the cells to introduce a biotin group on their surface. This can be performed for instance by covalent attachment of a biotin moiety through amide bond formation with lysine residues of membrane proteins [73] or via prior modification of cell surface monosaccharides such as sialic acid with a mild oxidizing agent to generate aldehyde groups followed by functionalization with a hydrazide-biotin crosslinker [74]. The biotinylated cells can then be directly treated with avidin, streptavidin or NeutrAvidin-modified particles [73,75] or further functionalized with free avidin and subsequently with biotin-modified particles [40].

Cheng et al. conjugated NeutrAvidin coated nanoparticles to human mesenchymal stem cells (hMSCs) that presented biotin moieties on the plasma membrane [73]. The cells

were first reacted with sulfosuccinimidyl-6-(biotinamido)hexanoate and then 40 nm diameter NeutrAvidin-modified polystyrene nanoparticles were anchored to the cell membrane. Although some nanoparticles were internalized, a substantial amount remained on the outer membrane and existed as large clusters, sitting on the main body of hMSCs. The clustering of nanoparticles was attributed (at least in part) to membrane reorganization and it was further hypothesized that the formation of clusters reduced nanoparticle internalization. These modified stem cells are ideal candidates for tumor-tropic cell-mediated delivery of nanoparticles. Nanoparticles decorated hMSCs were tested for their ability to sense and respond to tumor spheroid growth in vitro, which remained unaltered by the surface conjugation of nanoparticles. A similar strategy was used by Mooney et al. who decorated biotinylated NSCs with ~ 800 nm diameter polystyrene nanoparticles [75]. The aim of this study was to investigate whether tumor-tropic neural stem cells could help to improve the distribution and retention of nanoparticles in a brain tumor model. The modification had a negligible effect on the viability and tropism in vitro and the nanoparticles remained on the surface of the cells for at least 1 h after coupling, a time frame sufficient for NSCs to reach tumor foci in vivo after injection. The nanoparticle conjugated NSCs were injected adjacent to the intracerebral glioma, into the contralateral hemisphere or intravenously and in all cases showed improved intracranial nanoparticle targeting and retention as compared to their free counterparts. Surface conjugation to NSCs dramatically reduced nanoparticle clearance over a period of 4 days and anchored nanoparticles are retained at day 1 level, whereas 93% of free nanoparticles were cleared over the same period. The intravenous administration is of great clinical interest as it represents a much less invasive procedure for the patient than intratumoral injection, and this example represents the first successful example of > 200 nm particles penetrating the blood-tumor barrier after systemic administration.

Nanoparticle decorated neural stem cells have also been explored to improve the efficacy of docetaxel loaded nanoparticles in a triple negative breast cancer mouse model (Fig. 5) [40]. In this study, biotin moieties were introduced on the cell surface via hydrazone formation after oxidation of cell surface sialic acid residues and biotinylated poly(ethylene glycol)-b-poly((diisopropyl amino) ethyl methacrylate) (PEG-b-PDPAEMA) based nanoparticles were then conjugated to the NSCs using an avidin linker. This sophisticated delivery system exerts a dual pH responsive behavior. Upon reaching the mildly acidic tumor environment, docetaxel is either directly released from

the particles by disassembly of the PDPAEMA nanoparticle core or alternatively the entire particle is cleaved off from the NSC surface via hydrolysis of the pH labile hydrazone linkage. The polymer particles could then be taken up by tumor cells where the drug is released intracellularly with the decrease in pH along the endosomal pathway. Docetaxel loaded nanoparticles did not adversely affect NSC viability over 12 h and under physiological pH conditions, during which only a small fraction of the drug is released. Tumor tropism, however, was slightly affected because of the potent microtubule stabilizing effect of docetaxel, which is directly related to cell mobility. The efficacy of NSC coupled docetaxel loaded nanoparticles administered via intratumoral injection was eventually evaluated by monitoring tumor microvasculature, tumor cells proliferation and apoptosis over a period of 7 days. The conjugation of nanoparticles to NSCs decreased tumor vessel density and altered cell proliferation whereas freely administered nanoparticles were ineffective at this low drug dosage.

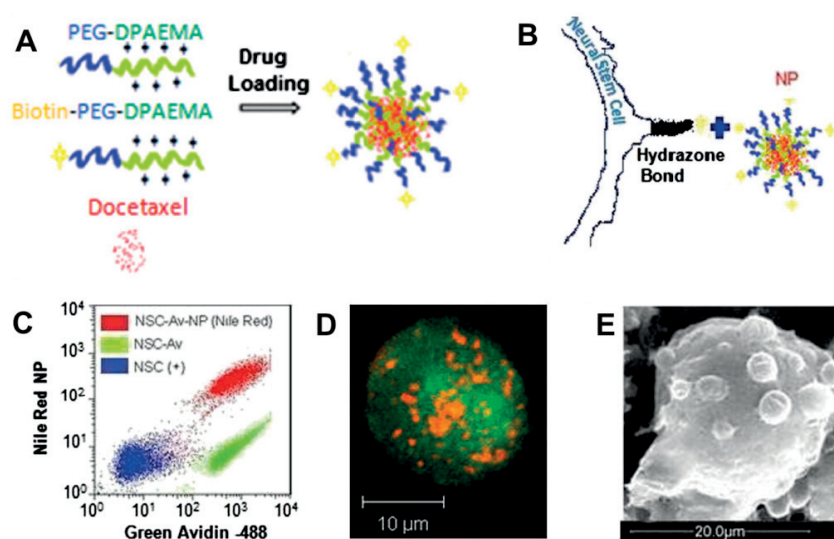


Figure 5. (A) Preparation of pH responsive, biotin functionalized and Docetaxel loaded poly(ethylene glycol)-b-poly((diisopropyl amino) ethyl methacrylate) block copolymer nanoparticles. (B) Schematic illustration of the conjugation of biotinylated nanoparticles onto a NSC surface, which presents hydrazone linked biotin moieties, via an avidin linker (C) Flow cytometric analysis of control NSCs (blue) and biotinylated NSCs after incubation with both fluorescein-conjugated avidin (green) and nile-red, biotinylated, pH responsive nanoparticles (red). (D) Confocal z-stack micrograph of a NSC-nanoparticle conjugate (NSC are shown in green and nanoparticles in red). (E) Scanning Electron microscopy micrograph of a nanoparticle modified NSC. Reprinted from J. Controlled Release, 191, R. Mooney, Y.M. Weng, E. Garcia, S. Bhojane,

L. Smith-Powell, S.U. Kim, A.J. Annala, K.S. Aboody, J.M. Berlin, Conjugation of pH-responsive nanoparticles to neural stem cells improves intratumoral therapy, 82-89, Copyright (2014), with permission from Elsevier [40].

Carbohydrate ligands that are present on the cell surface also provide opportunities for the selective non-covalent conjugation of synthetic nano- and microparticles. King and coworkers have taken advantage of the ability of E-selectin to bind to these cell surface ligands to decorate leukocytes with TRAIL functionalized liposomes [76]. E-selectin coated liposomes bearing TRAIL attach to leukocyte surfaces under shear by interacting with sialylated carbohydrates present on the cell membrane. This approach is highly effective in killing circulating tumors cells in vitro in human blood samples under flow conditions as well as in vivo in the peripheral circulation of mice by simple injection of a E-selectin/TRAIL-coated liposome solution in the circulation. This approach was also evaluated in a more advanced orthotopic xenograft animal model for prostate cancer and sustained delivery of E-selectin/TRAIL-coated liposomes efficiently eliminated circulating tumor cells and prevented the formation of metastasis in distant organs [77]. The same laboratory has also decorated NK cells with TRAIL-coated liposomes [78,79]. In this case cell surface conjugation was achieved by presentation of anti-CD57 or anti-NK1.1 antibodies on the liposome surface, which bind to the CD57 or to the NK1.1 cell surface proteins, respectively (Fig. 6). These enhanced NK cells, also named super NK cells by the authors, were able to induce apoptosis to several metastatic cancer cell lines (of three different cancer types i.e. prostate, colorectal and breast cancer) co-cultured in vitro in a lymph node mimetic system and were significantly more efficient than when co-cultured with unmodified NK cells or with TRAIL-functionalized liposomes only [78]. In vivo, this strategy also proved effective in preventing lymph node metastasis in mice bearing a subcutaneous human xenograft tumor model [79]. Super NK cells were formed within the tumor draining inguinal lymph node after subcutaneous injection of anti-NK1.1/TRAIL-functionalized liposomes. Tumor burden in the tumor draining inguinal lymph node dramatically decreased after treatment with anti-NK1.1/TRAIL liposomes whereas administration of soluble TRAIL by itself or TRAIL-functionalized liposomes did not hinder metastasis growth.

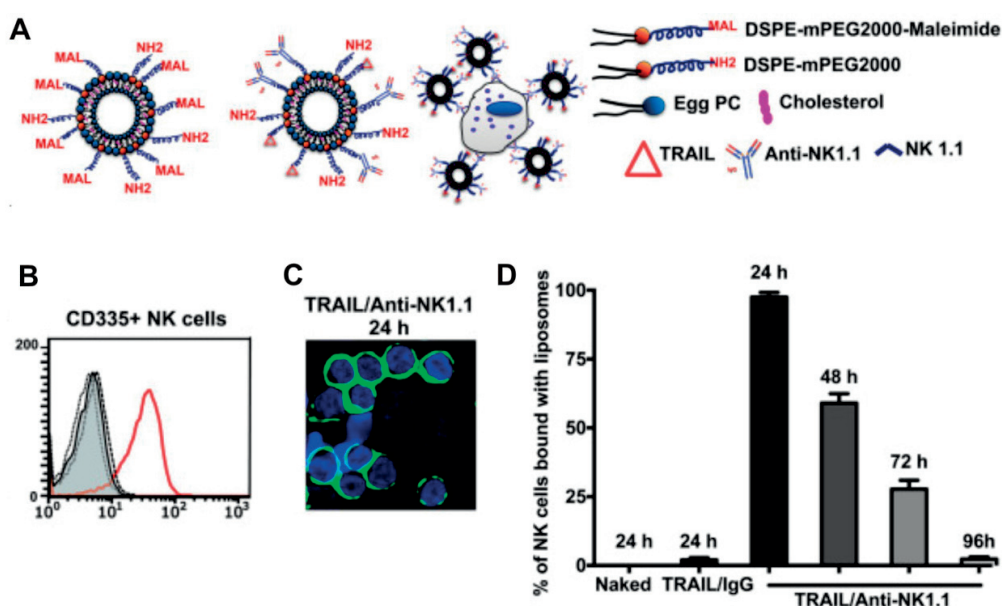


Figure 6. (A) Formulation and immobilization of TRAIL and anti-NK1.1 functionalized liposomes on NK cells. (B) Flow cytometry analysis: histograms from liposome fluorescence (FITC conjugated anti-human TRAIL) from CD335+ NK cells from the inguinal lymph nodes of mice injected with buffer (filled), naked liposomes (-----), TRAIL/IgG liposomes (.....) or TRAIL/Anti-NK1.1 liposomes (red) 24 h post-injection. (C) Fluorescent confocal micrograph of NK cells isolated from the inguinal lymph nodes of mice subcutaneously injected with TRAIL/Anti-NK1.1 liposomes (at t=24 h). (D) Numerical quantification of the percentage of NK cells bound with liposomes with different functionalizations. Bars represent the mean and standard deviation from 10 different confocal images for each time point. Reprinted from Biomaterials, 77, S. Chandrasekaran, M.F. Chan, J. Li, M.R. King, Super natural killer cells that target metastases in the tumor draining lymph nodes, 66-76, Copyright (2016), with permission from Elsevier [79].

In a series of reports, Bertozzi and coworkers have explored the highly selective binding properties of lectins to decorate living cells with carbon and boron nitride nanotubes. In a first report, carbon nanotubes were coated with a biomimetic glycopolymer, prepared by post-polymerization modification of a C₁₈ lipid tail functionalized poly(methyl vinyl ketone) with α -N-acetylgalactosamine residues. The lipid tail was used to anchor the synthetic polymer to the surface of the carbon nanotube via hydrophobic interactions and at the same time to reduce the cytotoxicity of the carbon nanotubes. The polymer coated carbon nanotubes were then modified by addition of *Helix pomatia* agglutinin (HPA) (a hexavalent lectin) and then added to the cell suspension (CHO cells or Jurkat cells) or alternatively the cells were treated with HPA

prior to addition of the coated nanotubes. HPA specifically recognizes α -N-acetylgalactosamine residues and is used to mediate crosslinking between cell-surface glycoproteins and the glycopolymer coated carbon nanotubes [80]. The use of the poly(methyl vinyl ketone) based glycopolymers to modify the carbon nanotubes, however, resulted in irregular surface coatings of non-uniform thickness. To overcome these problems, the Bertozzi laboratory prepared bifunctional glycodendrimers composed of a pyrene tail that can bind to the carbon nanotube surface via π - π interactions as well as a number of peripheral carbohydrate units that can be used to mediate cell surface immobilization. In this way, G2-mannose modified glycodendrimers were used to selectively bind carbon nanotubes to the surface of CHO cells in the presence of the lectin *Canavalia ensiformis* agglutinin (Con A) [81]. Boron nitride nanotubes, isosteres of carbon nanotubes, are more chemically inert and structurally stable than their carbon counterpart. They have similar mechanical and thermal properties. However, their most attractive feature is that they are inherently noncytotoxic. Boron nitride nanotubes were successfully assembled on the surface of CHO cells using the same glycodendrimers, which were discussed above for the cell surface immobilization of carbon nanotubes [82]. These nanotubes offer then an interesting alternative to carbon nanotubes in living systems and have the potential to be useful in therapy or diagnosis.

1.3.2. Covalent cell surface modification

Synthetic nano- and microparticles can be covalently attached to cell surfaces either via the native functional groups that are present on the cell surface such as amine or thiol groups or by using non-natural functional groups, which can be introduced onto the cell surface e.g. using metabolic strategies [83] or by chemically generating reactive groups such as aldehydes on the cell surface. Even though there is a vast range of chemoselective and bioorthogonal reactions that have been successfully used to modify peptides, proteins and polysaccharides [84], not all of these are suitable for the surface modification of living cells as the reaction conditions may impair the viability of the cells. The remainder of this section will highlight several covalent cell surface conjugation strategies that have been reported for the modification of specific natural and non-natural functional groups present on the cell surface.

1.3.2.1. Modification of cell surface amine groups

The concentration of amino groups on the cell surface is high and lysine residues on membrane surface proteins are usually readily accessible [85]. However, while they have been frequently used as anchors to introduce biotin moieties (which are then subsequently used to facilitate (strept)avidin mediated non-covalent cell surface conjugation), amine groups have been scarcely used for the direct covalent attachment of synthetic nano- or microparticles. There are, however, a few reports that describe the direct covalent conjugation of synthetic polymers to amine groups on the cell surface. For instance, poly(ethylene glycol) (PEG) was grafted on the surface of Langerhans islets using either isocyanate or *N*-hydroxysuccinimide end-functionalized PEGs [86,87]. Another example are red blood cells, which have been modified with cyanuric chloride end-functionalized PEGs [88], succinimidyl functionalized hyperbranched polyglycerols [89] as well as with ATRP synthesized polymers [90].

1.3.2.2. Maleimide-thiol coupling

Cysteine thiol groups are attractive anchors for covalent cell surface modification as they are relatively abundant [91] and can undergo various chemoselective reactions. Covalently anchoring nanoparticles via Michael type addition to cell surface cysteine residues was first proposed by Irvine and coworkers [92]. Maleimide functionalized liposomes, multilamellar liposomes and lipid coated PLGA nanoparticles in the range of 100–300 nm were efficiently conjugated to the surface of CD8⁺ T lymphocytes and hematopoietic stem cells (HSCs) commonly used in cell therapy (Fig. 7). Coupling of up to 100–120 nanoparticles on the surface of lymphocytes did not activate them and particles were retained on the surface of the cells for several days. Proliferation profiles were not affected after lymphocyte activation by DC and transendothelial migration efficiencies were similar to those of unmodified cells, with the exception of the more rigid lipid-coated PLGA nanoparticles, which showed a tendency to inhibit T cell migration and were not retained as well as liposomes after migration. Adoptively transferred T cells with surface conjugated 300 nm multilamellar liposomes kept tumor-homing properties in a subcutaneous EL4 tumor model and transported their nanoparticulate cargo with a 176-fold increased accumulation into the tumor tissue as compared to their freely administered counterparts. One of the limitations of adoptive cell therapy lies in the rapid decline of cell viability and function after transplantation. Co-administration of adjuvants such as cytokines during cell therapy is usually necessary and the high systemic levels required induce dose-limiting toxicities. A mixture of

interleukins loaded into surface-tethered multilamellar liposomes significantly improved the therapeutic efficacy of the transplanted cells by continuously delivering the cytokines in the direct surroundings of the particle-carrying cells at doses that are typically inefficient if they were administered systemically [92]. This approach markedly amplified T cell expansion and function during adoptive transfer in mice melanoma lung and bone marrow tumors models and efficiently prevented tumor growth after a 30 days T cell treatment. Further investigation of T cells decorated with nanoparticles using thiol-maleimide coupling chemistry revealed that the nanoparticles compartmentalize at the uropod of polarized T cells after seeding them onto a confluent endothelial cell monolayer (Fig. 7) [93]. Interestingly, nanoparticle compartmentalization was reversed when a T cell forms an immunological synapse with an antigen presenting cell. Surface-bound particles were repolarized to the contact zone with the antigen presenting cell after T cell receptor activation (Fig. 7). Nanoparticle-binding proteins were identified by mass spectrometry and predominantly consisted of the leukocyte common antigen CD45 as well as an additional small set of other surface proteins such as LFA-1, CD2 or CD97, which are all recruited to the immunological synapse during antigen recognition. This could be exploited to alleviate the effect of suppressive ligand upregulation by tumor cells occurring in the immunological synapse, which effectively prevents tumor cells recognition by the immune system. Inhibiting this tumor-induced suppression effect, locally, directly in the contact zone between the tumor cells and T cells was achieved by loading potent immunomodulators into the surface-bound nanoparticles that are translocated in the immunological synapse during plasma membrane proteins reorganization. Local and accurate delivery could avoid the severe adverse side effects and autoimmune risks associated with the systemic administration of these drugs.

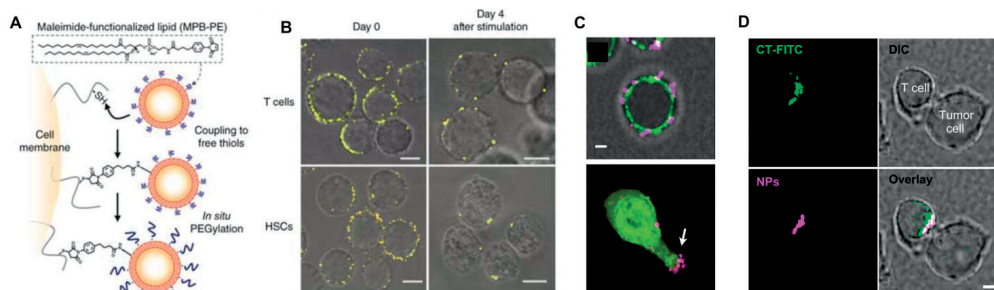


Figure 7. (A) Maleimide-thiol cell surface conjugation of lipid nanoparticles. MPB-PE: 1,2-dioleoyl-sn-glycero-3-phosphoethanolamine-N-[4-(p-maleimidophenyl)butyramide]. (B) Confocal microscopy images of CD8⁺ effector T cells and hematopoietic stem cells (HSCs) immediately

after conjugation with fluorescent 1,1-dioctadecyl-3,3,3,3-tetramethylindodicarbocyanine (DiD)-labeled multilamellar lipid nanoparticles (left) and after 4-d in vitro expansion (right). Scale bars, 2 μm . (C) Confocal micrographs of lipid nanoparticle-conjugated CD8⁺ effector T cells. Top: T cells surface stained with FITC-cholera toxin (green) immediately after surface-conjugation of fluorescent nanoparticles (magenta) or Bottom CFSE-labeled T-cells (green) conjugated with particles (magenta) migrating on an endothelial cell monolayer toward a chemoattractant. Scale bar 2 μm . (D) CD8⁺ effector T-cells conjugated with multilayer vesicles were incubated with tumor cells for 20 min, then fixed and stained with FITC-cholera toxin to mark lipid rafts known to accumulate at the immunological synapse. Shown are confocal images of a T-cell forming a synaptic contact with a tumor cell. Nanoparticles were fluorescently labelled with rhodamine-conjugated lipid (magenta). Scale bar: 2 μm . Reprinted by permission from Macmillan Publishers Ltd: Nature Medicine, [92] copyright (2010). Reprinted from Biomaterials, 33, M.T. Stephan, S.B. Stephan, P. Bak, J.Z. Chen, D.J. Irvine, Synapse-directed delivery of immunomodulators using T-cell-conjugated nanoparticles, Biomaterials, 5776-5787, Copyright (2012), with permission from Elsevier [93].

In another example, the Irvine lab used thiol-maleimide coupling chemistry to modify T cells with liposomes coated with the chemotherapeutic agent SN-38 to actively target disseminated tumors [94]. SN-38 is a potent chemotherapeutic agent, which has limited in vivo efficacy due to its poor pharmacokinetics and high toxicity but could potentially be very effective if it were delivered with high precision. Tumor dissemination in multiple organs is characteristic of lymphomas for instance and represents a real challenge for therapy because of the restricted access to tumors in lymph nodes, which can serve as niche for tumor cells survival during chemotherapy. Tumor-bearing lymph nodes were not sensitive to chemotherapy using free SN-38 or a liposome formulation of this drug, presumably because of the lack of a leaky vasculature around the tumor that does not allow passive accumulation of the drug in tumor tissues by the enhanced permeation and retention (EPR) effect. Since targeting lymph nodes was primarily sought, polyclonal T cells, which intrinsically express lymph node homing receptors and migrate throughout lymphoid organs as part of their normal function, were proposed as delivery vectors for SN-38 loaded nanocarriers rather than tumor specific T cells. SN-38 loaded nanocarrier-T cells accumulated in tumor-bearing lymph nodes 20 h after transfer and SN-38 concentration in lymph nodes was 63-fold higher than that achieved with free nanocarriers, resulting in a significant beneficial therapeutic effect, extending survival of mice up to 12 days at relatively low therapeutic doses (7 mg/kg) (Fig. 8). Since many receptors required for T cell trafficking to a variety of organs, such as lungs, skin, gut and

brain as well as that the stimuli required to induce expression of these markers are known [95], the authors proposed that T cells as chaperones potentially offer a means of selective delivery to virtually any of these organs without resorting to antigen specific T cells. Moreover, in the case in which tumor-specific T cells could be readily obtained, the concomitant chemotherapeutic agent delivery could in principle be combined with tumor-antigen specific T cells [94].

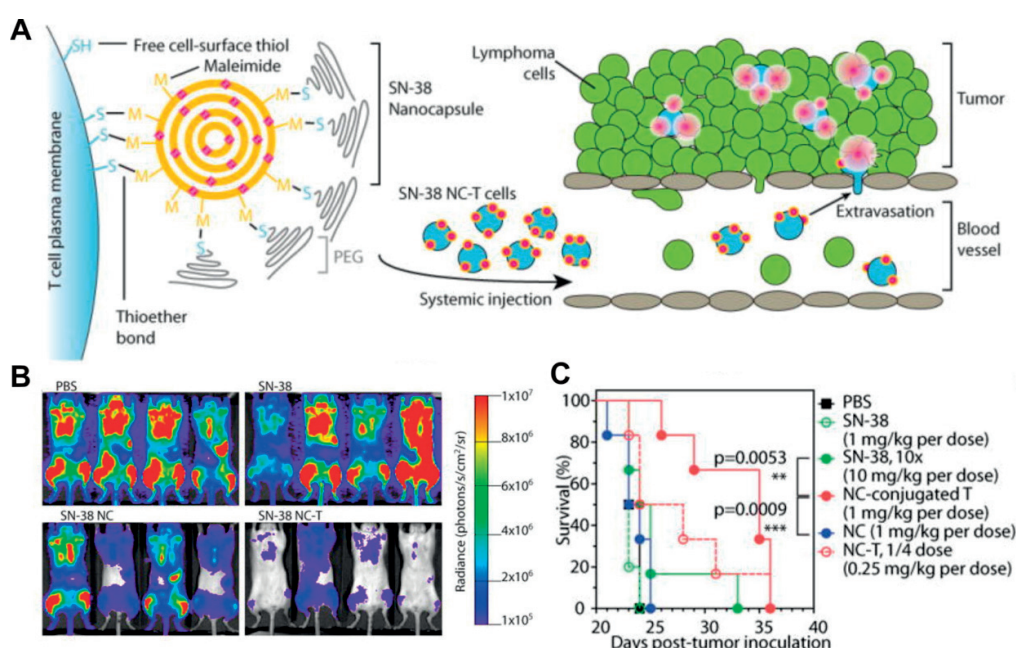


Figure 8. (A) T cell functionalization and cell-mediated delivery of SN-38 nanocapsules (NCs) into tumors. (B) Bioluminescence images of tumor burden on day 16 for mice treated with PBS, SN-38, SN-38 nanocapsules and SN-38 nanocapsules tethered to a T cell carrier (NC-T). (C) Overall survival. ***P < 0.001 by log-rank test. From [94]. Reprinted with permission from AAAS.

1.3.2.3. Conjugation through disulfide bond formation

In addition to covalent attachment of maleimide functionalized liposomes or polymer nanoparticles, cell surface thiol groups also provide the possibility to anchor nano- or microsized carriers via disulfide bonds. Wayteck et al. e.g. used this strategy to attach pyridyldithiopropionate functionalized liposomes to the surface of CD8⁺ T cells [96]. These surface-engineered T cells were proposed to serve two purposes: (i) to allow direct killing of tumor cells and (ii) to enhance the delivery of drug loaded liposomes to the tumor tissue and kill T cell refractory tumor cells. The reversible nature of the disulfide

linkage is envisioned as a tumor-specific trigger for liposome detachment in the tumor microenvironment where higher extracellular concentration of glutathione arises from dead cells and where several thiolytic proteins, such as thioredoxin are overexpressed. Liposome conjugation to T lymphocytes did not interfere with cell proliferative capacity after T cell activation, nor affected their cytotoxic function. In vitro liposome detachment was effective at glutathione concentrations of 2 mg/mL and accounted for the release of approx. 50% of all surface bound nanocarriers.

1.3.2.4. Conjugation through Schiff base formation

Yang and coworkers coupled quantum dots and PAMAM dendrimers which were modified with amine derivatized PEG to the surface of RAW 264.7 macrophages via Schiff base formation [97]. To this end, first the RAW 264.7 macrophages were pretreated with sodium periodate to generate aldehyde groups on the cell surface. Then, the cells were treated with amine functionalized dendrimers or quantum dots. If desired, the imine bond could subsequently be reduced with sodium cyanoborohydride to form a stable secondary amine linkage. The distribution of nanoparticles was assessed by confocal microscopy. Although partly internalized, the fate of these nanoparticles (typically in the range of 10 nm or smaller) depends on the nature of the covalent linkage and showed a bias for cell wall immobilization that was more pronounced when nanoparticles were linked to the cell surface via reductive amination.

1.3.2.5. Coupling through strain-promoted azide-alkyne cycloaddition (SPAAC)

The Yang laboratory also reported the surface modification of RAW 264.7 macrophages with PAMAM dendrimers using a metal free, bioorthogonal click reaction [98]. In this example, first azide moieties were metabolically incorporated into the cell surface. The cell surface azide groups were subsequently reacted with cyclooctyne functionalized PAMAM dendrimers in a strain-promoted azide-alkyne cycloaddition reaction. Dendrimers are interesting in this context as they can transport a high payload of anticancer drugs. Cell surface attachment predominantly yielded membrane bound dendrimers and significantly reduced their uptake as compared to unfunctionalized dendrimers which were mostly internalized. The hybridization process using this bioorthogonal ligation has a negligible effect on macrophage viability and their motility also remained unaffected after functionalization.

1.4. Conclusions and outlook

The aim of this article has been to provide an overview on the use of surface-engineered cells to mediate the delivery of synthetic nano- and microparticles. This is a very exciting and rapidly evolving area of research with great clinical potential. The variety of cell types that has been explored as well as the diversity of cell surface conjugation chemistries that are available provide a wide range of opportunities to generate nano- or microparticle decorated cells that are tailored towards a specific indication. Important challenges related to cell surface modification with synthetic nano- and microparticles are (i) whether cellular function remains intact after modification and (ii) whether the nano- or microcarrier remains attached to the cell surface in the systemic circulation upon exposure to shear forces, cell-cell and cell-wall interactions or during endothelial diapedesis. The development of novel, refined cell surface conjugation approaches could help to address these challenges. Genetic engineering [99] or evolutionary methods such as cell-SELEX and phage display could provide interesting solutions to selectively attach a synthetic material to the cell surface with high avidity and without compromising cellular functions. Ideally, cell-mediated drug delivery should enhance targeting of the drug loaded synthetic nano- or microcarrier and reduce off-target delivery. Although surface modified cells have been successfully used to facilitate delivery of nano- and microparticle-based carriers to the target site, a challenge that has received only comparably little attention is the release of the drug and/or drug loaded carrier from the cell surface upon arrival at the target site. This release and the mechanism that triggers it depends on the microenvironment where the drug is to be delivered and then on the nature of the pathological condition. The targeted release of nanoparticles at the tissue-level in the context of cell-mediated delivery is closely related to the field of stimuli-responsive nanomedicines and the same mechanisms can be applied here for delivery to tumor microenvironment, sites of inflammation or infection for instance [100,101]. There are in principle three main endogenous stimuli that can be used to trigger the liberation of nano- or microparticles from a cell surface: a lowered interstitial pH, a difference in redox status or an increased level of extracellular enzymes such as protease, phospholipase or glycosidases. For example, using a pH sensitive linkage or a pH sensitive polymer or biodegradable nano- or microparticles may promote the release of the drug-loaded carriers or of the encapsulated drug in a slightly acidic environment typically encountered in tumor tissues. Furthermore, and in particular in case drugs are used that act on intracellular targets, the nano- or microcarrier needs to be

designed such as to e.g. enhance cellular internalization as well as trafficking and delivery of the active compound to the appropriate organelle, taking advantage of the different intracellular pH, redox status and enzyme concentration. Ultimately, combining cell-mediated delivery with precision polymer nanocarriers could allow (i) an initial delivery mediated by a cellular vehicle to the site of disease and in a second step (ii) liberation of an effective nanomedicine that will precisely release its drug component directly at its site of action. An interesting first proof of principle study that demonstrates the feasibility of this approach was reported by Mooney et al. who decorated neural stem cells with docetaxel loaded pH responsive particles via a pH cleavable linker [40]. The concept of cell mediated delivery can be taken one step further if cells are not only used to mediate transport of nano- or microparticle based carriers, but also play an active therapeutic role. A nice example of this approach is the work by Wayteck et al. [96], which synergistically combines the direct tumor cell killing properties of cytotoxic T-cells with their ability to enhance delivery of drug-loaded nanoparticles to tumor tissue. The nanoparticles are liberated from their cellular carriers via a redox-sensitive linkage. This last example represents the state-of-the art technology in term of combination of cell therapy and cell-mediated drug delivery.

1.5. References

- [1]. R. Duncan, Polymer conjugates as anticancer nanomedicines, *Nature Reviews Cancer*, 6 (2006) 688-701.
- [2]. R. Duncan, The dawning era of polymer therapeutics, *Nature Reviews Drug Discovery*, 2 (2003) 347-360
- [3]. T.M. Allen, Ligand-targeted therapeutics in anticancer therapy, *Nature Reviews Cancer*, 2 (2002) 750-763.
- [4]. F. Danhier, To exploit the tumor microenvironment: Since the EPR effect fails in the clinic, what is the future of nanomedicine?, *J. Controlled Release*, 244 (2016) 108-121.
- [5]. E.V. Batrakova, H.E. Gendelman, A.V. Kabanov, Cell-mediated drug delivery, *Expert Opin. Drug Deliv.*, 8 (2011) 415-433.
- [6]. A.C. Anselmo, S. Mitragotri, Cell-mediated delivery of nanoparticles: Taking advantage of circulatory cells to target nanoparticles, *J. Controlled Release*, 190 (2014) 531-541.

- [7] Y. Su, Z. Xie, G.B. Kim, C. Dong, J. Yang, Design Strategies and Applications of Circulating Cell-Mediated Drug Delivery Systems, *ACS Biomaterials Science & Engineering*, 1 (2015) 201-217.
- [8] C. Eyileten, K. Majchrzak, Z. Pilch, K. Tonecka, J. Mucha, B. Taciak, K. Ulewicz, K. Witt, A. Boffi, M. Krol, T.P. Rygiel, Immune Cells in Cancer Therapy and Drug Delivery, *Mediators Inflamm.*, (2016).
- [9] M.T. Stephan, D.J. Irvine, Enhancing cell therapies from the outside in: Cell surface engineering using synthetic nanomaterials, *Nano Today*, 6 (2011) 309-325.
- [10] C.D. Porada, G. Almeida-Porada, Mesenchymal stem cells as therapeutics and vehicles for gene and drug delivery, *Adv. Drug Del. Rev.*, 62 (2010) 1156-1166.
- [11] V.R. Muzykantov, Drug delivery by red blood cells: vascular carriers designed by mother nature, *Expert Opin. Drug Deliv.*, 7 (2010) 403-427.
- [12] E.M. Pasini, M. Kirkegaard, P. Mortensen, H.U. Lutz, A.W. Thomas, M. Mann, In-depth analysis of the membrane and cytosolic proteome of red blood cells, *Blood*, 108 (2006) 791-801.
- [13] F. Pierige, S. Serafini, L. Rossi, A. Magnani, Cell-based drug delivery, *Adv. Drug Del. Rev.*, 60 (2008) 286-295.
- [14] T.F. Gajewski, H. Schreiber, Y.-X. Fu, Innate and adaptive immune cells in the tumor microenvironment, *Nat. Immunol.*, 14 (2013) 1014-1022.
- [15] W.A. Muller, Leukocyte-endothelial-cell interactions in leukocyte transmigration and the inflammatory response, *Trends Immunol.*, 24 (2003) 327-334.
- [16] L. Griffiths, K. Binley, S. Iqbal, O. Kan, P. Maxwell, P. Ratcliffe, C. Lewis, A. Harris, S. Kingsman, S. Naylor, The macrophage - a novel system to deliver gene therapy to pathological hypoxia, *Gene Ther.*, 7 (2000) 255-262.
- [17] C. Shi, E.G. Pamer, Monocyte recruitment during infection and inflammation, *Nature Reviews Immunology*, 11 (2011) 762-774.
- [18] P.J. Murray, T.A. Wynn, Protective and pathogenic functions of macrophage subsets, *Nature Reviews Immunology*, 11 (2011) 723-737.
- [19] J. Cros, N. Cagnard, K. Woollard, N. Patey, S.Y. Zhang, B. Senechal, A. Puel, S.K. Biswas, D. Moshous, C. Picard, J.P. Jais, D. D'Cruz, J.L. Casanova, C. Trouillet, F. Geissmann, Human CD14(dim) Monocytes Patrol and Sense Nucleic Acids and Viruses via TLR7 and TLR8 Receptors, *Immunity*, 33 (2010) 375-386.

- [20] C. Auffray, M.H. Sieweke, F. Geissmann, Blood monocytes: development, heterogeneity, and relationship with dendritic cells, *Annu. Rev. Immunol.*, 27 (2009) 669-692.
- [21] N. Doshi, S. Mitragotri, Macrophages Recognize Size and Shape of Their Targets, *PLoS One*, 5 (2010).
- [22] N. Doshi, A.J. Swiston, J.B. Gilbert, M.L. Alcaraz, R.E. Cohen, M.F. Rubner, S. Mitragotri, Cell-Based Drug Delivery Devices Using Phagocytosis-Resistant Backpacks, *Adv. Mater.*, 23 (2011) H105-H109.
- [23] T.W. LeBien, T.F. Tedder, B lymphocytes: how they develop and function, *Blood*, 112 (2008) 1570-1580.
- [24] M.I. Yuseff, P. Pierobon, A. Reversat, A.M. Lennon-Dumenil, How B cells capture, process and present antigens: a crucial role for cell polarity, *Nature Reviews Immunology*, 13 (2013) 475-486.
- [25] U.H. von Andrian, C.R. Mackay, Advances in immunology: T-cell function and migration - Two sides of the same coin, *New Engl. J. Med.*, 343 (2000) 1020-1033.
- [26] A.D. Luster, R. Alon, U.H. von Andrian, Immune cell migration in inflammation: present and future therapeutic targets, *Nat. Immunol.*, 6 (2005) 1182-1190.
- [27] E.J. Kunkel, E.C. Butcher, Plasma-cell homing, *Nature Reviews Immunology*, 3 (2003) 822-829.
- [28] M. Barry, R.C. Bleackley, Cytotoxic T lymphocytes: All roads lead to death, *Nature Reviews Immunology*, 2 (2002) 401-409.
- [29] M. DuPage, J.A. Bluestone, Harnessing the plasticity of CD4(+) T cells to treat immune-mediated disease, *Nature Reviews Immunology*, 16 (2016) 149-163.
- [30] L. Zamai, C. Ponti, P. Mirandola, G. Gobbi, S. Papa, L. Galeotti, L. Cocco, M. Vitale, NK Cells and Cancer, *The Journal of Immunology*, 178 (2007) 4011-4016.
- [31] A. Poli, T. Michel, M. Thérésine, E. Andrès, F. Hentges, J. Zimmer, CD56bright natural killer (NK) cells: an important NK cell subset, *Immunology*, 126 (2009) 458-465.
- [32] K. Cheent, S.I. Khakoo, Natural killer cells: integrating diversity with function, *Immunology*, 126 (2009) 449-457.
- [33] M.F. Corsten, K. Shah, Therapeutic stem-cells for cancer treatment: hopes and hurdles in tactical warfare, *Lancet Oncol.*, 9 (2008) 376-384.

- [34] A.J. Wagers, I.L. Weissman, Plasticity of adult stem cells, *Cell*, 116 (2004) 639-648.
- [35] D.J. Anderson, F.H. Gage, I.L. Weissman, Can stem cells cross lineage boundaries?, *Nat. Med.*, 7 (2001) 393-395.
- [36] D.L. Clarke, C.B. Johansson, J. Wilbertz, B. Veress, E. Nilsson, H. Karlstrom, U. Lendahl, J. Frisen, Generalized potential of adult neural stem cells, *Science*, 288 (2000) 1660-1663.
- [37] L.S. Sasportas, R. Kasmieh, H. Wakimoto, S. Hingtgen, J.A.J.M. van de Water, G. Mohapatra, J.L. Figueiredo, R.L. Martuza, R. Weissleder, K. Shah, Assessment of therapeutic efficacy and fate of engineered human mesenchymal stem cells for cancer therapy, *Proceedings of the National Academy of Sciences*, 106 (2009) 4822-4827.
- [38] M. Ehteshami, P. Kabos, A. Kabosova, T. Neuman, K.L. Black, J.S. Yu, The use of interleukin 12-secreting neural stem cells for the treatment of intracranial glioma, *Cancer Res.*, 62 (2002) 5657-5663.
- [39] A.U. Ahmed, M.A. Tyler, B. Thaci, N.G. Alexiades, Y. Han, I.V. Ulasov, M.S. Lesniak, A Comparative Study of Neural and Mesenchymal Stem Cell-Based Carriers for Oncolytic Adenovirus in a Model of Malignant Glioma, *Mol. Pharm.*, 8 (2011) 1559-1572.
- [40] R. Mooney, Y.M. Weng, E. Garcia, S. Bhojane, L. Smith-Powell, S.U. Kim, A.J. Annala, K.S. Aboody, J.M. Berlin, Conjugation of pH-responsive nanoparticles to neural stem cells improves intratumoral therapy, *J. Controlled Release*, 191 (2014) 82-89.
- [41] A. Uccelli, L. Moretta, V. Pistoia, Mesenchymal stem cells in health and disease, *Nature Reviews Immunology*, 8 (2008) 726-736.
- [42] M. Studeny, F.C. Marini, R.E. Champlin, C. Zompetta, I.J. Fidler, M. Andreeff, Bone marrow-derived mesenchymal stem cells as vehicles for interferon-beta delivery into tumors, *Cancer Res.*, 62 (2002) 3603-3608.
- [43] K. Nakamura, Y. Ito, Y. Kawano, K. Kurozumi, M. Kobune, H. Tsuda, A. Bizen, O. Honmou, Y. Niitsu, H. Hamada, Antitumor effect of genetically engineered mesenchymal stem cells in a rat glioma model, *Gene Ther.*, 11 (2004) 1155-1164.
- [44] K.S. Aboody, J. Najbauer, N.O. Schmidt, W. Yang, J.K. Wu, Y. Zhuge, W. Przybecki, R. Carroll, P.M. Black, G. Perides, Targeting of melanoma brain

- metastases using engineered neural stem/progenitor cells, *Neuro Oncol.*, 8 (2006) 119-126.
- [45] A.E. Karnoub, A.B. Dash, A.P. Vo, A. Sullivan, M.W. Brooks, G.W. Bell, A.L. Richardson, K. Polyak, R. Tubo, R.A. Weinberg, Mesenchymal stem cells within tumour stroma promote breast cancer metastasis, *Nature*, 449 (2007) 557-U554.
- [46] B. Ljubic, M. Milovanovic, V. Volarevic, B. Murray, D. Bugarski, S. Przyborski, N. Arsenijevic, M.L. Lukic, M. Stojkovic, Human mesenchymal stem cells creating an immunosuppressive environment and promote breast cancer in mice, *Sci. Rep.*, 3 (2013).
- [47] K.L. Lye, N. Nordin, S. Vidyadaran, K. Thilakavathy, Mesenchymal stem cells: From stem cells to sarcomas, *Cell Biol. Int.*, 40 (2016) 610-618.
- [48] F.-J. Muller, E.Y. Snyder, J.F. Loring, Gene therapy: can neural stem cells deliver?, *Nat. Rev. Neurosci.*, 7 (2006) 75-84.
- [49] P. Kabos, M. Ehtesham, A. Kabosova, K.L. Black, J.S. Yu, Generation of Neural Progenitor Cells from Whole Adult Bone Marrow, *Exp. Neurol.*, 178 (2002) 288-293.
- [50] X.P. Yuan, J.W. Hu, M.L. Belladonna, K.L. Black, J.S. Yu, Interleukin-23-expressing bone marrow-derived neural stem-like cells exhibit antitumor activity against intracranial glioma, *Cancer Res.*, 66 (2006) 2630-2638.
- [51] E. Chambers, S. Mitragotri, Prolonged circulation of large polymeric nanoparticles by non-covalent adsorption on erythrocytes, *J. Controlled Release*, 100 (2004) 111-119.
- [52] E. Chambers, S. Mitragotri, Long circulating nanoparticles via adhesion on red blood cells: Mechanism and extended circulation, *Exp. Biol. Med.*, 232 (2007) 958-966.
- [53] D. Pan, O. Vargas-Morales, B. Zern, A.C. Anselmo, V. Gupta, M. Zakrewsky, S. Mitragotri, V. Muzykantov, The Effect of Polymeric Nanoparticles on Biocompatibility of Carrier Red Blood Cells, *PLoS One*, 11 (2016) e0152074-e0152074.
- [54] A.C. Anselmo, S. Kumar, V. Gupta, A.M. Pearce, A. Ragusa, V. Muzykantov, S. Mitragotri, Exploiting shape, cellular-hitchhiking and antibodies to target nanoparticles to lung endothelium: Synergy between physical, chemical and biological approaches, *Biomaterials*, 68 (2015) 1-8.

- [55] A.C. Anselmo, V. Gupta, B.J. Zern, D. Pan, M. Zakrewsky, V. Muzykantov, S. Mitragotri, Delivering Nanoparticles to Lungs while Avoiding Liver and Spleen through Adsorption on Red Blood Cells, *Acs Nano*, 7 (2013) 11129-11137.
- [56] P. Zhang, J. Guan, Fabrication of Multilayered Microparticles by Integrating Layer-by-Layer Assembly and MicroContact Printing, *Small*, 7 (2011) 2998-3004.
- [57] Z. Wang, J. Xia, Y. Yan, A.-C. Tsai, Y. Li, T. Ma, J. Guan, Facile functionalization and assembly of live cells with microcontact-printed polymeric biomaterials, *Acta Biomater.*, 11 (2015) 80-87.
- [58] J.F. Xia, Z.B. Wang, D.T. Huang, Y.W. Yan, Y. Li, J.J. Guan, Asymmetric Biodegradable Microdevices for Cell-Borne Drug Delivery, *Acs Applied Materials & Interfaces*, 7 (2015) 6293-6299.
- [59] P.P. Zhang, J.F. Xia, Z.B. Wang, J.J. Guan, Gold nanoparticle-packed microdisks for multiplex Raman labelling of cells, *Nanoscale*, 6 (2014) 8762-8768.
- [60] A.J. Swiston, C. Cheng, S.H. Um, D.J. Irvine, R.E. Cohen, M.F. Rubner, Surface Functionalization of Living Cells with Multilayer Patches, *Nano Lett.*, 8 (2008) 4446-4453.
- [61] A.J. Swiston, J.B. Gilbert, D.J. Irvine, R.E. Cohen, M.F. Rubner, Freely Suspended Cellular "Backpacks" Lead to Cell Aggregate Self-Assembly, *Biomacromolecules*, 11 (2010) 1826-1832.
- [62] R. Polak, R.M. Lim, M.M. Beppu, R.N.M. Pitombo, R.E. Cohen, M.F. Rubner, Liposome-Loaded Cell Backpacks, *Advanced Healthcare Materials*, 4 (2015) 2832-2841.
- [63] R. Polak, T. Crouzier, R.M. Lim, K. Ribbeck, M.M. Beppu, R.N.M. Pitombo, R.E. Cohen, M.F. Rubner, Sugar-Mediated Disassembly of Mucin/Lectin Multilayers and Their Use as pH-Tolerant, On-Demand Sacrificial Layers, *Biomacromolecules*, 15 (2014) 3093-3098.
- [64] F.C. Vasconcellos, A.J. Swiston, M.M. Beppu, R.E. Cohen, M.F. Rubner, Bioactive Polyelectrolyte Multilayers: Hyaluronic Acid Mediated B Lymphocyte Adhesion, *Biomacromolecules*, 11 (2010) 2407-2414.
- [65] J.B. Gilbert, J.S. O'Brien, H.S. Suresh, R.E. Cohen, M.F. Rubner, Orientation-Specific Attachment of Polymeric Microtubes on Cell Surfaces, *Adv. Mater.*, 25 (2013) 5948-5952.

- [66] C. Gómez-Moutón, J.L. Abad, E. Mira, R.A. Lacalle, E. Gallardo, S. Jiménez-Baranda, I. Illa, A. Bernad, S. Mañes, C. Martínez-A., Segregation of leading-edge and uropod components into specific lipid rafts during T cell polarization, *Proceedings of the National Academy of Sciences*, 98 (2001) 9642-9647.
- [67] A.C. Anselmo, J.B. Gilbert, S. Kumar, V. Gupta, R.E. Cohen, M.F. Rubner, S. Mitragotri, Monocyte-mediated delivery of polymeric backpacks to inflamed tissues: a generalized strategy to deliver drugs to treat inflammation, *J. Controlled Release*, 199 (2015) 29-36.
- [68] L. Li, Y. Guan, H. Liu, N. Hao, T. Liu, X. Meng, C. Fu, Y. Li, Q. Qu, Y. Zhang, S. Ji, L. Chen, D. Chen, F. Tang, Silica Nanorattle-Doxorubicin-Anchored Mesenchymal Stem Cells for Tumor-Tropic Therapy, *Acs Nano*, 5 (2011) 7462-7470.
- [69] N.M. Green, Avidin, *Adv. Protein Chem.*, 29 (1975) 85-133.
- [70] N.M. Green, AVIDIN AND STREPTAVIDIN, *Methods Enzymol.*, 184 (1990) 51-67.
- [71] E.P. Diamandis, T.K. Christopoulos, THE BIOTIN (STREPT)AVIDIN SYSTEM - PRINCIPLES AND APPLICATIONS IN BIOTECHNOLOGY, *Clin. Chem.*, 37 (1991) 625-636.
- [72] G. Paganelli, P. Magnani, F. Zito, E. Villa, F. Sudati, C. Rossetti, F. Fazio, Three-Step Monoclonal Antibody Tumor Targeting in Carcinoembryonic Antigenpositive Patients, *Cancer Res.*, 51 (1991) 5960-5966.
- [73] H. Cheng, C.J. Kastrup, R. Ramanathan, D.J. Siegwart, M.L. Ma, S.R. Bogatyrev, Q.B. Xu, K.A. Whitehead, R. Langer, D.G. Anderson, Nanoparticulate Cellular Patches for Cell-Mediated Tumoritropic Delivery, *Acs Nano*, 4 (2010) 625-631.
- [74] Y. Krishnamachari, M.E. Pearce, A.K. Salem, Self-assembly of cell-microparticle hybrids, *Adv. Mater.*, 20 (2008) 989-+.
- [75] R. Mooney, Y.M. Weng, R. Tirughana-Sambandan, V. Valenzuela, S. Aramburo, E. Garcia, Z.Q. Li, M. Gutova, A.J. Annala, J.M. Berlin, K.S. Aboody, Neural stem cells improve intracranial nanoparticle retention and tumor-selective distribution, *Future Oncology*, 10 (2014) 401-415.
- [76] M.J. Mitchell, E. Wayne, K. Rana, C.B. Schaffer, M.R. King, TRAIL-coated leukocytes that kill cancer cells in the circulation, *Proc. Natl. Acad. Sci. U. S. A.*, 111 (2014) 930-935.

- [77] E.C. Wayne, S. Chandrasekaran, M.J. Mitchell, M.F. Chan, R.E. Lee, C.B. Schaffer, M.R. King, TRAIL-coated leukocytes that prevent the bloodborne metastasis of prostate cancer, *J. Controlled Release*, 223 (2016) 215-223.
- [78] S. Chandrasekaran, M.J. McGuire, M.R. King, Sweeping lymph node micrometastases off their feet: an engineered model to evaluate natural killer cell mediated therapeutic intervention of circulating tumor cells that disseminate to the lymph nodes, *Lab on a Chip*, 14 (2014) 118-127.
- [79] S. Chandrasekaran, M.F. Chan, J. Li, M.R. King, Super natural killer cells that target metastases in the tumor draining lymph nodes, *Biomaterials*, 77 (2016) 66-76.
- [80] X. Chen, U.C. Tam, J.L. Czapinski, G.S. Lee, D. Rabuka, A. Zettl, C.R. Bertozzi, Interfacing carbon nanotubes with living cells, *J. Am. Chem. Soc.*, 128 (2006) 6292-6293.
- [81] P. Wu, X. Chen, N. Hu, U.C. Tam, O. Blixt, A. Zettl, C.R. Bertozzi, Biocompatible Carbon Nanotubes Generated by Functionalization with Glycodendrimers, *Angew. Chem. Int. Ed.*, 47 (2008) 5022-5025.
- [82] X. Chen, P. Wu, M. Rousseas, D. Okawa, Z. Gartner, A. Zettl, C.R. Bertozzi, Boron Nitride Nanotubes Are Noncytotoxic and Can Be Functionalized for Interaction with Proteins and Cells, *J. Am. Chem. Soc.*, 131 (2009) 890-891.
- [83] J.A. Prescher, C.R. Bertozzi, Chemistry in living systems, *Nat. Chem. Biol.*, 1 (2005) 13-21.
- [84] M.A. Gauthier, H.-A. Klok, Peptide/protein-polymer conjugates: synthetic strategies and design concepts, *Chem. Commun.*, (2008) 2591-2611.
- [85] M.B. Ulmschneider, M.S.P. Sansom, Amino acid distributions in integral membrane protein structures, *Biochim. Biophys. Acta*, 1512 (2001) 1-14.
- [86] J.L. Panza, W. R. Wagner, H.L.R. Rilo, R. Harsha Rao, E.J. Beckman, A.J. Russell, Treatment of rat pancreatic islets with reactive PEG, *Biomaterials*, 21 (2000) 1155-1164.
- [87] D.Y. Lee, K. Yang, S. Lee, S.Y. Chae, K.-W. Kim, M.K. Lee, D.-J. Han, Y. Byun, Optimization of monomethoxy-polyethylene glycol grafting on the pancreatic islet capsules, *J. Biomed. Mater. Res.*, 62 (2002) 372-377.
- [88] M.D. Scott, K.L. Murad, F. Koumpouras, M. Talbot, J.W. Eaton, Chemical camouflage of antigenic determinants: Stealth erythrocytes, *Proc. Natl. Acad. Sci. U. S. A.*, 94 (1997) 7566-7571.

- [89] N.A.A. Rossi, I. Constantinescu, R.K. Kainthan, D.E. Brooks, M.D. Scott, J.N. Kizhakkedathu, Red blood cell membrane grafting of multi-functional hyperbranched polyglycerols, *Biomaterials*, 31 (2010) 4167-4178.
- [90] W.P. Clafshenkel, H. Murata, J. Andersen, Y. Creeger, R.R. Koepsel, A.J. Russell, The Effect of Covalently-Attached ATRP-Synthesized Polymers on Membrane Stability and Cytoprotection in Human Erythrocytes, *PLoS One*, 11 (2016).
- [91] B. Sahaf, K. Heydari, L.A. Herzenberg, L.A. Herzenberg, Lymphocyte surface thiol levels, *Proc. Natl. Acad. Sci. U. S. A.*, 100 (2003) 4001-4005.
- [92] M.T. Stephan, J.J. Moon, S.H. Um, A. Bershteyn, D.J. Irvine, Therapeutic cell engineering with surface-conjugated synthetic nanoparticles, *Nat. Med.*, 16 (2010) 1035-1041.
- [93] M.T. Stephan, S.B. Stephan, P. Bak, J.Z. Chen, D.J. Irvine, Synapse-directed delivery of immunomodulators using T-cell-conjugated nanoparticles, *Biomaterials*, 33 (2012) 5776-5787.
- [94] B. Huang, W.D. Abraham, Y. Zheng, S.C. Bustamante Lopez, S.S. Luo, D.J. Irvine, Active targeting of chemotherapy to disseminated tumors using nanoparticle-carrying T cells, *Sci. Transl. Med.*, 7 (2015) 291ra294.
- [95] D. Masopust, J.M. Schenkel, The integration of T cell migration, differentiation and function, *Nature Reviews Immunology*, 13 (2013) 309-320.
- [96] L. Wayteck, L. Dewitte, L. De Backer, K. Breckpot, J. Demeester, S.C. De Smedt, K. Raemdonck, Hitchhiking nanoparticles: Reversible coupling of lipid-based nanoparticles to cytotoxic T lymphocytes, *Biomaterials*, 77 (2016) 243-254.
- [97] C.A. Holden, Q. Yuan, W.A. Yeudall, D.A. Lebman, H. Yang, Surface engineering of macrophages with nanoparticles to generate a cell-nanoparticle hybrid vehicle for hypoxia-targeted drug delivery, *Int J Nanomed*, 5 (2010) 25-36.
- [98] L. Xu, O.Y. Zolotarskaya, W.A. Yeudall, H. Yang, Click hybridization of immune cells and polyamidoamine dendrimers, *Adv Healthc Mater*, 3 (2014) 1430-1438.
- [99] X.L. Wang, W.C. Chang, C.W. Wong, D. Colcher, M. Sherman, J.R. Ostberg, S.J. Forman, S.R. Riddell, M.C. Jensen, A transgene-encoded cell surface

- polypeptide for selection, in vivo tracking, and ablation of engineered cells, *Blood*, 118 (2011) 1255-1263.
- [100] S. Mura, J. Nicolas, P. Couvreur, Stimuli-responsive nanocarriers for drug delivery, *Nature Materials*, 12 (2013) 991-1003.
- [101] S. Ganta, H. Devalapally, A. Shahiwala, M. Amiji, A review of stimuli-responsive nanocarriers for drug and gene delivery, *J. Controlled Release*, 126 (2008) 187-204

2. T cell-mediated delivery of polymer nanoparticles across the blood brain barrier

2.1. Introduction

Efficient delivery of drugs across the blood-brain barrier (BBB) is key to the diagnosis and treatment of diseases of the central nervous system (CNS). The BBB is composed of endothelial cells and is characterized by unique junctional complexes that prohibit free passage of polar compounds via the paracellular route [1, 2]. In addition, transcellular passage of these molecules is hindered by the low pinocytotic activity of the BBB. Due to its restrictive nature, movement across the BBB is essentially limited to lipophilic compounds with molecular weight less than 400 Da [3]. But even these small lipophilic molecules are difficult to accumulate in the CNS because they are efficiently removed by efflux pumps [2]. These are major limitations, as a large number of drug candidates to treat brain related diseases do not fulfil these requirements, especially peptide and protein therapeutics which yet hold great promises as treatment for neurodegenerative diseases [4] or also cannot be transported across the BBB by specific transporters.

Nanoparticles have been extensively investigated to enhance drug delivery across the BBB. Nanoparticle carriers can facilitate access to the CNS in a number of ways: (i) by opening tight junction or inducing local toxic effects that leads to local permeabilization of the BBB; (ii) by transcytosis of the nanoparticles across the BBB, (iii) by endocytosis, followed by intracellular release and exocytosis of their payload and (iv) by a combination of these pathways [5]. The ability of nanoparticles to enhance delivery to the CNS can be quantified by determining the percentage of the injected nanoparticle dose (% ID) that reaches the brain tissue [6]. For nanoparticles the % ID that accumulates in the brain typically ranges from 0.01-0.5% [6]. While these numbers are small, in some cases uptake of only a very small fraction of the injected dose is sufficient to induce a therapeutic effect. An example is morphine with a % ID of 0.02 %, which is however sufficient to produce analgesia [6]. Obviously, the % ID required to produce a therapeutic effect depends on the indication and the drug that is used. There is a variety of, in

particular acute conditions that requires high therapeutic doses, which calls for alternative approaches to further enhance transport of therapeutic nanoparticle to the CNS.

Cell based carriers offer unique opportunities to improve targeted delivery of therapeutic nanoparticles, to enhance their blood circulation times and to facilitate transport of therapeutic nanoparticles across challenging physiological barriers [7-9]. While cell-mediated delivery of nanoparticles has been explored in a number of cases to combat cancer, only relatively little effort has been made to use this concept to enhance drug delivery to the CNS. Until recently cell-mediated delivery to the brain [10] essentially relied on nanomaterials loaded inside a cell-carrier used as a Trojan horse. In a series of studies, bone marrow derived macrophages were used as a delivery vehicle for catalase nanoparticles in the context of Parkinson's disease, taking advantage of their migratory properties to actively target sites of inflammation [11-13]. The delivery of catalase nanoparticles to the CNS may not exclusively work through a Trojan horse effect but it has been postulated that other pathways such as the release of catalase into the blood stream or directly to brain endothelial cells may also take place [14, 15]. Therapeutic nanomaterials internalization may not be applicable to all kind of therapeutic agents, especially in the case of cytotoxic agents used in chemotherapy [16] and additionally internalization of nanocarriers is also almost exclusively limited to the phagocytic cell repertoire. An interesting example, published recently, resorted to surface conjugation of nanoparticles on neural stem cell for brain tumor delivery. Large (>800 nm) polymer nanoparticles coupled to the surface of neural stem cells showed improved targeting and retention in a brain tumor model [17]. The nanoparticle functionalized neural stem cells were delivered via intracranial or intravenous injection, which in the latter case represents an important achievement towards cell-mediated delivery of nanomaterials across the blood-tumor barrier [17].

Another potentially very attractive class of cell to enhance drug delivery to the CNS are encephalitogenic $CD4^{+} T_{EM}$ cells. These cells are optimized to reach the brain via the blood stream and although these activated T cells can trigger experimental autoimmune encephalomyelitis (EAE) if transferred to naïve syngeneic recipients, they do not cause disease in allogenic or heterologous transfer and as such can be used safely for diagnostic or therapeutic purposes. $CD4^{+} T_{EM}$ cells are able to diapedese across the BBB in the absence or presence of neuroinflammation as schematically illustrated in Figure 1 via a multistep process that is mediated by a series of adhesion and signaling molecules on the immune cells as well as on the endothelial cells. The sequence of event involves T-cell

rolling and arresting on BBB endothelium, followed by T cells crawling which is mediated by the adhesion molecules ICAM-1 and ICAM-2 eventually leading to T-cell migration across the BBB at a junctional or non-junctional site permissive for diapedesis [18, 19]. $CD4^+$ T_{EM} cells are potentially highly attractive carrier to mediate transport of nanoparticles across the BBB for a number of reasons: (i) the initial organ targeting: with nanoparticle enrichment due to the migration of brain seeking T cells across brain microvessels (ii) active transport of nanoparticles across the BBB during T-cell diapedesis. Additionally and since the passage of T cells from the systemic circulation to the perivascular space is a function of the activated state of the T cell rather than its antigen-specificity [20], the delivery of nanoparticles across the BBB using an allogenic or heterologous transfer of encephalitogenic T-cell carriers is potentially applicable to a wide range of neuroinflammatory conditions irrespective of their antigen such as multiple sclerosis, brain tumors and brain metastasis, as well as neurodegenerative diseases.

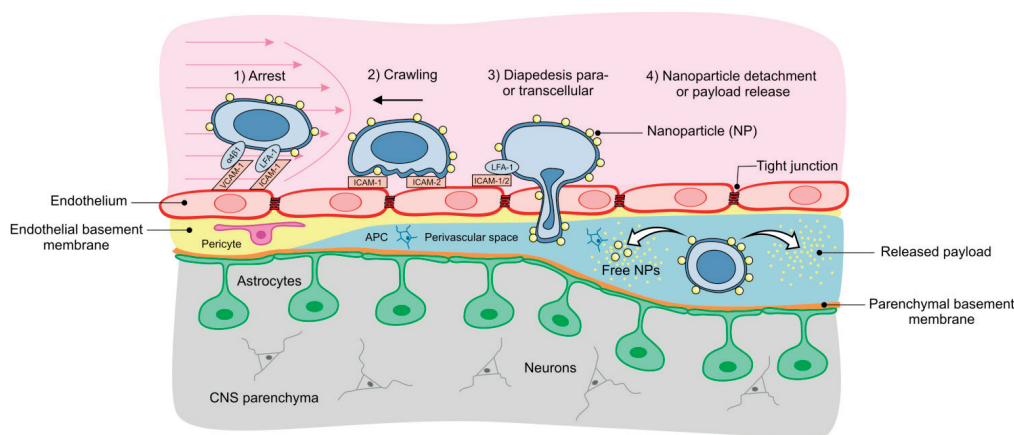


Figure 1. Schematic view of $CD4^+$ T cell-mediated transfer of drug-loaded nanocarriers across the BBB. The cartoon illustrates the putative transfer of nanoparticles conjugated to the T-cell surface across the BBB endothelium, followed by drug release and/or nanoparticle detachment upon arrival in the CNS (APC = antigen presenting cell, NPs = nanoparticles).

In this report, we explored the feasibility of using $CD4^+$ T_{EM} to facilitate transport of 200 nm diameter polystyrene model nanoparticles across the BBB. The PEG chains that constitute the corona of the nanoparticles contain a maleimide group at the polymer chain end, which was used to covalently couple the nanoparticles to thiol group present on the cell surface. The conjugation was first evaluated over a period of 24 hours in complete growth medium to assess the stability and toxicity of the modification. The localization

and distribution of the nanoparticles on the T-cell surface was measured through confocal microscopy experiments. T-cell surface coupling of the nanoparticles was not found to lead to necrosis and apoptosis and also did not alter T-cell ability to bind to ICAM-1. Nanoparticle decorated T cells were then investigated for their ability to cross a mouse BBB model *in vitro* under static condition in a two-chamber assay. Finally, nanoparticle functionalized T cells crossing this BBB model *in vitro* under physiological flow conditions were monitored by time-lapse live cell imaging. This latest part represents a major step towards understanding the mechanism and the limitations of nanoparticle surface conjugation for their cell-mediated delivery across the BBB and builds the fundamentals of effective nanoparticle delivery to the brain using brain-seeking T cell subsets as the initial carrier.

2.2. Experimental Section

2.2.1. Materials

Amine-modified yellow-green FluoSpheres (d= 200 nm), CellTrace Violet, WGA-Texas Red conjugate, Annexin V-Alexa Fluor 647 conjugate, Annexin buffer and Prolong Gold mounting media, Dubelcco's Phosphate-buffered saline (DPBS), RPMI 1640 and FBS were purchased from Thermofischer scientific. Methoxy-PEG₅₀₀₀-succinimidyl valerate and maleimide-PEG₅₀₀₀-succinimidyl valerate were obtained from Laysan Bio Inc.. Poly(L-lysine) 0.1 % w/v solution, 4',6-Diamidine-2'-phenylindole dihydrochloride (DAPI) and 1 mM Staurosporine solution in DMSO were purchased from Sigma-Aldrich.

2.2.2. Methods

Particle size and zeta potential were measured by dynamic light scattering (DLS) using a Zetasizer Nano Zs instrument (Malvern). ¹H-NMR spectra were recorded on Bruker Avance III 400 MHz spectrometer. Flow cytometry analysis was performed on a Beckmann Coulter Gallios instrument. Confocal microscopy images were recorded on a Zeiss LSM700 Inverted microscope (Carl Zeiss, Feldbach, Switzerland). Cell-counting for binding assay was performed using an Olympus CKX41 inverted microscope equipped with a 10 mm x 10 mm / 10 divisions counting reticle and a 20x objective.

2.2.3. Procedures

2.2.3.1. Cell lines and cell cultures

Encephalitogenic CD4⁺ effector/memory proteolipid protein (PLP) peptide aa139-153 specific T cells (line SJL/PLP7) were cultured as previously described [21]. In brief, SJL/PLP7 T cells were cultured in RPMI 1640 glutamax medium (Gibco) supplemented with 10% fetal bovine serum (FBS) (Gibco), 1% penicillin/streptomycin (Gibco), 1% non-essential amino acid (Gibco), 1% Na-pyruvate (Gibco), 0.4% β -mercaptoethanol (Gibco) and 1% IL-2 supernatant (self-made). Cells were typically used for modification and in functional assays at day 3 or 4 after restimulation.

Isolation and culture of *primary mouse brain microvascular endothelial cells (pMBMECs)* was performed as described before [22-24]. In brief: cortices from 6-8 weeks old C57BL/6 mice were isolated by removing cerebellum, striatum, optic nerves and brain white matter. Outer vessels and meninges were then removed using dry cotton swabs. Preparations were pooled and homogenized in wash buffer (HBSS containing 10 mM HEPES and 0.1% BSA). The resulting homogenate was mixed with 30% dextran (v/v, molecular weight 100 000 – 200 000 Da) in wash buffer. This suspension was centrifuged at 3000 g for 25 min at 10°C. The neural component and the dextran layer were discarded, the pellet containing the vascular component was filtered through a nylon mesh with 60 μ m pore size. The capillary-enriched filtrate was digested in collagenase/dispase (2 mg/mL) in wash buffer supplemented with 10 μ g/mL DNase I and 0.147 μ g/mL TLCK (Tosyl-L-lysyl-chloromethane hydrochloride) for 30 min at 37°C. Digestion was stopped by adding an excess of wash buffer and the suspension was filtered through a nylon mesh of 20 μ m pore size. The resulting digested capillary suspension was seeded onto a tissue culture-treated dish or insert. Culture medium was DMEM supplemented with 20% FBS, 2% sodium pyruvate, 2% non-essential amino acids, 50 μ g/mL gentamycin, 1 ng/mL basic fibroblast growth factor and for the first 48 h with 4 μ g/ml puromycin. 24 h after plating, red blood cells, cell debris and non-adherent cells were removed by washing with medium. Afterwards, the medium was changed every second day and pMBMECs were used on day 7 or 8 after isolation.

2.2.3.2. Preparation of PEGylated nanoparticles

In a typical procedure, 50 μ L of 2% w/v solid 200 nm amine-modified yellow-green polystyrene microspheres (approx. 0.85 μ mol of -NH₂ groups) were washed twice with

200 μ L MilliQ water, resuspended in 50 μ L MilliQ water and sonicated for 10-15 min. Then 5 eq (approx. 20 mg, 4.25 μ mol) of maleimide-PEG₅₀₀₀-succinimidyl valerate (or methoxy-PEG₅₀₀₀-succinimidyl valerate for control unfunctionalized particles) were dissolved in 50 μ L MilliQ water and added to the particle solution. The reaction mixture (solid concentration, 1% w/v) was left on an orbital shaker (600 rpm) at room temperature for 60 minutes. Excess PEG was removed by 3 centrifugal washing cycles (30'000 x g) and particles were resuspended to the desired working concentration in MilliQ water and stored at 4° C until used. Particle size and zeta potential were measured in MilliQ water and in 1 mM sodium chloride solution (conductivity approx. 0.12 mS/cm and pH measured of 6.5) respectively. Diameter of the methoxy-PEGylated and maleimide-functionalized PEGylated particles were 242 ± 3 (PDI: 0.036 ± 0.009) nm and 255 ± 4 nm (PDI: 0.106 ± 0.020), respectively. PEGylation resulted in a change of the zeta potential from $+17.7 \pm 1.3$ mV for the amine-modified nanoparticles to near neutral values for the PEGylated nanoparticles. The grafting density of PEG was estimated by ¹H-NMR analysis of the freeze-dried particles dissolved in CDCl₃ knowing the specific surface area of the FluoSpheres and was approx 0.2 chains/nm². ¹H-NMR spectra of the methoxy-PEGylated and the maleimide PEGylated nanoparticles as well as particle size distributions and zeta potentials are provided in Supporting Information Figures S1-S3.

2.2.3.3. T-cell surface modification with maleimide functionalized PEGylated nanoparticles

T-Cells were washed twice with DPBS (centrifuged at 250 x g for 7 min) and resuspended to a concentration of 30 mio cells/mL in DPBS. Then 100 μ L of cell suspension (i.e. 3 mio cells) were added to each well (Nunc, 96 well round bottom plate, low cell binding, Sigma-Aldrich) containing 100 μ L MilliQ water only, control particles (unfunctionalized methoxy-PEGylated particles) or maleimide-functionalized particles dispersed in MilliQ water at a concentration of 5000 particles/cell. The conjugation was performed at 37° C for 30 minutes with gentle pipette mixing every 10 minutes. Unreacted maleimide groups were quenched by addition of 20 μ L of a 1 mM solution of *N*-acetylcysteine and the cell suspension was left for another 10 minutes at 37° C. Subsequently, cells were washed trice with approx. 10 mL of DPBS (centrifuged at 250 RCF for 7 min) to remove unbound and loosely bound particles.

2.2.3.4. Proliferation assay

T-cell proliferation was monitored with CellTrace Violet according to the manufacturer's protocol. In short, cells were washed once and resuspended into DPBS at a concentration of 1 mio cells/mL. 1 μ L of CellTrace Violet stock solution in DMSO (5 mM) was added per milliliter of cell suspension and left for 20 minutes at 37° C in the dark. Excess dye was removed by addition of approx. 5 times the staining volume of complete growth medium. Cells were then pelleted, washed once with DPBS and resuspended in complete growth medium until use for cell-surface modification experiments. Fluorescence intensities were measured by flow cytometry, directly after surface modification and 24 hours after modification.

2.2.3.5. Confocal microscopy and image analysis

Nanoparticle modified and CellTrace Violet stained T cells were additionally stained with a membrane marker, WGA-Texas Red X for 30 minutes on ice in DPBS at a concentration of 1 mio cells/mL. Cells were then seeded on a Poly-(L-Lysine) coated 12 mm diameter, 0.17 mm thickness borosilicate glass precision microscopy coverslip (Carl Roth GmbH), washed twice with DPBS and fixed for 10 minutes with a 4% paraformaldehyde solution in DPBS at room temperature. Fixed cells were finally mounted on a microscopy glass slide with Prolong Gold. The slides were left to dry overnight before images were acquired on a Zeiss LSM700 microscope with a 63x/1.4NA lens. Voxel sizes were optimized for deconvolution (XYZ 30 nm x 30 nm x 130 nm). (Digital gain, pinhole size) was set as follows for each channel (1.0, 49 μ m) for the whole cell channel (CellTrace Violet); (1.25, 48 μ m) for the membrane channel (WGA-Texas Red-X) and (1.3, 47 μ m) for the nanoparticle channel (BODIPY). Gain was optimized for each z-stack.

2.2.3.6. Cell viability

Viability assays were performed using Annexin V – Alexa Fluor 647 and DAPI as a dead cell stain. Briefly, unmodified or surface-modified T cells were washed once with DPBS and 0.3 mio cells were resuspended in Annexin buffer containing 1 μ g/mL DAPI at a concentration of 1 mio cells/mL. 15 μ L Annexin V - Alexa Fluor 647 conjugate were added to the cell suspension and cells were incubated at room temperature for 15 minutes in the dark. Subsequently, 400 μ L Annexin buffer was added and cells were analyzed by flow cytometry directly after modification. The assay was repeated 12 hours and 24 hours after modification. As a positive control for apoptosis, T cells were incubated in complete

growth medium supplemented with 1 μ M staurosporine for at least 6 hours. Staurosporine treated cells were used to gate cell population as follow: viable cells, apoptotic cells and apoptotic/necrotic cells gated as quadrant Q4, Q3 and Q2 respectively in Figure S4.

2.2.3.7. Binding assay

ICAM-1 coated slides were prepared as previously reported [25]. In brief, standard 12 well diagnostic slides (ER-202W-CE24, ThermoFisher Scientific) were coated with a protein A (BioVision, Lausen, Switzerland) solution at a concentration of 20 mg/mL in PBS (pH 9) for 1 h at 37°C. The protein A incubation was followed by three PBS washes and subsequently a blocking step using with 1.5% bovine serum albumin (BSA) in PBS overnight at 4°C. Wells were then washed once with PBS pH 7.4 and protein A was exposed to recombinant purified cell-adhesion molecule (100 mM) mouse ICAM-1-Fc chimera (R&D Systems, Abingdon, U.K.) for 2 hours at 37°C and finally the wells blocked with 1.5% BSA in PBS for 30 min at room temperature and washed once with PBS before used in a binding assay. As a control DNER-Fc (R&D Systems, Abingdon, U.K.) chimera was used instead of mouse ICAM-1-Fc chimera.

For the binding assay, T cells were collected at 10 mio cells/mL in migration assay medium (MAM: DMEM, 25 mM HEPES, 5% FBS, 2% L-glutamine) and 1×10^5 cells were added to each well and the slide was incubated for 30 minutes at room temperature on a rotating platform. The slides were finally washed twice by dipping them into PBS and fixed for 2 h in 2.5% v/v glutaraldehyde in PBS. The number of adherent cells was evaluated by counting the number of bound cells per field of view using a 20x objective mounted on an Olympus CKX41 inverted microscope equipped with a 10 mm x 10 mm / 10 divisions counting reticle. Each dot in Figure 6 represents a single cell count from the diagonal of the reticle. 3 counts per well (i.e. per replicate) were recorded in a total of two independent experiments performed in triplicate).

2.2.3.8. Transendothelial migration assay under static conditions

Transmigration assays were performed as described before [26] using a two chamber Transwell system. In brief, pMBMECs were seeded on 6.5 mm filter inserts with a 5 μ m pore size (Costar, Bodenheim, Germany) previously coated with laminin and matrigel. In order to prevent the pMBMECs from sprouting through the pores of the filter, they were grown to confluency without medium in the lower compartment. Prior to the experiment, pMBMECs were stimulated with recombinant murine tumor necrosis factor alpha, TNF- α (10 ng/mL) for 16 h. At the beginning of the transmigration assay, pMBMEC inserts were

washed twice with migration assay medium (MAM: DMEM (Gibco), 2 % L-Glutamine, 25 mM HEPES (Gibco), 5 % FBS (Gibco)) before being transferred into a new 24-well Costar plate well containing 600 μ L MAM. Then 100 μ L MAM containing 100'000 T cells were added per insert and T cells were allowed to transmigrate for 6 h at 37°C. Additionally, aliquots of 100'000 T cells were kept in 600 μ L MAM and used as representative for the input. The number of transmigrated T cells and the number of the cells in input samples were assessed by flow cytometry (FACS calibur) using BD Trucount tubes (BD biosciences). The percentage of migrated T cells was calculated referring to the inputs as 100 %. Finally, the inserts were washed twice in PBS and fixed in 1%PFA. Fixed inserts were stained with phalloidin-rhodamin and DAPI and mounted on glass slides in order to confirm the confluency of the endothelial monolayer of each filter after the assay.

2.2.3.9. T-cell extravasation under physiological flow

In vitro live cell imaging of T cell extravasation across pMBMECs cultured on matrigel coated cell culture surfaces (μ -dish35 mm-low, ibidi Vitaris, Baar, Switzerland) was performed as described before [27]. The pMBMECs were stimulated with recombinant murine tumor necrosis factor alpha (TNF- α , 10 ng/mL) for 16-24 h prior to the experiment. A small custom-made flow chamber was used here [27]. The inlet tubing of the flow chamber was filled with MAM and the flow chamber placed on the endothelial cells. Flow was then applied by connecting the outlet tubing to a syringe automatically drawn up by a precision pump (Harvard Apparatus, Holliston, MA, USA). For microscopic imaging, the assembled flow chamber was placed on the stage of an inverted microscope (AxioObserver.Z1, Carl Zeiss, Feldbach, Switzerland) equipped with a temperature-controlled chamber (37°C). Image acquisition was performed through computer control using the ZEN software (Carl Zeiss) at a rate of 10 images per min and with a 20-fold (Objective LD "Plan-Neofluar" 20 \times /0,4 Korr Ph2 M27) magnification using a monochrome CCD camera (AxioCam MRmRev, Carl Zeiss).

Aspiration of T cells from a reservoir via the inlet tubing was performed at 1.5 dyne/cm² until the T cells appear in the field of view. To allow settling of the T cells on the endothelial surface, the flow rate was reduced to 0.2 dyne/cm² and accumulation was terminated after 5 min by increasing the flow to 1.5 dyne/cm² (closely mimicking physiological flow conditions within CNS post-capillary venules). Image recording in time-lapse mode was started at the beginning of the accumulation phase and continued for up to 30 min. The dynamic interaction of T cells with the endothelium was evaluated by

assigning a migratory phenotype to each T cell using ImageJ software (National Institute of Health, Bethesda, MD, USA). To this end, each arrested T cell is assigned a digit 30 sec after the end of the accumulation phase. The behavior of each individual T cell was analyzed throughout the complete movie and then accordingly assigned to one category. T cells that continuously crawl are categorized as “Crawling”. T cells that are probing without crawling or diapedesis are categorized as “Probing”. T cells that diapedesis after having crawled to or having probed at a site of diapedesis are categorized as “Diapedesis”. T cells that have partially diapedesis through the endothelial monolayer are categorized as “Incomplete diapedesis”. Arrested T cells that enter or leave the field of view during the recording time are excluded from the evaluation.

2.3. Results and Discussion

2.3.1. Particle synthesis

To explore the feasibility of CD4⁺ T_{EM} cells to facilitate transport of therapeutic cargo across the BBB, this study has used model nanoparticles, which were obtained by surface modification of 200 nm diameter, fluorescently labeled (BODIPY) amine functionalized polystyrene beads. These polystyrene beads were modified with a heterobifunctional PEG derivative to introduce maleimide groups on the surface of the nanoparticles, which are subsequently used to conjugate the nanoparticles to thiol groups that are present on the T-cell surface (Figure 2). Modification of the amine functionalized nanoparticles with the maleimide or methoxy PEG derivatives was accompanied by a change in zeta potential from $+17.7 \pm 1.3$ mV for the amine functionalized particles to near neutral values for the PEGylated particles (see Supporting Information Figure S3). From ¹H-NMR, the PEG grafting density was estimated to be ~ 0.2 chains/nm² which corresponds to an average distance between two grafting sites $D \approx 20$ Å. This distance is significantly smaller than the Flory radius R_F of the PEG spacer ($R_F \approx 60$ Å), indicating that the PEG chains adopt a stretched brush-like conformation [28]. As they present a large number of maleimide groups on their surface, coupling of these nanoparticles to thiol groups on the cell surface is most likely to result in multipoint attachment. Control nanoparticles that present a methoxy-PEG brush layer were produced in the same way as their maleimide functionalized counterparts.

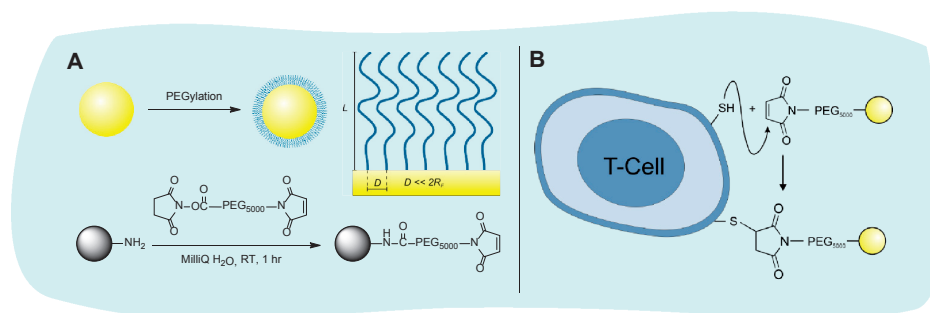


Figure 2. (A) Synthesis of maleimide functionalized PEGylated polystyrene nanoparticles. (B) Coupling of maleimide functionalized PEGylated nanoparticles to thiol groups present on T cell surface. For simplification, only one PEG chain is shown per nanoparticle.

2.3.2. T-cell surface modification and characterization

Cell surface conjugation of the maleimide functionalized polystyrene nanoparticles was performed as shown in Figure 2B and followed a strategy reported earlier by Irvine and coworkers for the coupling of liposomal nanoparticles to the surface of B cells, T cells and hematopoietic stem cells [29]. The conjugation reactions were performed by addition of a suspension of 5000 nanoparticles/cell in MilliQ water to a suspension of 30 mio cells/mL in DPBS. After 30 minutes the reaction was stopped and unreacted maleimide groups were quenched with *N*-acetylcysteine. Unbound and physically adsorbed nanoparticles were removed by three washing cycles. As a control experiment, cells were exposed to methoxy-functionalized PEGylated polystyrene nanoparticles. Surface modification of the T cells with the polystyrene nanoparticles was followed using flow cytometry (Figure S5). While these experiments indicated that non-specific binding of the control particles also takes place, the use of the maleimide functionalized particles resulted in a > 100 -fold increase in fluorescence intensity illustrating the successful covalent coupling of the maleimide functionalized polystyrene nanoparticles to the cell surface thiol groups.

The localization and distribution of the nanoparticles on the cell surface directly after cell surface attachment as well as after 24h was studied by flow cytometry and confocal microscopy. For the flow cytometry experiments, prior to cell surface conjugation, the cells were stained with a proliferation marker (CellTrace Violet), which allowed to simultaneously monitor T cell proliferation and nanoparticle cell surface attachment over a period of 24h. The flow cytometry results which are presented in Figure 3A show that

after 24 hours the cells have gone through one cycle of cell division. Monitoring the nanoparticle-associated fluorescence (BODIPY) by flow cytometry revealed that nanoparticles remained attached during cell division, however it is accompanied by approximately a 4-fold decrease in the BODIPY (nanoparticle-associated) fluorescence indicating a partial loss of surface attached nanoparticles. In addition a significant broadening of the nanoparticle associated fluorescence distribution is observed upon cell division. This indicates an uneven distribution of the nanoparticles on the daughter cells, which could be the consequence of a heterogeneous distribution of the nanoparticles on the initial cell surface (vide infra).

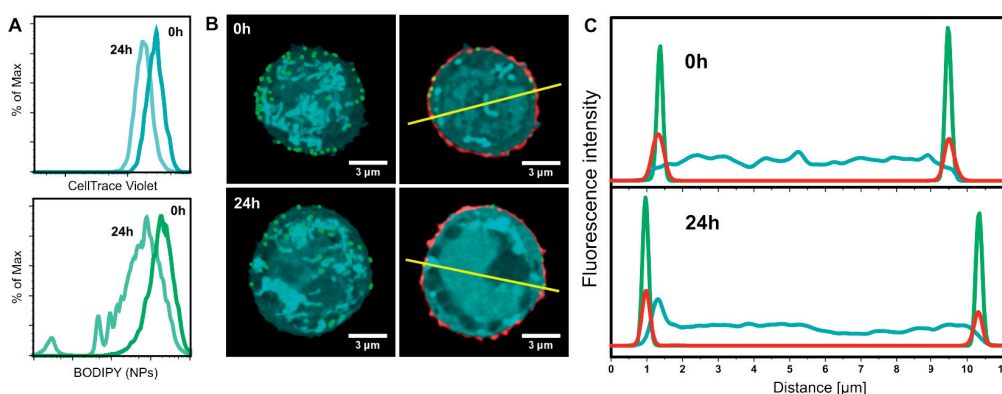


Figure 3. (A) Flow cytometry measurement directly after modification and 24 hours later. Top view shows a histogram of scatter gated live T cells stained with CellTrace violet to observe cell division over 24h. Bottom view shows a histogram of scatter gated live cells for nanoparticle retention assessed using BODIPY labelled fluorescent nanoparticles. (B) left: 3D-reconstruction of confocal micrographs of nanoparticle (green) decorated T Cells (cyan). The cell was stained with CellTrace violet. Right: cross sectional confocal images of a T cell with an additional membrane WGA-Texas Red-X (red) staining. (C) Fluorescence intensity profiles (yellow line in B) directly after modification and 24 hours later showing the overlapping of nanoparticle associated fluorescence (green) and the membrane stain (red) on the edge of the whole cell stain (cyan).

To determine the number and distribution of nanoparticles on the cell surface, cells were stained with CellTrace Violet and WGA-Texas Red-X to visualize the whole cell, respectively, cell membrane and investigated by confocal microscopy. Figure 3B shows three-dimensional reconstructions of nanoparticle modified T cells as well as two-dimensional images of a cross sectional plane of these cells directly after modification and 24h later. Figure 3C presents fluorescence intensity profiles that are obtained from analyzing the two-dimensional cross sectional images in Figure 3B along the yellow

lines. The images in Figure 3B and the intensity profiles in Figure 3C clearly indicate that the nanoparticles colocalize with the cell membrane and that the position of the nanoparticles does not significantly change over a period of 24h. To determine the average number of nanoparticles per cell and to (semi-)quantitatively determine their position, three-dimensional reconstructions of 9 cells were analyzed, both directly after cell surface modification as well as after 24h. On average, 105 ± 39 nanoparticles were attached per cell directly after modification. After 24h, 34 ± 18 nanoparticles remained attached to the cell. The localization of the nanoparticles (green) was assessed both by measuring the distance between their position and the whole cell (CellTrace Violet, cyan) as well as by calculating the percentage of nanoparticles that colocalized with the membrane stain (WGA Texas Red-X, red). Figure 4 presents for a total number of 9 cells analyzed both at $t=0$ and 24h for each nanoparticle the distance between its position and the cell edge, which is defined as $0 \mu\text{m}$. Each dot represents a single nanoparticle and a red dot represents a nanoparticle that is colocalized with the membrane staining. On average, directly after modification, the nanoparticles are localized at a distance of approximately $-66 \pm 305 \text{ nm}$ from the edge. A very similar number is measured after 24 hours, i.e. $-65 \pm 256 \text{ nm}$. Approximately 90% of the nanoparticles were found to colocalize with the WGA Texas Red-X membrane stain, both directly after cell surface modification and after 24h. The confocal microscopy experiments indicate that the nanoparticles are located at the cell surface and remain there at least for a period of 24h. During the time course of these experiments there was no indication for nanoparticle internalization by the T cells.

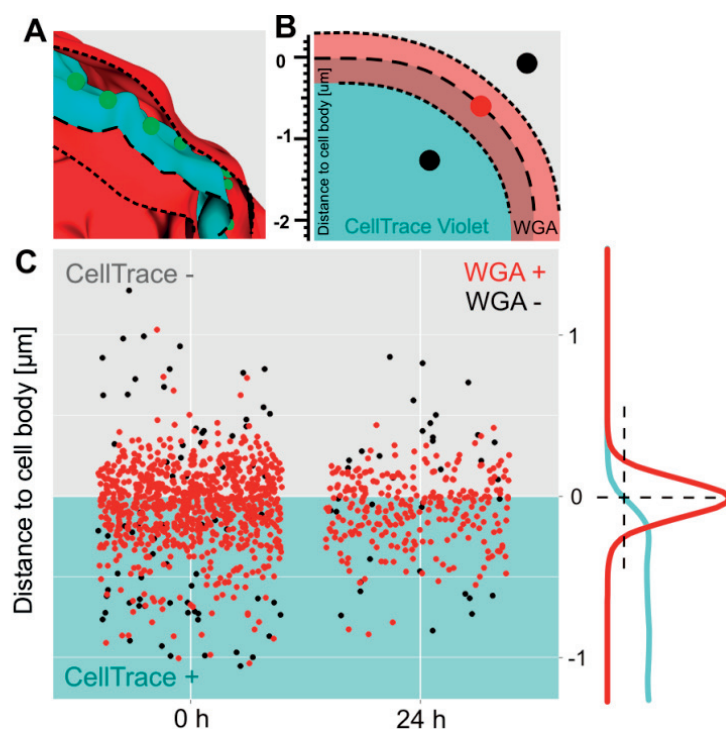


Figure 4. (A) Surface generated from image processing (Imaris software: Bitplane, Oxford Instrument) showing the edge of CellTrace Violet (cyan) whole cell staining (— — — —), inner and outer boundaries of the WGA-Texas Red-X (red) membrane staining (— — — —) and 200 nm nanoparticles (green) (B) Schematic explanation for the nanoparticle distribution observed in (C) around the cell edge. (C) Statistical distribution of nanoparticles with respect to their distance to the whole cell edge (CellTrace Violet). Each dot represents a single nanoparticle. Red dots represent nanoparticles which are found between the inner and outer boundaries outlined by the membrane staining (WGA-Texas Red X) and black dots those which are not. Right: typical fluorescence intensity profiles for the CellTrace Violet and WGA-Texas Red-X channels around the cell edge.

To investigate the possible effect of cell surface modification on the viability of the T cells, nanoparticle decorated T cells as well as unmodified T cells were studied using an Annexin V – DAPI apoptosis/necrosis assay. T-cell viability was assessed directly after surface modification as well as at 12h and 24h. The flow cytometry results of these experiments are provided in Figure S4 and Figure 5 presents the T-cell viability results from the flow cytometry data. As a positive control for apoptosis, T cells were treated with staurosporine. The results in Figure 5 show that while there is an initial decrease in viability (%) directly after cell surface modification, the T cells seem to recover as time

progressed. The percentage of viable cells increased from ~ 67% directly after T-cell surface modification to > 80 % after 12h and longer.

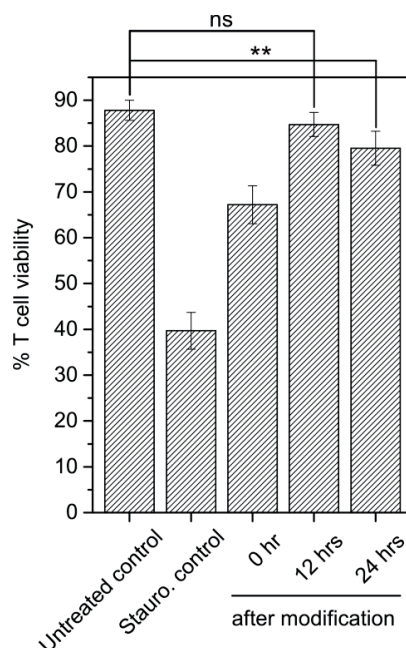


Figure 5. T-cell viability assay: untreated control T cells and staurosporine treated control T cells (24 hours). Then nanoparticles functionalized T cells directly after modification, 12h and 24h after modification. The results are shown for two independent experiments performed in triplicate. Error bars on the histograms represent standard deviation. P-values were determined by *t* test (ns: $P > 0.05$ ** $P < 0.01$ is).

2.3.3. Functional assays

The functional properties of the nanoparticle decorated $CD4^+$ T_{EM} cells were investigated in three different experiments. In a first experiment, the ability of the surface modified T cells to bind to immobilized recombinant intercellular adhesion molecule-1 (ICAM-1) was assessed. This experiment was performed since ICAM-1 has been identified as a critical adhesion molecule mediating T-cell crawling in the multi-step extravasation of $CD4^+$ T_{EM} cells across the BBB [19, 30]. For this experiment, ICAM-1 was coated on a 12-well standard PTFE diagnosis slide at a concentration of 100 nM and unmodified control T cells or nanoparticle carrying T cells (100'000 cells/well) were incubated under moderate shear condition. Figure 6 plots the number of cells counted per field of view upon analysis of the slide with a counting reticle. The results in Figure 6

demonstrate that the presence of 100 polystyrene nanoparticles on the T cell surface does not compromise the ability of $CD4^+$ T_{EM} cells to bind recombinant ICAM-1. The total surface area covered by 100 nanoparticles with a diameter of 200 nm can be estimated to be less than 1%. The absence of adherent cells on the delta/notch-like epidermal growth factor (DNER) coated wells indicates that binding of the T cells to ICAM-1 is a selective (LFA-1) mediated process.

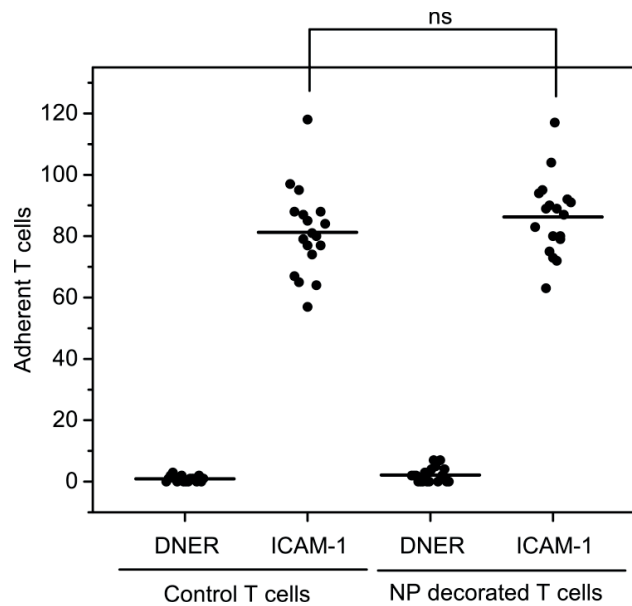


Figure 6. T-cell binding to ICAM-1. Cell count of a binding assay on ICAM-1 coated wells and DNER coated wells for unmodified control cells and nanoparticle (NP) decorated T cells performed at room temperature for 30 minutes under moderate shear conditions. Each dot represents one cell count from the diagonal of a 10 mm x 10 mm / 10 divisions counting reticle using a 20x objective. The figure represents the results of two independent assays performed in triplicate. Each well (i.e. replicate) was counted at 3 different positions. The horizontal bar represents the mean over all counts. P-value was determined by *t* test (ns: $P > 0.05$).

In a second experiment, the question whether nanoparticle decorated $CD4^+$ T_{EM} cells retain their ability to cross the BBB was assessed *in vitro*. To this end, a transendothelial migration assay across a primary mouse brain microvascular endothelial cell (pMBMEC) monolayer was performed under static conditions (Figure 7A). This model retains BBB characteristics *in vitro* such as complex tight junctions and low permeability [24]. The assay was performed on both TNF- α stimulated as well as unstimulated pMBMEC monolayers for a period of 6 hours. TNF- α stimulation of endothelial cells increases the

expression of adhesion molecules such as ICAM-1 on the surface of the barrier mimicking an inflamed BBB, which is typically found in many neuroinflammatory related disorders. Flow cytometry analysis revealed that 24 ± 7 % of nanoparticle modified T cells migrated across the TNF- α stimulated- and 18 ± 5 % across the unstimulated pMBMEC monolayer (Figure 7B). These percentages were comparable to those of unmodified control T cells migrating across TNF- α stimulated and unstimulated pMBMEC monolayers under the same static conditions, which were 23 ± 10 % and 23 ± 6 % respectively. The nanoparticle payload was partially transported across the pMBMEC monolayer as can be seen from Figure 7C. Flow cytometry analysis revealed that 79 ± 2 % of the nanoparticle modified CD4⁺ T_{EM} cells were able to transport part of their initial cargo across the pMBMEC monolayer (Figure 7C). Comparison of the flow cytometry results of the input T cells and the transmigrated T cells, however, shows a 9-fold and 13-fold decrease in nanoparticle associated fluorescence for the nanoparticle decorated CD4⁺ T_{EM} cells that migrated across non-stimulated and TNF- α stimulated pMBMEC monolayers respectively. This decrease in fluorescence intensity indicates a partial loss of the nanoparticle payload and may be attributed to shear forces associated with the squeezing of the T cells through paracellular or transcellular pores of the endothelial layer, the clustering of nanoparticles at the uropod during T cell polarization and migration as well as the possible loss of integrins from the T cell surface to which nanoparticles could be tethered. Nanoparticles that were shed from T cell surface during transmigration remain associated with the pMBMEC monolayer as observed by epifluorescence microscopy (Figure S6). Confocal images of a nanoparticle modified T cells after transmigration showed presence of nanoparticle clustering at the uropod. Nanoparticle accumulation at the uropod (Figure 7D) was also reported elsewhere during T cell migration on an endothelial cell monolayer toward a chemoattractant [31] and was essentially attributed to membrane protein reorganization during T cell polarization [32].

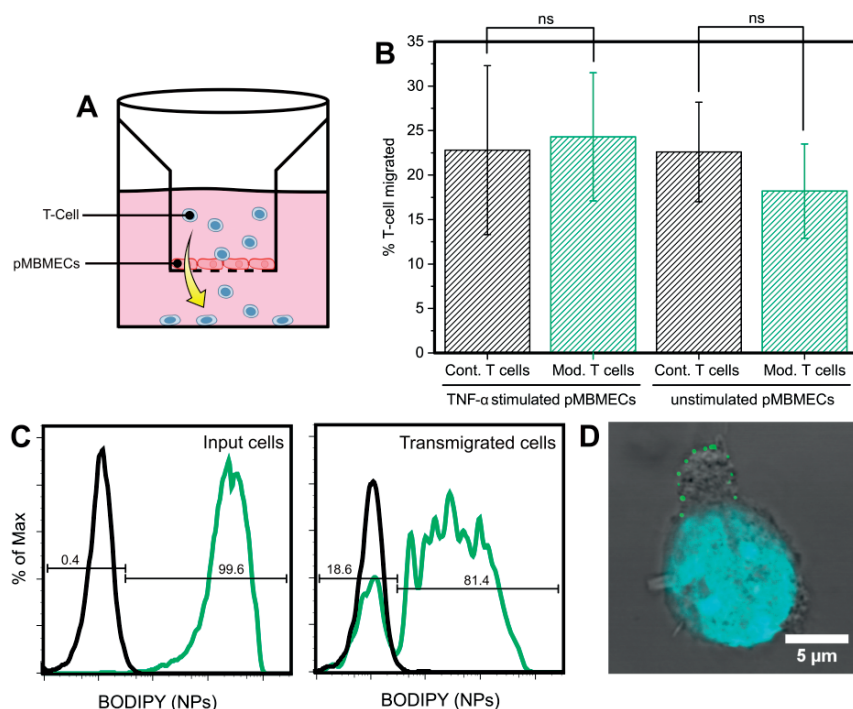


Figure 7. (A) Schematic overview of the two-chamber *in vitro* transendothelial migration assay (TEM). (B) Percentage of migrated T cells through TNF- α stimulated and unstimulated pMBMEC monolayers: comparison between unmodified control (Cont.) T cells and nanoparticle decorated T cells (Mod.). P-values were determined by *t* test (ns: P > 0.05). The histogram present the results of two independent experiments performed in triplicate and the error bars are standard deviations. (C) Flow cytometry analysis showing histograms of nanoparticle associated fluorescence of scatter gated live T cells. (left) T cell input for TEM assay across a TNF- α stimulated pMBMEC monolayer and (right) migrated T cells. Black: control unmodified T cells; green: nanoparticle functionalized T cells. (D) Confocal micrograph of a nanoparticle (green) functionalized T cell (transmission image, nucleus stained with DAPI), which migrated across a TNF- α stimulated pMBMEC monolayer.

In a final experiment, the ability of the nanoparticle decorated CD4⁺ T_{EM} cells to migrate across an *in vitro* BBB model under physiological flow was investigated using a microfluidic set-up. The same TNF- α stimulated endothelial BBB model as described above was used. The behavior of nanoparticle modified T cells was compared to that of control unmodified T cells with time-lapse live cell imaging using differential interference contrast (DIC) to detect both T cells and pMBMECs and epifluorescence to detect the nanoparticles (green). T cells were allowed to initiate interaction with the pMBMEC monolayer at a reduced flow rate of 0.2 dyne/cm² during an accumulation

period of 5 minutes. The flow rate was then increased to 1.5 dyne/cm² to mimic physiological flow conditions typically encountered within CNS post-capillary venules. Figure 8 shows a sequence of eight images that illustrates the diapedesis of a nanoparticle decorated CD4⁺ T_{EM} cell across the BBB (video is available as Supporting Information). First, a nanoparticle modified T cell adheres to the endothelial surface during the accumulation phase (image time 03:10 [min:sec]). At this stage, the T cell is surrounded by a halo of light showing that it interacts with the luminal side of the pMBMEC monolayer and the nanoparticles (green) are visible on the T cell. Following attachment and polarization, the T cell crawls and nanoparticles cluster at the uropod as visible in the image taken at 04:10. The T cell then was observed to further crawl against the direction of flow (white arrow) and to eventually reach a site on the pMBMEC monolayer permissive for diapedesis (image time 06:20). Then, the nanoparticle modified T cell can be seen during extravasation, partially through the pMBMEC monolayer in the two images recorded at 08:20 and 11:00. Only the uropod with a nanoparticle cluster remains above the pMBMEC monolayer at this stage. The largest part of the T cell has migrated across the pMBMEC monolayer and is visible as a dark protrusion below the endothelial cells. The extravasation of the nanoparticle modified T cells takes approximately 6 minutes in total from the point that the T cell found a site permissive of diapedesis until the entire cell is found below the pMBMEC monolayer (image at 12:10). Once the T cell is under the pMBMEC monolayer it continues to crawl below carrying its nanoparticulate cargo along (images at 21:50 and 25:10). Towards the end of the sequence, some nanoparticles are released from the T cells surface, a behavior that has been observed many times during or after diapedesis of modified T cells.

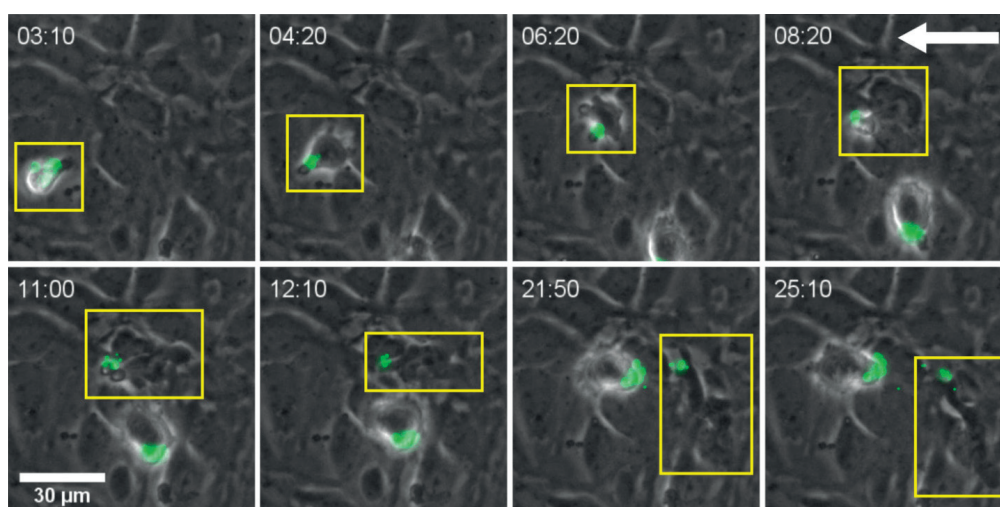


Figure 8. Live cell imaging of a nanoparticle (green) decorated T cell (yellow rectangle) arresting (image at [03:10]), crawling against the flow (images at [04:20] and [06:20]), migrating across a pMBMEC monolayer (images from [08:20] to [12:10]) and finally crawling below the pMBMEC layer (images at [21:50] and [25:10]). The white arrow (top right corner) indicates the direction of the flow. Time is indicated in left corners of each images as [min:sec].

To quantitatively describe the interaction of the nanoparticle decorated T cells with the pMBMEC monolayer under flow, each arrested T cell was assigned a behavioral category and the total number of T cells within a particular category presented as a percentage of arrested T cells. T cells that entered or left the field of view during the recorded period were excluded from the analysis. T cells that continuously crawled were categorized as “Crawling” and T cells that remained stationary while sending out protrusions as “Probing”. The category “Diapedesis” encompasses T cells that performed a complete diapedesis across the pMBMEC monolayer after crawling or probing. Finally, a category accounting for incomplete diapedesis after crawling or probing was defined as “Incomplete diapedesis”. A total of 582 nanoparticle modified T cells in 10 different movies were compared to 278 control T cells from 5 different movies for an observation time of 25 to 30 minutes recorded at a rate of 6 frames per minute. Figure 9 shows the percentages of each behavioral category assigned to T cells interacting with pMBMEC under flow for unmodified and nanoparticle modified T cells (a supplementary Figure and movie can be found for each behavioral category as supporting information: Figures S7-S10). A clear alteration of behavior when T cells are carrying a nanoparticle cargo was observed. While after 30 minutes 65% of arrested unmodified T cells had crossed the TNF- α stimulated monolayer only 23 % nanoparticle modified T cells managed to cross

the pMBMEC monolayer during the same time. This discrepancy may partly be explained by the duration difference of the flow assay compared to the transendothelial assay under static conditions that is typically performed for six hours. In fact, this longer timeframe allowed nanoparticle decorated T cells to reach a similar extent of migration across the pMBMEC monolayer to that of unmodified control T cells. It is possible that this difference in diapedesis rate after 30 minutes under flow condition is only due to a delay effect caused by a temporal partial functional impairment of nanoparticle decorated T cells, which can be seen by increased percentages in other migratory categories. Notably a 6-fold increase in *incomplete diapedesis* was observed and is illustrated in Figure and Movie S9 where a nanoparticle decorated T cell with a highly functionalized uropod (visually estimated as highly functionalized) tend to remain blocked half way through the pMBMEC layer during transmigration. An explanation of this behavior may lie in the nanoparticles clustering at the uropod, creating an important stress on this part of the membrane, which in turn causes the inability of this T cell to complete diapedesis in this short timeframe. There is at least one other case where functional impairment could be observed by time-lapse live cell imaging under flow condition during this assay. Figure and Movie S11 shows a T cell that is stuck below the pMBMEC monolayer from its site of diapedesis and which is unable to continue crawling below the BBB as normal control T cells do. These two observations were only possible in this sophisticated set-up which mimic *in vivo* conditions encountered in the CNS and suggest that nanoparticle decoration alter T cell function at least temporarily.

Finally determining the exact amount of nanoparticles transported across the BBB after T-cell diapedesis across the pMBMEC monolayer was not possible with precision because transmigrated T cells could not be analyzed by flow cytometry. We have however observed individual T cells which dropped their nanoparticle load during or after diapedesis below the pMBMEC monolayer (Figure and Movie S12). Alternatively, the nanoparticle functionalized uropod was detached from the rest of the T cell during diapedesis leaving nanoparticles at the luminal surface of the pMBMEC monolayer (Figure and Movie S13). These observations confirm the observations obtained under static conditions namely that part of the nanoparticulate payload may not be completely transported together with the T cells across the BBB.

Based on the experiments performed we can estimate the potential of T cell-mediated delivery of nanoparticle across the BBB using CD4⁺ T_{EM} cell as a vehicle to be in the range of approx. 2 %. This was calculated assuming that a proportion of 23% of

nanoparticle decorated T cells are able to cross the BBB under physiological flow condition in a very short time of 30 minutes and taking into account that a part of the initial nanoparticulate cargo (approx. 10-fold decrease in fluorescence intensity in static assay) may not be transported through the BBB. This number has the potential to be increased if cells are allowed to interact with the pMBMEC monolayer for longer period under flow condition. The overall efficiency of cell-mediated delivery to the CNS using this platform is also likely to be improved by modulating parameters such as nanoparticle size or type, for instance using polymersomes as well as the conjugation method to prevent nanoparticle from clustering at the uropod.

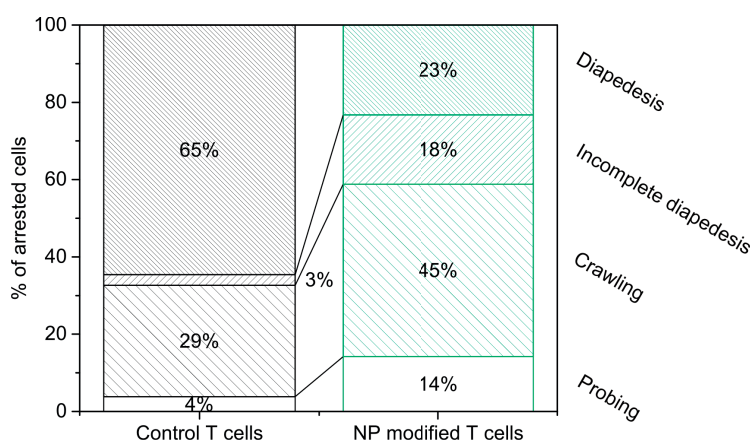


Figure 9. Percentage of control and nanoparticle modified T cell behavior during the multi-step extravasation across the BBB under physiological flow condition *in vitro*. The results are presented for a total of 582 nanoparticle modified T cells recorded in 10 different movies and compared to 278 control T cells from 5 different movies for an observation time of 30 minutes.

2.4. Conclusions

In this report the functionalization of $CD4^+$ T_{EM} cells with approx. 100 model fluorescent PEGylated nanoparticles coupled via maleimide-thiol conjugation chemistry was shown to be non-toxic and stable over a period of 24h as demonstrated by flow cytometry and confocal microscopy. T cells remained functional after modification and were able to bind to immobilized ICAM-1 as well as to transmigrate across the BBB *in vitro*. These nanoparticle modified T cells could transport their nanoparticulate cargo across the BBB in two complementary experiments, a simple two-chamber assay that provided insight in the amount of transported cargo and a T cell extravasation assay

carried out under physiological flow conditions mimicking *in vivo* conditions of CNS post-capillary venules. Our study shows for the first time diapedesis of nanoparticle functionalized T cells across the BBB under physiological flow by live cell imaging and revealed the clustering of nanoparticle at the uropod during T cell polarization, crawling and diapedesis and their transport to the abluminal side of the BBB. The current state-of-the-art approaches in nanomedicine explored for transport of nanoparticles across the BBB, essentially rely on targeting receptors at the luminal side of the BBB endothelium. Our approach using a cell carrier for nanoparticle transport thus represents an innovative step in drug delivery development to the CNS and is here for the first time applied to an intact BBB model. The potential of this cell-based approach in nanoparticle uptake in the CNS is substantial compared to traditional nanoparticle delivery approaches. Finally, our method allows to target the BBB in the presence or absence of neuroinflammation and thus provides a broad basis for the diagnosis and treatment of a wide range of neuroinflammatory disorders.

2.5. References and Notes

- [1] N.J. Abbott, A.A.K. Patabendige, D.E.M. Dolman, S.R. Yusof, D.J. Begley, Structure and function of the blood–brain barrier, *Neurobiol. Dis.*, 37 (2010) 13-25.
- [2] S. Krol, Challenges in drug delivery to the brain: nature is against us, *J. Control. Release*, 164 (2012) 145-155.
- [3] W.M. Pardridge, Drug transport across the blood-brain barrier, *J. Cereb. Blood Flow Metab.*, 32 (2012) 1959-1972.
- [4] I. Brasnjevic, H.W.M. Steinbusch, C. Schmitz, P. Martinez-Martinez, R. European NanoBioPharmaceutics, Delivery of peptide and protein drugs over the blood-brain barrier, *Prog. Neurobiol.*, 87 (2009) 212-251.
- [5] C. Saraiva, C. Praça, R. Ferreira, T. Santos, L. Ferreira, L. Bernardino, Nanoparticle-mediated brain drug delivery: Overcoming blood–brain barrier to treat neurodegenerative diseases, *J. Controlled Release*, 235 (2016) 34-47.
- [6] I. van Rooy, S. Cakir-Tascioglu, W.E. Hennink, G. Storm, R.M. Schiffelers, E. Mastrobattista, In Vivo Methods to Study Uptake of Nanoparticles into the Brain, *Pharm. Res.*, 28 (2011) 456-471.

- [7] A.C. Anselmo, S. Mitragotri, Cell-mediated delivery of nanoparticles: Taking advantage of circulatory cells to target nanoparticles, *J. Controlled Release*, 190 (2014) 531-541.
- [8] Y. Su, Z. Xie, G.B. Kim, C. Dong, J. Yang, Design Strategies and Applications of Circulating Cell-Mediated Drug Delivery Systems, *ACS Biomaterials Science & Engineering*, 1 (2015) 201-217.
- [9] M. Ayer, H.-A. Klok, Cell-mediated delivery of synthetic nano- and microparticles, *J. Controlled Release*.
- [10] E.V. Batrakova, A.V. Kabanov, Cell-mediated drug delivery to the brain, *J. Drug Deliv. Sci. Technol.*, 23 (2013) 419-433.
- [11] E.V. Batrakova, S. Li, A.D. Reynolds, R.L. Mosley, T.K. Bronich, A.V. Kabanov, H.E. Gendelman, A Macrophage–Nanozyme Delivery System for Parkinson's Disease, *Bioconjugate Chem.*, 18 (2007) 1498-1506.
- [12] A.M. Brynskikh, Y.L. Zhao, R.L. Mosley, S. Li, M.D. Boska, N.L. Klyachko, A.V. Kabanov, H.E. Gendelman, E.V. Batrakova, Macrophage delivery of therapeutic nanozymes in a murine model of Parkinson's disease, *Nanomedicine*, 5 (2010) 379-396.
- [13] Y. Zhao, M.J. Haney, V. Mahajan, B.C. Reiner, A. Dunaevsky, R.L. Mosley, A.V. Kabanov, H.E. Gendelman, E.V. Batrakova, Active Targeted Macrophage-mediated Delivery of Catalase to Affected Brain Regions in Models of Parkinson's Disease, *Journal of nanomedicine & nanotechnology*, Suppl 4 (2011) 003.
- [14] M.J. Haney, P. Suresh, Y. Zhao, G.D. Kanmogne, I. Kadiu, M. Sokolsky-Papkov, N.L. Klyachko, R.L. Mosley, A.V. Kabanov, H.E. Gendelman, E.V. Batrakova, Blood-Borne Macrophage-Neural Cell Interactions Hitchhike Endosome Networks for Cell-Based Nanozyme Brain Delivery, *Nanomedicine (London, England)*, 7 (2012) 815-833.
- [15] M.J. Haney, Y. Zhao, S. Li, S.M. Higginbotham, S.L. Booth, H.-Y. Han, J.A. Vetro, R.L. Mosley, A.V. Kabanov, H.E. Gendelman, E.V. Batrakova, Cell-mediated Transfer of Catalase Nanoparticles from Macrophages to Brain Endothelial and Neural Cells, *Nanomedicine (London, England)*, 6 (2011) 1215-1230.

- [16] U. Steinfeld, C. Pauli, N. Kaltz, C. Bergemann, H.H. Lee, T lymphocytes as potential therapeutic drug carrier for cancer treatment, *Int. J. Pharm.*, 311 (2006) 229-236.
- [17] R. Mooney, Y.M. Weng, R. Tirughana-Sambandan, V. Valenzuela, S. Aramburo, E. Garcia, Z.Q. Li, M. Gutova, A.J. Annala, J.M. Berlin, K.S. Aboody, Neural stem cells improve intracranial nanoparticle retention and tumor-selective distribution, *Future Oncology*, 10 (2014) 401-415.
- [18] B. Engelhardt, R.M. Ransohoff, Capture, crawl, cross: the T cell code to breach the blood-brain barriers, *Trends Immunol.*, 33 (2012) 579-589.
- [19] O. Steiner, C. Coisne, R. Cecchelli, R. Boscacci, U. Deutsch, B. Engelhardt, R. Lyck, Differential Roles for Endothelial ICAM-1, ICAM-2, and VCAM-1 in Shear-Resistant T Cell Arrest, Polarization, and Directed Crawling on Blood-Brain Barrier Endothelium, *J. Immunol.*, 185 (2010) 4846-4855.
- [20] B. Engelhardt, R.M. Ransohoff, The ins and outs of T-lymphocyte trafficking to the CNS: anatomical sites and molecular mechanisms, *Trends Immunol.*, 26 (2005) 485-495.
- [21] B. Engelhardt, M. Laschinger, M. Schulz, U. Samulowitz, D. Vestweber, G. Hoch, The development of experimental autoimmune encephalomyelitis in the mouse requires alpha 4-integrin but not alpha 4 beta 7-integrin, *J. Clin. Invest.*, 102 (1998) 2096-2105.
- [22] C. Coisne, L. Dehouck, C. Faveeuw, Y. Delplace, F. Miller, C. Landry, C. Morissette, L. Fenart, R. Cecchelli, P. Tremblay, B. Dehouck, Mouse syngenic in vitro blood-brain barrier model: a new tool to examine inflammatory events in cerebral endothelium, *Lab. Invest.*, 85 (2005) 734-746.
- [23] R. Lyck, N. Ruderisch, A.G. Moll, O. Steiner, C.D. Cohen, B. Engelhardt, V. Makrides, F. Verrey, Culture-induced changes in blood-brain barrier transcriptome: implications for amino-acid transporters in vivo, *J. Cereb. Blood Flow Metab.*, 29 (2009) 1491-1502.
- [24] O. Steiner, C. Coisne, B. Engelhardt, R. Lyck, Comparison of immortalized bEnd5 and primary mouse brain microvascular endothelial cells as in vitro blood-brain barrier models for the study of T cell extravasation, *J. Cereb. Blood Flow Metab.*, 31 (2011) 315-327.
- [25] G. Martin-Blondel, B. Pignolet, S. Tietz, L. Yshii, C. Gebauer, T. Perinat, I. Van Weddingen, C. Blatti, B. Engelhardt, R. Liblau, Migration of encephalitogenic

- CD8 T cells into the central nervous system is dependent on the alpha 4 beta 1-integrin, *Eur. J. Immunol.*, 45 (2015) 3302-3312.
- [26] R.K. Röhnelt, G. Hoch, Y. Reiss, B. Engelhardt, Immunosurveillance modelled in vitro: naive and memory T cells spontaneously migrate across unstimulated microvascular endothelium, *Int. Immunol.*, 9 (1997) 435-450.
- [27] C. Coisne, R. Lyck, B. Engelhardt, Live cell imaging techniques to study T cell trafficking across the blood-brain barrier in vitro and in vivo, *Fluids Barriers CNS*, 10 (2013) 7.
- [28] F. Meng, G.H. Engbers, J. Feijen, Polyethylene glycol-grafted polystyrene particles, *J. Biomed. Mater. Res. A*, 70 (2004) 49-58.
- [29] M.T. Stephan, J.J. Moon, S.H. Um, A. Bershteyn, D.J. Irvine, Therapeutic cell engineering with surface-conjugated synthetic nanoparticles, *Nat. Med.*, 16 (2010) 1035-1041.
- [30] Y. Reiss, G. Hoch, U. Deutsch, B. Engelhardt, T cell interaction with ICAM-1-deficient endothelium in vitro: essential role for ICAM-1 and ICAM-2 in transendothelial migration of T cells, *Eur. J. Immunol.*, 28 (1998) 3086-3099.
- [31] M.T. Stephan, S.B. Stephan, P. Bak, J.Z. Chen, D.J. Irvine, Synapse-directed delivery of immunomodulators using T-cell-conjugated nanoparticles, *Biomaterials*, 33 (2012) 5776-5787.
- [32] C. Gómez-Moutón, J.L. Abad, E. Mira, R.A. Lacalle, E. Gallardo, S. Jiménez-Baranda, I. Illa, A. Bernad, S. Mañes, C. Martínez-A., Segregation of leading-edge and uropod components into specific lipid rafts during T cell polarization, *Proceedings of the National Academy of Sciences*, 98 (2001) 9642-9647.

2.6. Supporting information

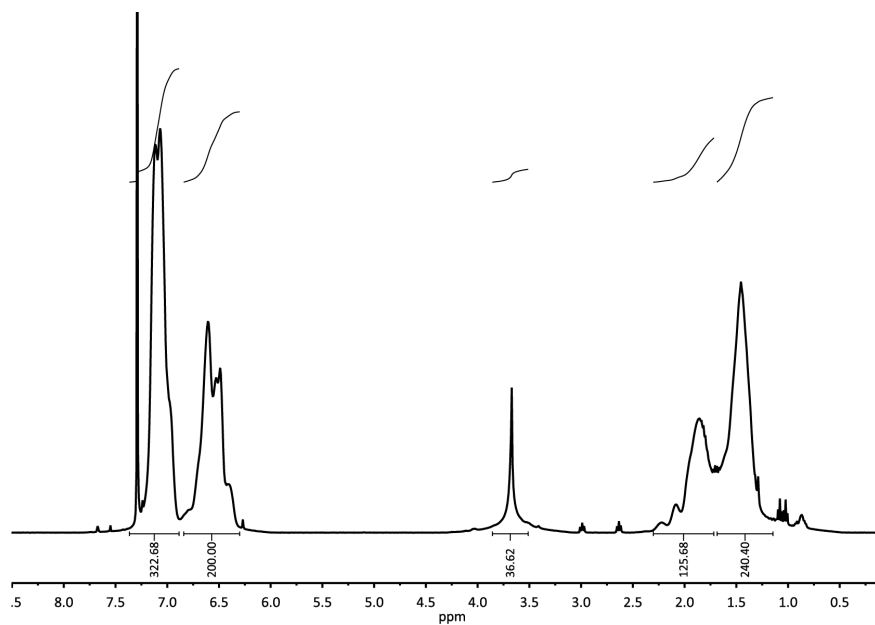


Figure S1. ¹H-NMR spectrum of freeze-dried unfunctionalized PEGylated amine-modified FluoSpheres dissolved in CDCl₃.

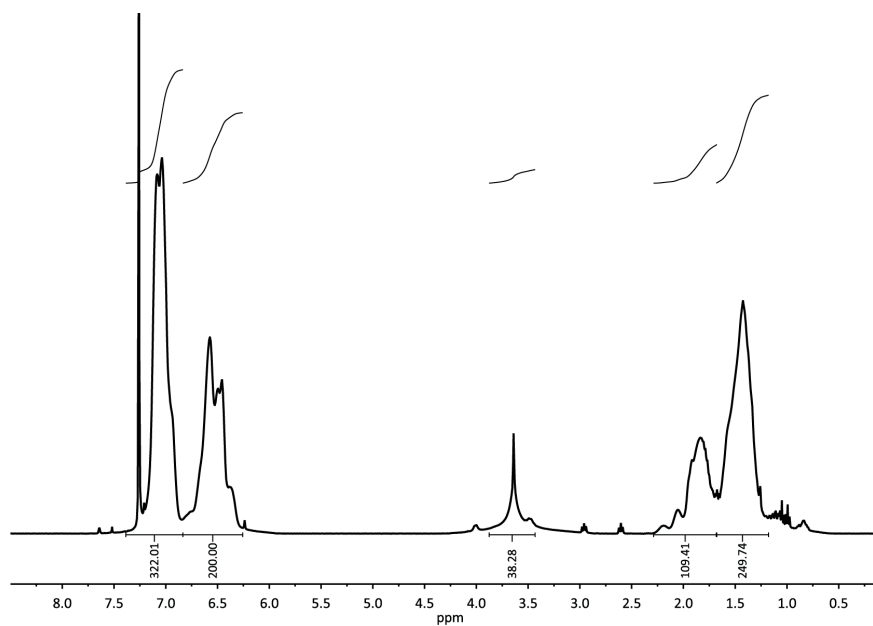


Figure S2. ¹H-NMR spectrum of freeze-dried maleimide functionalized PEGylated amine-modified FluoSpheres dissolved in CDCl₃.

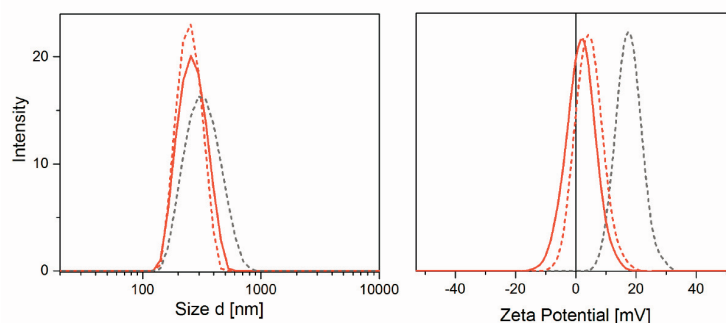


Figure S3. Size and zeta potential measurement of (solid red) Maleimide functionalized PEGylated polystyrene nanoparticles; (dash red) Methoxy-PEGylated polystyrene nanoparticles; (dash gray) amine modified polystyrene nanoparticles (commercial product).

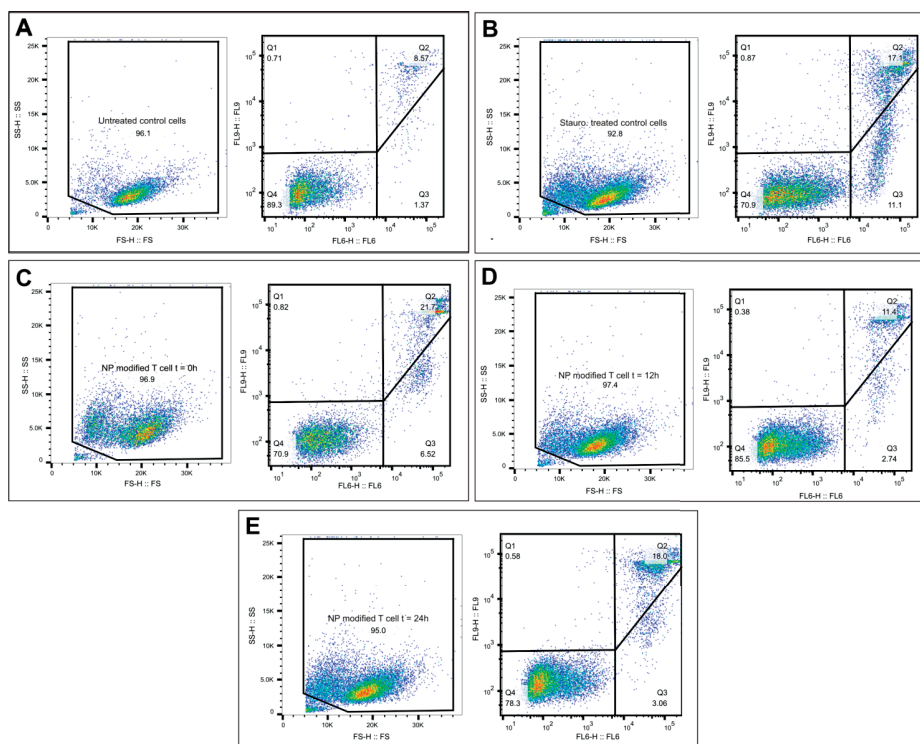


Figure S4. Annexin V-Alexa 647 / DAPI viability assay. For each box: (Left) Forward and side scatter gated population for viability assay and (right) plot of fluorescence of Annexin V-Alexa 647 (FL-6) versus fluorescence of DAPI (FL-9) (A) untreated control T cells. (B) Staurosporine treated (for 6h) control T cells. (C) Nanoparticle modified T cells directly after functionalization. (D) Nanoparticle modified T cells 12h after functionalization. (E) Nanoparticle modified T cells 24h after functionalization. Quadrant Q4 show live T cells, Q3 apoptotic T cells and Q2 apoptotic/necrotic T cells as gated from the two controls: untreated control T cells (A) and staurosporine treated T cells (B) plots.

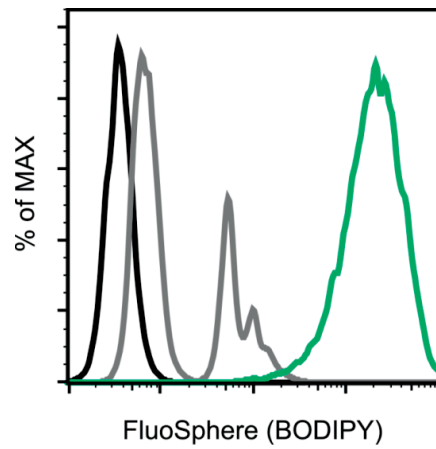


Figure S5. Flow cytometry results showing the specific binding of maleimide functionalized PEGylated nanoparticle. The figure shows histograms of scatter gated live T cells for nanoparticle associated fluorescence. Control untreated T cells are shown in black; T cells treated with methoxy-PEGylated nanoparticles in grey and T cells treated with maleimide-functionalized PEGylated nanoparticles in green. This result is representative of two independent experiments performed in triplicate.

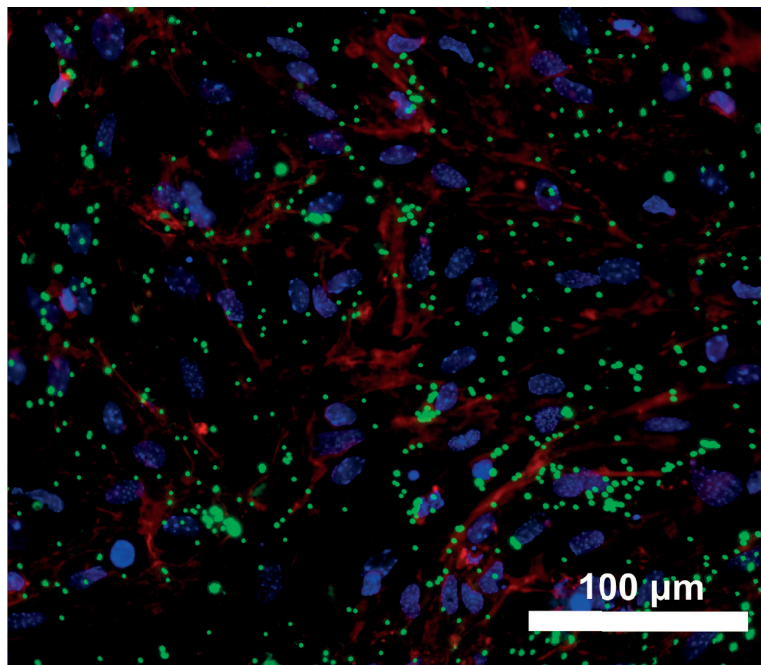


Figure S6. Fluorescence image of a pMBMEC monolayer stained with DAPI (blue) and phalloidin-rhodamin (red) after nanoparticle (green) modified T cells transmigration under static condition. Nanoparticles that were shed from T cell surface during transmigration remain associated with the pMBMEC monolayer.

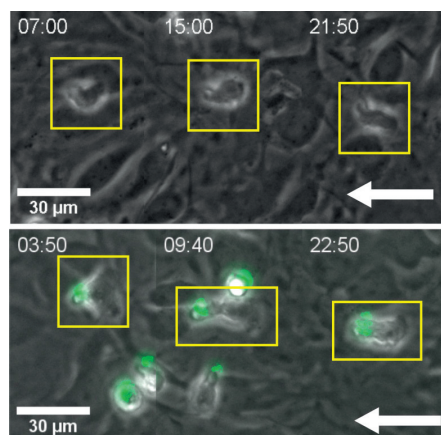


Figure S7. T-cell crawling. Continuous sequence of three images recorded during time-lapse live cell imaging of (top) a control T cell and (bottom) a nanoparticle (green) decorated T cell crawling on a pMBMEC monolayer under physiological flow. The yellow rectangles indicate the position of the cell of interest as a function of time. The white arrow indicates the direction of the flow. Time is indicated in left corners of each images as [min:sec].

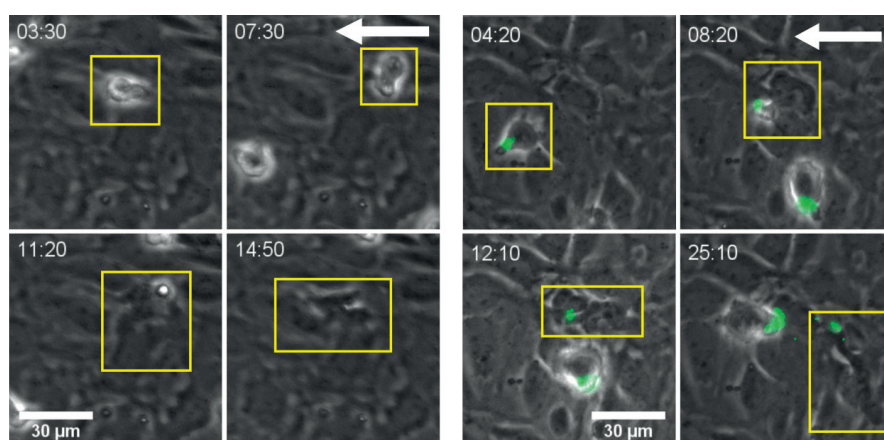


Figure S8. T-cell diapedesis. Sequence of four images recorded during time-lapse live cell imaging of a control T cell (left) and a nanoparticle modified T cell (right) performing complete diapedesis across a pMBMEC monolayer under physiological flow. The yellow rectangles indicate the position of the cell of interest as a function of time. The white arrow (top right corner) indicates the direction of the flow. Time is indicated in left corners of each images as [min:sec].

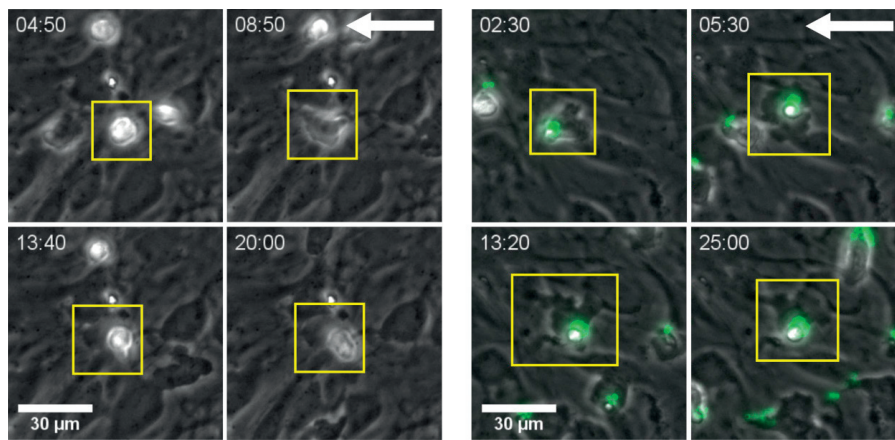


Figure S9. Incomplete diapedesis of T cells. Sequence of four images recorded during time-lapse live cell imaging of (left) a control T cell and (right) a nanoparticle (green) decorated T cell performing an incomplete diapedesis across a pMBMEC monolayer under physiological flow. In both cases, the uropod remains on the luminal side of the pMBMEC monolayer. Nanoparticles are clustering at the uropod in the image sequence on the right. The yellow rectangles indicate the position of the cell of interest as a function of time in both left and right image series. The white arrow (top right corner) indicates the direction of the flow. Time is indicated in left corners of each images as [min:sec].

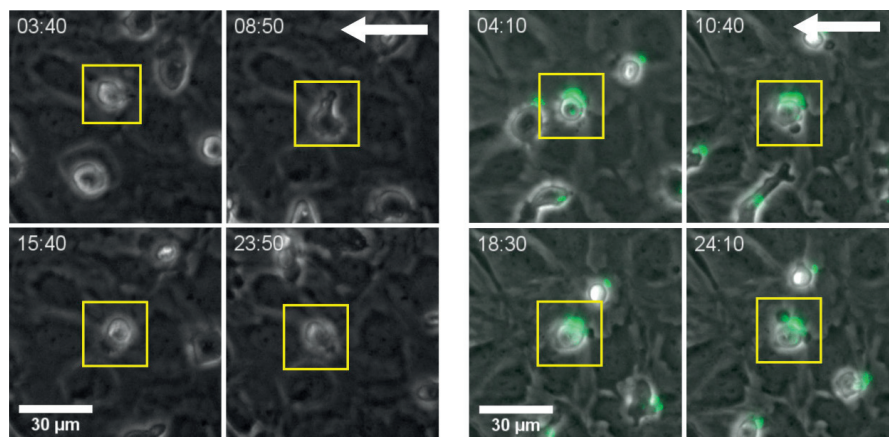


Figure S10. T-cell probing. Sequence of four images recorded during time-lapse live cell imaging of (left) a control T cell and (right) a nanoparticle (green) decorated T cell probing on the luminal side of a pMBMEC monolayer under physiological flow. The yellow rectangles indicate the position of the cell of interest as a function of time in both left and right image series. The white arrow (top right corner) indicates the direction of the flow. Time is indicated in left corners of each images as [min:sec].

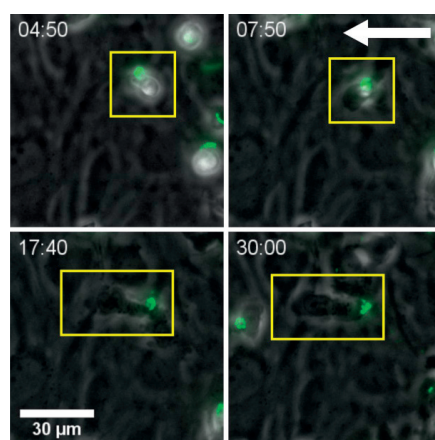


Figure S11. T cell stuck after diapedesis. Sequence of four images recorded during time-lapse live cell imaging of a nanoparticle (green) decorated T cell being stuck after diapedesis across a pMBMEC monolayer under physiological flow. On the image taken at 17:40 the modified T cell is below the pMBMEC monolayer but is prevented from further moving away from its site of diapedesis until the end of the recording time. The yellow rectangles indicate the position of the cell of interest as a function of time in the image series. The white arrow (top right corner) indicates the direction of the flow. Time is indicated in left corners of each images as [min:sec].

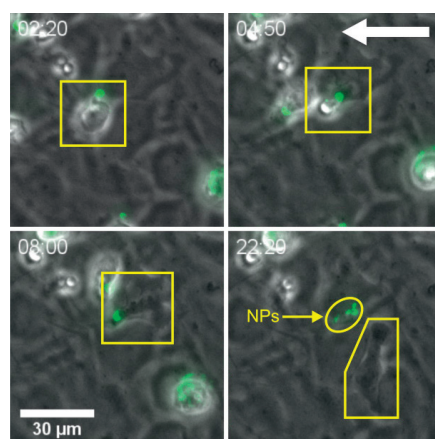


Figure S12. Nanoparticle dropped after diapedesis. Sequence of four images recorded during time-lapse live cell imaging of a nanoparticle (green) decorated T cell dropping its nanoparticle cargo after diapedesis across a pMBMEC monolayer under physiological flow. The yellow rectangles indicate the position of the cell of interest as a function of time. At the end of the sequence (image at 22:20) dropped nanoparticles (NPs) are marked with a yellow circle and the T cell is marked with a yellow polygon. The white arrow (top right corner) indicates the direction of the flow. Time is indicated in left corners of each images as [min:sec].

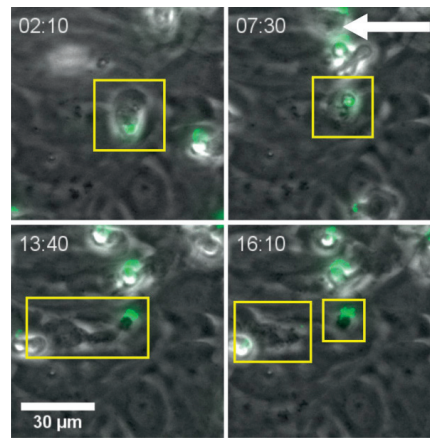


Figure S13. T cell breaking apart, losing its nanoparticle functionalized uropod. Sequence of four images recorded during time-lapse live cell imaging of a nanoparticle (green) decorated T cell losing its nanoparticle decorated uropod after diapedesis across a pMBMEC monolayer under physiological flow. The yellow rectangles indicate the position of the cell of interest as a function of time in the image series. On the image taken at 16.10 the modified T cell is broken apart and the functionalized uropod is left on the luminal side of the pMBMEC monolayer. The white arrow (top right corner) indicates the direction of the flow. Time is indicated in left corners of each images as [min:sec].

3. Biotin-NeutrAvidin mediated immobilization of polymer nanoparticles on T lymphocytes

3.1. Introduction

Circulatory cells have received increasing attention as carriers for the delivery of synthetic nano- and microparticle-based therapeutics [1-3]. Cell based delivery systems hold enormous promise to help overcome some of the limitations of nano- and microparticle therapeutics. This includes, among others, the possibility to allow highly specific targeted delivery [4], to facilitate delivery across challenging physiological barriers as well as the opportunity to generate long circulating delivery systems [5].

One way to use circulatory cells as carriers for therapeutic nano- and microparticles involves immobilization of the particle based cargo on the cell surface [1]. While an increasing number of reports have explored surface modified cells as delivery systems, only relatively little effort has been made to systematically investigate and understand the effect of cell surface immobilization chemistries, particle size and surface concentration on the properties and performance of the cell based drug delivery systems. A closely related challenge is the need for methods that allow to monitor and determine the precise location and distribution of particles on a cell surface.

The immobilization of nano- and microparticles on cell surfaces can be monitored using conventional bright field or epifluorescence microscopy. These techniques, however, provide images that are 2D projections of the entire surface modified cells and as a consequence provide limited possibilities to identify the precise location of the particle payload (e.g. on the cell surface or internalized). These methods can be nevertheless sufficient in some very specific cases, where particles are in the micron-size range [6] and/or for cells lacking phagocytic competences [7]. Confocal fluorescence microscopy is a very powerful technique to study cells that have been modified with nano- and microparticles. Confocal microscopy allows to reconstruct 3D images of surface-modified cells from images obtained from different focal planes throughout the cell. As a consequence detailed information on the position and distribution of the particle payload on the cell surface can be obtained. So far, however, confocal microscopy has

been mainly used to qualitatively analyzed particle modified cells [4, 8-10]. Determining the localization of objects in the nano-size range with respect to the cell surface or membrane is far from trivial even using confocal microscopy techniques because the plasma membrane as well as nanoparticles with a diameter smaller than 200 nm have a size that is below the maximum resolution of confocal microscopy and thus requires careful analysis after image acquisition. Electron microscopy, in particular scanning electron microscopy (SEM) has been alternatively used to characterized nanoparticle decorated cells [11]. SEM can very accurately detect surface-bound nanomaterials but cannot detect internalized particles, which may be disadvantageous in cases where internalization may not be negligible.

This study uses the non-covalent, biotin-NeutrAvidin mediated conjugation strategy [11] to functionalize T lymphocytes with fluorescent polystyrene nano- and microparticles of three different sizes. To characterize the particle decorated cells, a semi-quantitative method to analyze confocal 3D reconstructions of the cells was developed. This method was used to investigate the influence of particles size on the position and distribution of the particles over a period of 24h and across two cell lines. The first cell line used were Jurkat cells, which are T lymphocytes established from an acute leukemia human patient. The Jurkat cell line is a robust and easy cell line for culture which is very useful to investigate and explore various cell-surface modification strategies. The second type of T cells that was used are SJL/PLP7 T cells, which are primary mouse CD4⁺ effector/memory proteolipid protein (PLP) specific T cells. These T cells are potentially attractive as carriers to facilitate drug delivery to the central nervous system. In a final experiment, the ability of the nanoparticle decorated CD4⁺ T_{EM} cells to bind to a key protein involved in the migration across the blood-brain barrier was investigated [12, 13].

3.2. Experimental Section

3.2.1. Materials

NeutrAvidin coated yellow-green polystyrene FluoSpheres (d = 1 μ m, 200 nm and 40 nm), NeutrAvidin Oregon Green 488 conjugate, CellTrace Violet, WGA-Texas Red conjugate, 6-((6-((biotinoyl)amino)hexanoyl)amino)hexanoic acid, sulfosuccinimidyl ester, sodium Salt (Biotin-XX, SSE), Prolong Gold mounting media, Dubelcco's Phosphate-buffered saline (DPBS), RPMI 1640 and FBS were

purchased from Thermofischer scientific. mPEG₂₀₀₀-Biotin was were obtained from Laysan Bio Inc. Poly(L-lysine) (0.1 % w/v solution), paraformaldehyde (PFA) and sodium azide were purchased from Sigma-Aldrich.

3.2.2. Methods

Flow cytometry was performed on a Beckmann Coulter Gallios instrument. Confocal microscopy images were recorded on a Zeiss LSM700 Inverted microscope (Carl Zeiss, Feldbach, Switzerland). Cell-counting for binding assay was performed using an Olympus CKX41 inverted microscope equipped with a 10 mm x 10 mm / 10 divisions counting reticle and a 20x objective.

3.2.3. Procedures

3.2.3.1. Cell lines and cell cultures

Jurkat cells were cultured in RPMI 1640 glutamax medium (Gibco) supplemented with 10% fetal bovine serum (FBS) (Gibco), 1% penicillin/streptomycin (Gibco), 1% Na-pyruvate (Gibco). Cells were maintained between 1×10^5 and 1×10^6 cells/mL in Corning T175 flasks.

Encephalitogenic CD4⁺ effector/memory proteolipid protein (PLP) peptide aa139-153 specific T cells (line SJL/PLP7) were cultured as previously described [14]. In brief, PLP-specific T cells were cultured in RPMI 1640 glutamax medium (Gibco) supplemented with 10% fetal bovine serum (FBS) (Gibco), 1% penicillin/streptomycin (Gibco), 1% non-essential amino acid (Gibco), 1% Na-pyruvate (Gibco), 0.4% β -mercaptoethanol (Gibco) and 1% IL-2 supernatant (self-made). Cells were typically used for modification and in functional assays at day 3 or 4 after restimulation.

3.2.3.2. Biotinylation of T cells

First, T cells were washed trice with DPBS (centrifuged at $250 \times g$ for 7 min) and finally resuspended at a concentration 25 mio cells/mL in DPBS. Cells were left to cool on ice for at least 5 minutes before Biotin-XX, SSE, a cell impermeable *N*-sulfosuccinimidyl reactive ester (Thermofisher scientific) was added to the cell suspension to a final concentration of approx. 0.05 mM or 0.5 mM or 1 mM. Cells were functionalized on ice for 30 minutes and then washed three times with DPBS and used directly for nanoparticle conjugation. The biotinylation of T cells was monitored by flow cytometry. In short, 0.5 mio cells were resuspended in 1 mL FACS buffer (DPBS, 2.5%

FBS, 0.1% sodium azide) containing 10 μ L of a 1 mg/mL solution of NeutrAvidin Oregon Green 488 conjugate and left on ice for 20 min in the dark, washed once with FACS buffer and resuspended in 1% PFA in DPBS for analysis.

3.2.3.3. T-cell surface modification

Freshly biotinylated T cells were resuspended at a concentration of 5 or 10 mio cells/mL in DPBS. Then, 100 μ L cell suspension (i.e. 0.5 to 1 mio cells) were added to each well (Greiner Bio-One, 96 well round bottom plate, with cell-repellent surface) followed by addition of 100 μ L of nanoparticle suspension (nanoparticle solution were prepared at a defined concentration according to the conditions for each particle size and cell line listed below). The conjugation was performed at room temperature, in the absence of light for 30 minutes with gentle pipette mixing every 10 minutes. After the conjugation, remaining binding sites were blocked by adding the cell and nanoparticle suspension to a solution of 10 mg/mL Biotin-PEG₂₀₀₀-OMe and left at room temperature for another 10 minutes at 37° C. Subsequently, cells were washed trice with approx. 10 mL of DPBS (centrifuged at 250 x g for 7 min) to remove unbound and loosely bound particles. Cells were then either resuspended in growth media or in 1% PFA in DPBS for flow cytometry, or prepared for confocal microscopy (see below). Specific conditions for each experiment are listed below. Jurkat cells were functionalized using the following conditions. For 200 nm nanoparticles: 0.5 mio Jurkat cells/well with 2000 nanoparticles/cell. For 40 nm nanoparticles: 1 mio Jurkat cells/well with 200'000 nanoparticles/cell. For 1 μ m nanoparticles: 1 mio Jurkat cells/well with 1800 nanoparticles/cell. SJL/PLP 7 T cells were functionalized with 200 nm nanoparticles in the following conditions: 0.5 mio cells/well and 8000 nanoparticles/cell.

3.2.3.4. Proliferation assay

T-cell proliferation was monitored with CellTrace Violet according to the manufacturer's protocol. In short, cells were washed once and resuspended in DPBS at a concentration of 1 mio cells/mL. 1 μ L of CellTrace Violet stock solution in DMSO (5 mM) was added per milliliter of cell suspension and left for 20 minutes at 37° C in the dark. Excess dye was removed by addition of approx. 5 times the staining volume of complete growth medium. Cells were then pelleted, washed once with DPBS and resuspended in complete growth medium until used for cell-surface modification experiments. Fluorescence intensities were measured by flow cytometry, directly after surface modification and 24 hours after modification.

3.2.3.5. Confocal microscopy and image analysis

Surface-modified and CellTrace Violet stained T cells were additionally stained with a membrane marker, WGA-Texas Red-X for 30 minutes on ice in DPBS at a concentration of 1 mio cells/mL. Cells were then seeded on a Poly(L-Lysine) coated 12 mm diameter, 0.17 mm thickness borosilicate glass precision microscopy coverslip (Carl Roth GmbH), washed twice with DPBS and fixed for 10 minutes with a 4% paraformaldehyde solution in DPBS at room temperature. Fixed cells were finally mounted on a microscopy glass slide with Prolong Gold. The slides were left to dry overnight before images were acquired on a Zeiss LSM700 microscope with a 63x/1.4NA lens. Voxel sizes were optimized for deconvolution (XYZ 30 nm x 30 nm x 130 nm). (Digital gain, pinhole size) was set as follows for each channel (1.0, 49 μ m) for the whole cell channel (CellTrace Violet); (1.25, 48 μ m) for the membrane channel (WGA-Texas Red-X) and (1.3, 47 μ m) for the nanoparticle channel (BODIPY). Gain was optimized for each z-stack.

3.2.3.6. Binding assay

ICAM-1 coated slides were prepared as previously reported [15]. In brief, standard 12 well diagnostic slides (ER-202W-CE24, ThermoFisher Scientific) were coated with a protein A (BioVision, Lausen, Switzerland) solution at a concentration of 20 mg/mL in PBS (pH 9) for 1 h at 37°C. The protein A incubation was followed by three PBS washes and subsequently a blocking step using 1.5% bovine serum albumin (BSA) in PBS overnight at 4 °C. Wells were then washed once with PBS pH 7.4 and protein A was exposed to recombinant purified 100 nm mouse ICAM-1-Fc chimera (R&D Systems, Abingdon, U.K.) for 2 hours at 37°C and finally the wells blocked with 1.5% BSA in PBS for 30 min at room temperature and washed once with PBS before used in a binding assay. As a control, DNER-Fc (R&D Systems, Abingdon, U.K.) chimera was used instead of mouse ICAM-1-Fc chimera.

For the binding assay, SJL/PLP7 T cells were collected at 10 mio cells/mL in migration assay medium (MAM: DMEM, 25 mM HEPES, 5% FBS, 2% L-glutamine) and 1×10^5 cells were added to each well and the slide was incubated for 30 minutes at room temperature on a rotating platform. The slides were finally washed twice by dipping them into PBS and fixed for 2 h in 2.5% v/v glutaraldehyde in PBS. The number of adherent cells was evaluated by counting the number of bound cells per field of view using a 20x objective mounted on an Olympus CKX41 inverted microscope equipped with a 10 mm x 10 mm / 10 divisions counting reticle. Each dot in Figure 7 represents a single cell count

from the diagonal of the reticle, 3 counts per well (i.e. per replicate) were recorded in a total of two independent experiments performed in triplicate).

3.3. Results and Discussion

3.3.1. T-cell surface modification and characterization

Figure 1 illustrates the different steps that are involved in the non-covalent attachment of NeutrAvidin-coated fluorescent polystyrene nano- and microparticles on the surface of Jurkat cells or SJL/PLP7 T cells. In the first step, biotin moieties are introduced on the T cell surface using an amine reactive biotinylating agent (Biotin-XX, SSE). After that, freshly biotinylated T cells are exposed to a NeutrAvidin-coated nanoparticle suspension for 30 minutes, after which the remaining free biotin binding sites are blocked with biotin-functionalized PEG and unbound nanoparticles were removed by three centrifugal cycles.

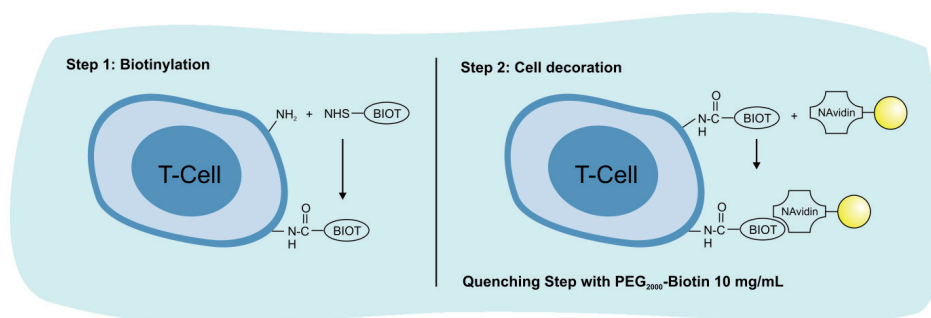


Figure 1: Biotin-NeutrAvidin mediated T cell surface immobilization of fluorescently labeled polystyrene nano- and microparticles. T cell biotinylation using a sulfosuccinimidyl ester-biotin cross-linker followed by attachment of NeutrAvidin (NAvidin)-coated particles on biotinylated cells and blocking of remaining biotin binding sites with PEG₂₀₀₀-Biotin.

Biotinylation of the T cells was typically performed by incubation of 25 mio cells/mL in DPBS and addition of Biotin-XX, SSE to a final concentration of 0.5 mM for 30 minutes on ice. This procedure ensures a high biotin cell surface concentration. These optimized conditions were obtained using 200 nm NeutrAvidin-coated nanoparticles in experiments in which Jurkat cells were exposed to 0.05 mM, 0.5 mM and 1.0 mM Biotin-XX, SEE. Throughout these experiments, the cell concentration and nanoparticle to cell ratio were kept constant at 0.5 mio cells/well and 2000 nanoparticles/cells. To validate the

presence of the biotin moieties on the cell surface and to monitor changes in the surface concentration of these groups upon varying the concentration of Biotin-XX, SSE, cells were treated with NeutrAvidin-Oregon Green 488 and analyzed by flow cytometry. As shown in Figure 2A, a gradual shift in the NeutrAvidin-Oregon Green 488 associated fluorescence can be observed when the concentration of Biotin-XX, SSE is increased from 0.05-1.0 mM, which is consistent with an increasing concentration of biotin groups on the cell surface (Figure S1B). When Jurkat cells that have been treated with 0.05 mM, 0.5 mM and 1 mM Biotin-XX, SSE are exposed to NeutrAvidin-coated 200 nm polystyrene nanoparticles, a similar shift is observed in the nanoparticle associated BODIPY fluorescence, demonstrating that the increased biotin cell surface concentration enhances the polystyrene nanoparticle binding capacity of the T cell. The concentration of 0.5 mM Biotin-XX, SSE is a balanced compromise between high cell surface nanoparticle functionalization and viability of cells that undergo biotinylation (as estimated by trypan blue cell counting using a hemocytometer). Using the same protocol, the extent of biotinylation for SJL/PLP7 T cells was approx. 1.6-fold higher than for Jurkat cells (Figure S1A). The biotin functionalization was also observed by confocal microscopy and the images show high and homogenous NeutrAvidin-Oregon Green 488 fluorescence on the surface of Jurkat cells and SJL/PLP 7 T cells (Figure S1B).

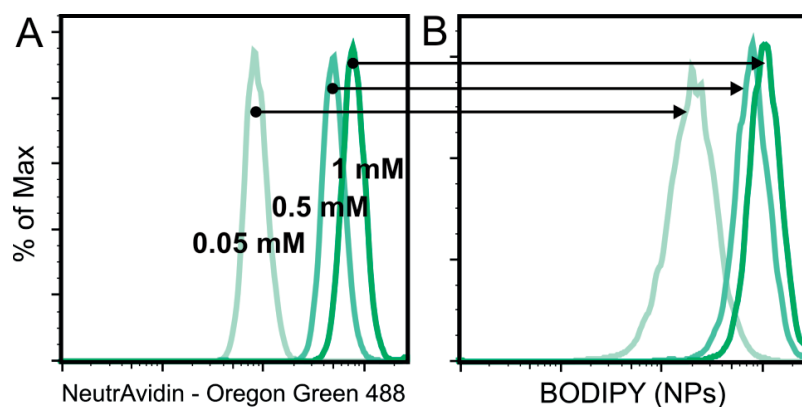


Figure 2. (A) Histogram of scatter gated live Jurkat cells stained with NeutrAvidin-Oregon Green 488 conjugate previously treated with an increasing concentration of biotinylating agent (Biotin-XX, SSE). (B) Histogram of scatter gated live Jurkat cells showing nanoparticle (NP) associated BODIPY fluorescence. NeutrAvidin-coated 200 nm nanoparticles are attached on Jurkat cells presenting an increasing concentration of biotin moieties on their surface.

The protocols for the attachment of nano- and microparticles were optimized for each particle size on the Jurkat cells and SJL/PLP7 T cells. For these experiments, cells were used, which had been treated with 0.5 mM Biotin-XX, SSE. As a control, to evaluate non-specific binding of the NeutrAvidin-coated particles, cells were used that had not been modified with Biotin-XX, SSE. For each particle size and cell type, the concentration of cells per well and the ratio of particles to cell was chosen such as to maximize specific, biotin-NeutrAvidin mediated binding versus non-specific binding. Although unspecific binding takes place in all cases, an approx. 14-fold increase in mean fluorescence intensity (MFI) was observed for 200 nm nanoparticles on biotinylated Jurkat cells versus control unmodified cells (Figure S2B) and an approx. 2.7-fold increase in the case in which 40 nm particles were used (Figure S2A). These increases account for the specific biotin-NeutrAvidin mediated binding of nanoparticles. An approx. 8-fold increase in mean fluorescence intensity was observed for 200 nm beads on biotinylated SJL/PLP7 T cells versus control unmodified cells (Figure S2C). Since NeutrAvidin by itself was not found to bind to non-biotinylated T cells as could be observed from flow cytometry experiments (Figure S1A), the non-specific binding that is observed in Figure S2 is attributed to the nanoparticles.

To remove loosely bound and excess particles, cells were subjected to three centrifugal washing cycles. While this procedure was very efficient for the 40 nm and 200 nm particles, purification of T cells decorated with 1 μ m polystyrene particles was challenging and it was difficult to produce T cells modified with 1 μ m particles that were free of unbound material. As a consequence, T cell modified with 1 μ m particles were only characterized by confocal microscopy.

To study proliferation of the nanoparticle decorated T cells, cells were stained with a proliferation marker, CellTrace Violet, prior to biotinylation. CellTrace Violet is a cell-penetrating and succinimidyl ester functionalized phenolic dye. The low concentration of CellTrace Violet (5 μ M for a typical staining protocol) affects only very mildly the subsequent biotinylation of T cells which is performed using a 100-fold higher concentration of amine reactive biotinylating agent. Subsequently, as the nanoparticles are also fluorescently labelled, flow cytometry allows to simultaneously monitor changes in both, CellTrace Violet as well as the nanoparticles associated fluorescence. Figure 3 presents the results of flow cytometry measurements directly after surface modification and 24h later. On average, after one division cycle, an approx 1.7-fold mean fluorescence intensity decrease from fluorescently labelled nanoparticles (both 200 nm and 40 nm) on

Jurkat cells was found. For SJL/PLP7 T cells an approx. 2-fold decrease in the nanoparticles associated fluorescence was observed after 24h. The decrease in nanoparticles associated fluorescence is consistent with the redistribution of the nanoparticles over daughter cells after one cycle of cell division.

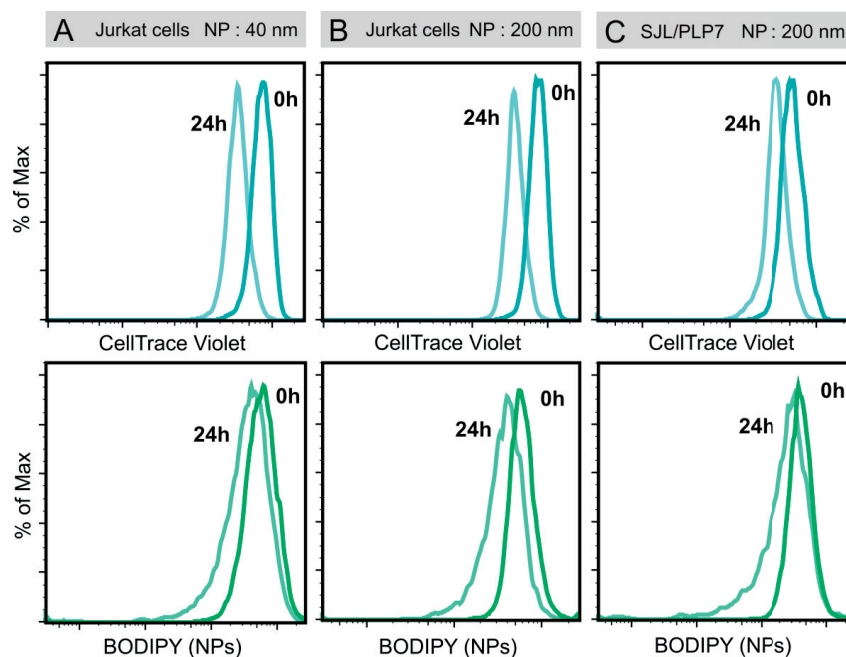


Figure 3. Histogram of scatter gated live cells directly after modification and 24 hours later. Top: cell division was observed using a CellTrace Violet staining. Bottom: nanoparticle retention was assessed using BODIPY labelled fluorescent nanoparticles. Data are shown for Jurkat cells functionalized with 40 nm nanoparticles (A) and with 200 nm nanoparticles (B) as well as SJL/PLP7 T cells functionalized with 200 nm nanoparticles (C).

The number of nanoparticles per cell and their position on the cell surface were determined by confocal microscopy. Figure 4A shows the workflow for the preparation of whole cell and membrane stained nanoparticle decorated T cells. After nanoparticle binding, T cells, which were previously stained with CellTrace Violet, were additionally labelled with a membrane dye, WGA-Texas Red-X. Wheat Germ Agglutinin (WGA) is a carbohydrate binding protein that selectively recognizes sialic acid and N-acetylglucosaminyl sugars present on the cell membrane and as such marks the surface of the cell. As mentioned above, CellTrace Violet is a cell-penetrating and amine reactive dye that binds covalently to amine groups both intracellularly and on the surface of the cell and therefore delineates the entire cell structure. The use of an amine reactive dye is

particularly interesting for long-term analysis as the dye is efficiently retained by the cell due to its covalent attachment to proteins. Figure 5 shows four sets of images of Jurkat cell modified with 40 nm, 200 nm and 1 μm particles as well as of SJL/PLP7 T cells modified with 200 nm nanoparticles. For each set, the left images represent 3D-reconstructs of nanoparticle decorated T cells and the right images are 2D cross sectional planes of these cells directly after modification or 24h later. The 2D cross sectional planes of Jurkat cells modified with 40 nm and 200 nm particles indicate that directly after immobilization nanoparticles are localized almost exclusively on the edge of the cell, whereas after 24h both surface-conjugated and internalized nanoparticles can be observed. Figure 5C shows large microparticles on Jurkat cells present on the cell edge both directly after modification and 24h later. Interestingly, the attachment of 200 nm nanoparticles on the primary cells almost only resulted in surface-bound nanoparticles. Even after 24h, accumulation of nanoparticles inside the cell could not be observed (Figure 5D), in contrast to Jurkat cells.

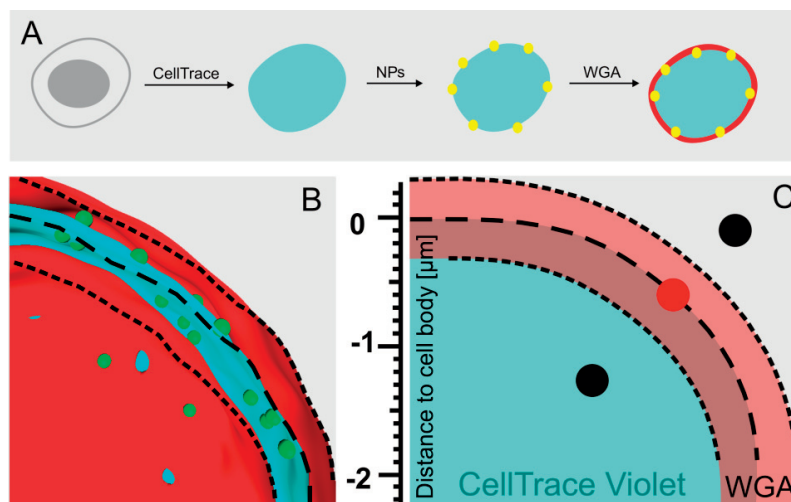


Figure 4. (A) Work flow for the preparation of nanoparticle (yellow) decorated T cells with a whole cell staining (cyan, CellTrace Violet) and membrane staining (red, WGA Texas Red-X). (B) Surface generated from image processing (Imaris) showing the edge of CellTrace Violet (cyan) whole cell staining (— — — — —), inner and outer bounds of the WGA-Texas Red-X (red) membrane staining (— — — — —) and 200 nm nanoparticles (green) (B) Schematic explanation for the nanoparticle distribution observed in Figure 6 around the cell edge based on 3D-reconstruction and image processing as shown in (B). The edge of CellTrace Violet (cyan) whole cell staining is represented by (— — — — —), inner and outer bounds of the WGA-Texas Red-X (red) membrane

staining as (----). When a nanoparticle appears as a red dot, this nanoparticle is colocalized with the membrane dye otherwise it is shown as a black dot in the statistical distribution of Figure 6.

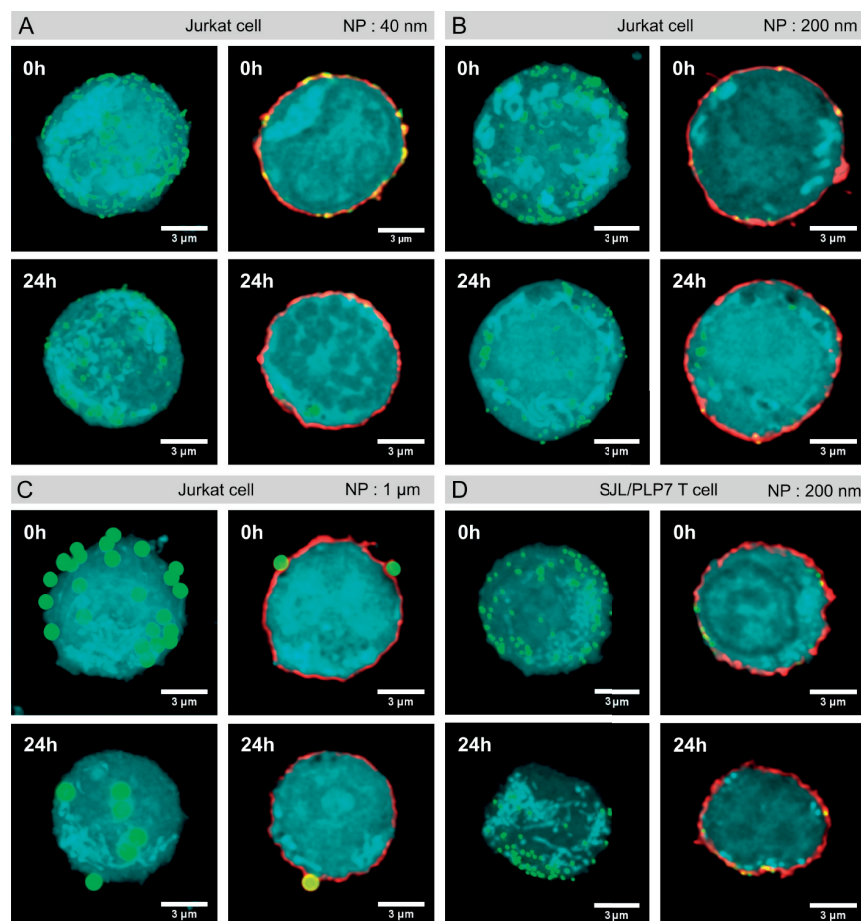


Figure 5. Each set of four images represent two 3D-reconstructions (images on the left) of confocal micrograph z-stacks of nanoparticle (green) decorated cells (cyan, CellTrace Violet) directly after modification (top) and 24h (later bottom) as well as two 2D-images of a cross sectional confocal plane (images on the right) of a nanoparticle modified T cell directly after modification (top) and 24h (later bottom) showing an additional membrane WGA-Texas Red X (red) staining. **(A)** A Jurkat cell modified with 40 nm nanoparticles. **(B)** A Jurkat cell modified with 200 nm nanoparticles. **(C)** A Jurkat cell modified with 1 µm particles. **(D)** An SJL/PLP 7 T cell modified with 200 nm nanoparticles.

To obtain insight in the average number of particles per cell as well as on the location of the particles, data were compiled for a set of 9 cells per condition, both directly after cell surface modification and 24h later. Figure 4B shows the results of a processed image to detect spheres (nanoparticles) and surfaces generated by the staining protocols. This

figure shows the surface generated from the edge of CellTrace Violet staining (cyan) and both the inner and outer boundaries of the WGA staining (red) and 200 nm nanoparticles detected as ellipsoids (green). Figure 4C provides an explanatory scheme for the interpretation of nanoparticle localization and distribution data that are summarized in Table 1 and Figure 6. In brief, each nanoparticle was assigned a distance from the surface generated by the CellTrace Violet staining. The edge of the CellTrace violet is defined as 0 μm in Figure 4B and 4C. Positive values are attributed to nanoparticles detected above the staining and negative values are attributed to nanoparticles found inside the CellTrace Violet staining. Additionally nanoparticles that are detected between the inner and outer boundaries of the WGA membrane staining appear as red dots in Figure 6, those which do not are shown as black dots. Figure 6 shows the distribution of nanoparticles with respect to their distance from the whole cell edge (CellTrace Violet) and as a function of occurrence within the membrane dye WGA-Texas Red-X boundaries. Table 1 summarize the average distance between the particles and the cell edge as well as the percentage of particles that are found in between the inner and outer boundaries of the WGA-Texas Red-X membrane staining for the different particles directly after cell surface modification as well as after 24h. Figure 6A shows the results for 1 μm particles on Jurkat cells. On average directly after modification 9 ± 4 microparticles can be found on the surface of the cell and 24h later there are still 5 ± 1 particles. The microparticles are localized on average at a distance of 537 ± 519 nm directly after modification and at 400 ± 240 nm 24h later, corresponding approx. to a distance equivalent to the radius of the fluorescent particles. Figure 6B illustrates the distribution of 200 nm nanoparticles on Jurkat cells. On average there are 124 ± 45 nanoparticles per cell at $t=0$ and 60 ± 25 nanoparticles 24h later. They are localized directly after modification at a distance on average of $-170 \text{ nm} \pm 250 \text{ nm}$ from the edge of the CellTrace Violet stain and $92 \pm 3.2 \%$ of all nanoparticles are found within the WGA membrane dye boundaries. At $t=24\text{h}$ the nanoparticles are on average at a distance of $-280 \text{ nm} \pm 523 \text{ nm}$ from the surface of the CellTrace Violet stain and the percentage of nanoparticles found within the WGA membrane dye boundaries falls down to $74.7 \pm 14.7 \%$, indicating that nanoparticle internalization occurred as can be observed from the increasing number of black dots distant from the edge of the whole cell staining (Figure 6B). Figure 6C shows the distribution of 40 nm particles from the cell edge. Because the size of these particles is below the resolution of a confocal microscope, it is important to note here that the detected ellipsoids (diameter of 200 nm in the xy plane and 300 nm in the z direction)

corresponds roughly to the smallest point spread (PSF) function for this channel. Therefore each single detected spot may in reality account for more than one nanoparticle. On average, 275 ± 84 ellipsoids at $t=0$ and 142 ± 43 24h later were detected. The spots were localized on average at a distance from the CellTrace Violet edge of $-16 \text{ nm} \pm 525$ and $92 \pm 3.6 \%$ are localized within the WGA membrane dye boundaries. After 24h the distance of the spots is on average $-307 \pm 639 \text{ nm}$ from the whole cell edge and the colocalization with the membrane dye dropped to $65.2 \pm 7.2 \%$. These values indicated an even more pronounced internalization of 40 nm nanoparticles compared to 200 nm beads on Jurkat cells. This expected trend i.e. increasing internalization with decreasing nanoparticle size can be very precisely detected with our semi-quantitative approach. SJL/PLP7 T cells modified with 200 nm particles were analyzed using the same procedure. On average, surface modification led to the attachment of 79 ± 19 nanoparticles per cell at $t=0$ and after 24h 48 ± 14 were still detected. The nanoparticles were localized on average at a distance of $-139 \pm 263 \text{ nm}$ from the edge of the CellTrace Violet stain directly after modification and $87 \pm 9 \%$ of nanoparticles are localized within the WGA membrane dye boundaries. 24h later the average nanoparticle distance from cell edge was $-86 \pm 216 \text{ nm}$ and $96.5 \pm 4.5 \%$ are found within the WGA membrane dye boundaries. This contrasts drastically with what was observed in the case of Jurkat cells modified with 200 nm particles. The internalization of 200 nm and 40 nm nanoparticles was statistically analyzed with a χ^2 test and was significant in Jurkat cells for both 200 nm and 40 nm over 24h, whereas for SJL/PLP7 T cells no statistically significant internalization could be detected during this period (Figure 6).

It is worthwhile noting that in Figure 6, in almost all cases, a certain percentage of nanoparticles detected close to the CellTrace Violet surface appear as black dots whereas they should in principle also be localized within the boundaries of the membrane dye. This bias often happens for nanoparticles that are detected on the top or the bottom of the cells. In fact due to the poorer resolution in the z direction, it is often the case that the surface generated during image processing for the WGA Texas Red-X stain are discontinuous in these regions, this could in principle be avoided by exclusion of these spots during analysis.

Table 1. Parameters obtained by image processing and statistical analysis of 3D-reconstructions acquired by confocal microscopy.

Cell line	NP size	Time	NPs / cell (or PSF)	Avg. Distance to cell edge [nm] (CellTrace Violet)	χ^2 test ⁽¹⁾ WGA+ WGA-	% NP localization between inner / outer WGA-Texas Red-X boundaries
Jurkat cells	40 nm	t_0	(275 ± 84)	-16 ± 525	ns	92 ± 4
		t_{24h}	(142 ± 43)	-307 ± 639	****	65 ± 7
	200 nm	t_0	124 ± 45	-170 ± 250	ns	92 ± 3
		t_{24h}	60 ± 25	-280 ± 523	****	75 ± 15
	1 μ m	t_0	9 ± 4	537 ± 519	N/A	> 98%
		t_{24h}	5 ± 1	400 ± 240	N/A	100
SJL/PLP7	200 nm	t_0	79 ± 19	-139 ± 263	ns	87 ± 9
		t_{24h}	48 ± 14	-86 ± 215	ns	96.5 ± 4.5

(1) Comparison between nanoparticle distribution at $t=0$ and $t=24h$ above a cut off threshold for the WGA+ and WGA- nanoparticle subsets to detect internalization. The threshold was set at -250 nm considering the lowest possible approximate point spread function (PSF) detection of a 200 nm or 40 nm nanoparticle (PSF = 200 nm) localized exactly at the inner boundary of the membrane WGA staining (PSF = 300 nm) (see Figure 6E for an explanatory scheme). P-value: (ns: $P > 0.05$; **** $P < 0.0001$). N/A = not available.

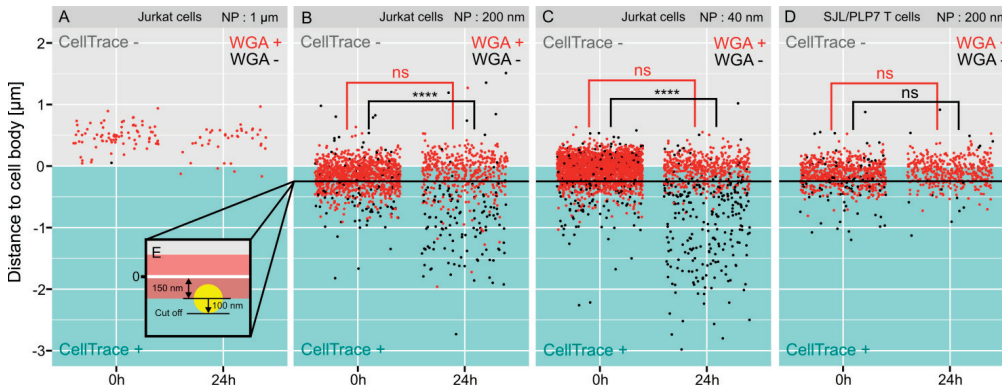


Figure 6. Statistical distribution of nanoparticles (NP) with respect to their distance to the whole cell edge (CellTrace Violet). Each dot represents a single nanoparticle. Red dots represent nanoparticles which are located between the inner and outer boundaries of the membrane staining (WGA-Texas Red-X) (see Figure 4 for details); black dots those which are not. **(A)** Jurkat cells decorated with 1 μ m particles **(B)** Jurkat cells decorated with 200 nm particles **(C)** Jurkat cells decorated with 40 nm particle **(D)** SJL/PLP7 T cells decorated with 200 nm particles. The statistical significance was evaluated by a χ^2 test (ns: $P > 0.05$; **** $P < 0.0001$) on WGA+ (red) and WGA- (black) nanoparticle subsets for the distribution below and above the cut off threshold (solid black line) at $t=0$ and $t=24h$. **(E)** The cut off threshold was set at -250 nm considering the lowest possible approximate point spread function (PSF) detection of a 200 nm or 40 nm nanoparticle (PSF = 200 nm) localized exactly at the inner boundary of the membrane WGA staining (PSF = 300 nm).

3.3.2. Binding assay

The SJL/PLP7 cell line is of interest since these T lymphocytes are able to cross the blood-brain barrier (BBB) during inflammation. This is highly attractive as it offers opportunities to us these T cells to facilitate delivery of nanoparticles to the central nervous system (CNS). One protein that has been identified to be crucial in the extravasation of CD4⁺ TEM cells across the BBB is intercellular adhesion molecule-1 (ICAM-1) [12, 16]. To investigate the ability of the nanoparticle decorated CD4⁺ TEM cells prepared in this study to recognize and bind to ICAM-1, a functional assay was performed using ICAM-1 coated well plates. As controls, non-modified T cells and wells mounted with delta/notch-like epidermal growth factor (DNER) were used. Figure 7 presents the number of adherent cells counted per field of view for nanoparticle decorated and unmodified T cells both on ICAM-1 and control DNER coated surfaces. The results in Figure 7 show that the biotin-NeutrAvidin conjugation of nanoparticles on the surface of these T cells does not impact their ability to bind ICAM-1, which is a selective (LFA-1) mediated process, as evidenced by the absence of adherent T cells in the DNER coated wells. There is in fact no significant difference with control unmodified T cells, which is quite impressive given the fact that the modified T cells are not only decorated with approximately 80 nanoparticles but that their entire surface is also highly functionalized with biotin moieties.

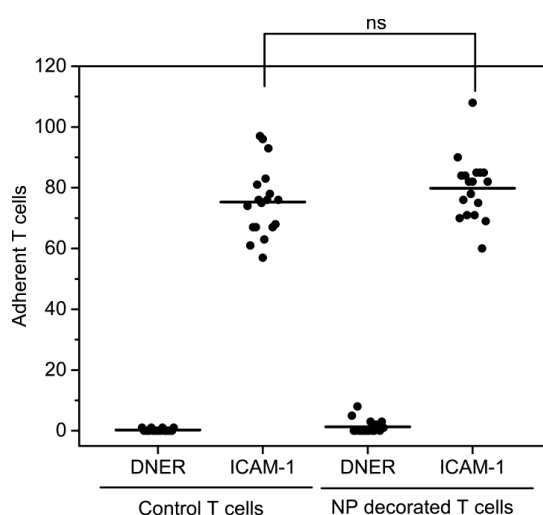


Figure 7. Cell count of a binding assay on ICAM-1 coated wells and DNER coated wells for unmodified control SJL/PLP7 T cells and nanoparticle (NP) decorated SJL/PLP7 T cells. Each dot represents one cell count from the diagonal of a 10 mm x 10 mm / 10 divisions counting reticle using a 20x objective. P-value was determined by *t* test (ns: $P > 0.05$).

3.4. Conclusions

Cell-surface modification is an emerging technology that has a great potential for therapeutic applications. This strategy allows to use circulatory cells such as T lymphocytes to mediate the transport of nanoparticles to sites of disease. This field has recently gained attention with impressive examples in cancer therapy [4, 17]. The positions and distribution of the nanoparticles on the surface may have a direct impact on the function of the T cell carrier and thus need to be carefully monitored. For clinical applications, it is also important to ensure that the nano- or microparticle cargo remains mainly on the T cell carrier surface during a therapeutically relevant timeframe and that internalization of the cargo by the cell carrier is minimized. Internalization depends on factors such as the cell type, the shape and the size of the cargo and potentially also on the immobilization chemistry used. In the present study, a method to determine the nanoparticle position and distribution as a function of time was developed using confocal microscopy and image processing. The protocol used two staining protocols to visualize both the entire cell structure as well as the plasma membrane to detect surface-conjugated versus internalized fluorescently labeled nano- and microparticles. The method was tested for polystyrene particles of various sizes (40 nm, 200 nm and 1 μ m) on Jurkat cells and was validated on a primary mouse cell line (SJL/PLP7 T cells). The method is able to discriminate surface-bound from internalized nanomaterials in a semi-quantitative manner.

3.5. References

- [1] M. Ayer, H.-A. Klok, Cell-mediated delivery of synthetic nano- and microparticles, *J. Controlled Release*.
- [2] A.C. Anselmo, S. Mitragotri, Cell-mediated delivery of nanoparticles: Taking advantage of circulatory cells to target nanoparticles, *J. Controlled Release*, 190 (2014) 531-541.
- [3] Y. Su, Z. Xie, G.B. Kim, C. Dong, J. Yang, Design Strategies and Applications of Circulating Cell-Mediated Drug Delivery Systems, *ACS Biomaterials Science & Engineering*, 1 (2015) 201-217.

- [4] B. Huang, W.D. Abraham, Y. Zheng, S.C. Bustamante Lopez, S.S. Luo, D.J. Irvine, Active targeting of chemotherapy to disseminated tumors using nanoparticle-carrying T cells, *Sci. Transl. Med.*, 7 (2015) 291ra294.
- [5] E. Chambers, S. Mitragotri, Prolonged circulation of large polymeric nanoparticles by non-covalent adsorption on erythrocytes, *J. Controlled Release*, 100 (2004) 111-119.
- [6] P. Zhang, J. Guan, Fabrication of Multilayered Microparticles by Integrating Layer-by-Layer Assembly and MicroContact Printing, *Small*, 7 (2011) 2998-3004.
- [7] Y. Krishnamachari, M.E. Pearce, A.K. Salem, Self-assembly of cell-microparticle hybrids, *Adv. Mater.*, 20 (2008) 989-+.
- [8] R. Mooney, Y.M. Weng, E. Garcia, S. Bhojane, L. Smith-Powell, S.U. Kim, A.J. Annala, K.S. Aboody, J.M. Berlin, Conjugation of pH-responsive nanoparticles to neural stem cells improves intratumoral therapy, *J. Controlled Release*, 191 (2014) 82-89.
- [9] M.T. Stephan, S.B. Stephan, P. Bak, J.Z. Chen, D.J. Irvine, Synapse-directed delivery of immunomodulators using T-cell-conjugated nanoparticles, *Biomaterials*, 33 (2012) 5776-5787.
- [10] M.T. Stephan, J.J. Moon, S.H. Um, A. Bershteyn, D.J. Irvine, Therapeutic cell engineering with surface-conjugated synthetic nanoparticles, *Nat. Med.*, 16 (2010) 1035-1041.
- [11] H. Cheng, C.J. Kastrup, R. Ramanathan, D.J. Siegwart, M.L. Ma, S.R. Bogatyrev, Q.B. Xu, K.A. Whitehead, R. Langer, D.G. Anderson, Nanoparticulate Cellular Patches for Cell-Mediated Tumortropic Delivery, *Acs Nano*, 4 (2010) 625-631.
- [12] O. Steiner, C. Coisne, R. Cecchelli, R. Boscacci, U. Deutsch, B. Engelhardt, R. Lyck, Differential Roles for Endothelial ICAM-1, ICAM-2, and VCAM-1 in Shear-Resistant T Cell Arrest, Polarization, and Directed Crawling on Blood-Brain Barrier Endothelium, *J. Immunol.*, 185 (2010) 4846-4855.
- [13] B. Engelhardt, R.M. Ransohoff, The ins and outs of T-lymphocyte trafficking to the CNS: anatomical sites and molecular mechanisms, *Trends Immunol.*, 26 (2005) 485-495.
- [14] B. Engelhardt, M. Laschinger, M. Schulz, U. Samulowitz, D. Vestweber, G. Hoch, The development of experimental autoimmune encephalomyelitis in the

- mouse requires alpha 4-integrin but not alpha 4 beta 7-integrin, *J. Clin. Invest.*, 102 (1998) 2096-2105.
- [15] G. Martin-Blondel, B. Pignolet, S. Tietz, L. Yshii, C. Gebauer, T. Perinat, I. Van Weddingen, C. Blatti, B. Engelhardt, R. Liblau, Migration of encephalitogenic CD8 T cells into the central nervous system is dependent on the alpha 4 beta 1-integrin, *Eur. J. Immunol.*, 45 (2015) 3302-3312.
- [16] Y. Reiss, G. Hoch, U. Deutsch, B. Engelhardt, T cell interaction with ICAM-1-deficient endothelium in vitro: essential role for ICAM-1 and ICAM-2 in transendothelial migration of T cells, *Eur. J. Immunol.*, 28 (1998) 3086-3099.
- [17] L. Wayteck, L. Dewitte, L. De Backer, K. Breckpot, J. Demeester, S.C. De Smedt, K. Raemdonck, Hitchhiking nanoparticles: Reversible coupling of lipid-based nanoparticles to cytotoxic T lymphocytes, *Biomaterials*, 77 (2016) 243-254.

3.6. Supporting Information

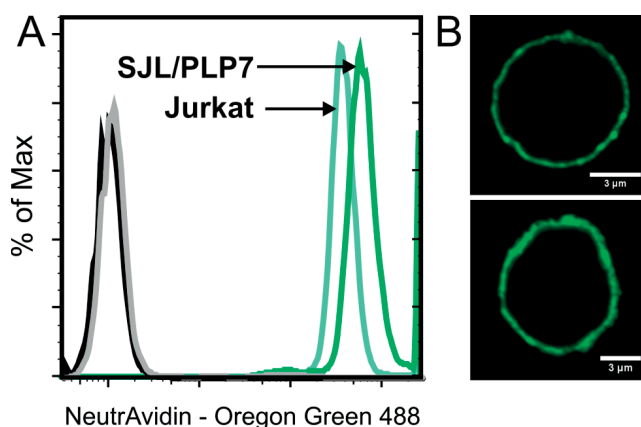


Figure S1. (A) Histogram of scatter gated live cells (Jurkat cells and SJL/PLP7 T cells) stained with NeutrAvidin-Oregon Green 488 conjugate previously treated with a constant 0.5 mM concentration of biotinylating agent (Biotin-XX, SSE). Black: control non-biotinylated Jurkat cells. Grey: non-biotinylated Jurkat cells exposed to NeutrAvidin-Oregon Green 488. (B) Confocal micrographs showing surface biotin detection with NeutrAvidin – Oregon Green 488 in a Jurkat cell (top) and an SJL/PLP 7 T cells.

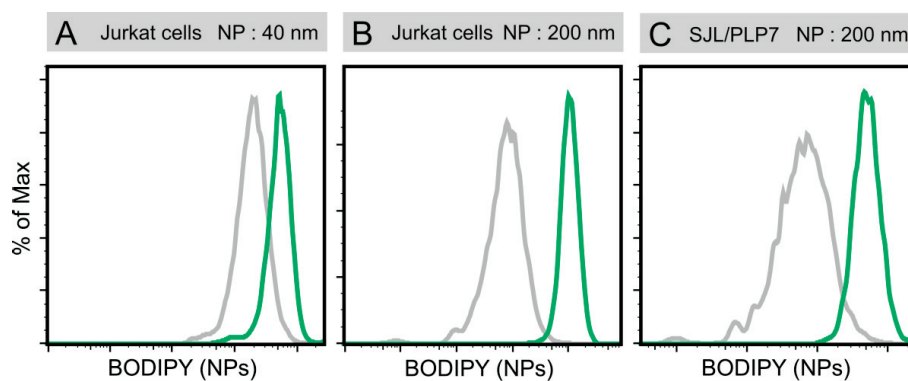


Figure S2. Histogram of scatter gated live cells (Jurkat cells or SJL/PLP7 T cells) directly after modification showing nanoparticle associated BODIPY fluorescence on biotinylated cells (green) versus non biotinylated cells (gray). The biotinylation was performed using a 0.5 mM Biotin XX, SSE.

4. Conclusions and Perspectives

The potential of cell-mediated drug delivery is immense and may contribute in the future to the improvement of targeted therapies, for example in cancer treatment, where T-cell therapy has already gained great interest and could potentially be used in combination with cell-mediated delivery of therapeutic nanomaterials. Some of the difficulties of cell-mediated approaches are related to the cross-disciplinary requirements in immunology, materials science and potentially genetic engineering to prepare effective and well-defined hybrid cell-nanomaterial vehicles suitable for a specific application and the associated cost to develop this method. The combination of cell-mediated delivery with highly engineered nanomedicines or together with cell-therapy provides very exciting opportunities in therapy to enhance efficacy of a treatment by a multicomponent approach. Cell-mediated drug delivery is also a very attractive strategy for central nervous system (CNS) delivery. The need for new treatments for CNS disorders such as Parkinson's or Alzheimer diseases, which have become public health priority will only go along with highly effective delivery strategy and hence the tremendous efforts in this area.

Following a comprehensive introduction on the topic of cell-surface modification with synthetic nanomaterials and their application in therapy (**Chapter 1**), the present work has focused on the preparation and characterization of nanoparticle decorated T cell carriers designed for the delivery of a model polymer cargo across the BBB (**Chapter 2**). This approach was based on covalent maleimide-thiol chemistry described previously and the obtained cell-nanomaterial hybrids were subjected to a series of functional assays to demonstrate the feasibility of using T lymphocytes as vehicles for the transport and delivery of nanoparticles across the BBB. This is the first study showing that nanoparticle modified T cells can cross an intact BBB model *in vitro* and transport their nanoparticle cargo across this highly impermeable barrier. This study also showed the importance of investigating these systems under physiological flow condition and revealed that nanoparticle surface modification change the migratory behavior of T cell carriers. The strategy described in this Thesis is very general and could in principle be applicable to a large variety of CNS disorders. It can be used in diagnostic as well as in therapy or in combination with other treatments, such as radiation therapy that induces localized inflammation and which could promote the migration of T cell carriers in these regions.

Cell-surface modification has gained interest recently with very nice examples of application in cancer therapy in combination with CD8⁺ T cell or for the targeting of disseminated tumors. The field of cell-surface modification still remains today a research niche and there are many opportunities to improve for example characterization of these new cell-nanomaterial hybrids. One important challenge is the development of methods that allow to monitor nanoparticle positions after surface-conjugation as a function of time. This was described in **Chapter 3**. The protocol used confocal microscopy techniques and image processing to precisely determine the position of nano- and microparticles on the surface or inside a T cell carrier. This section has highlighted the difference that exists in terms of internalization across two different cells lines for different particle sizes and showed the importance of carefully characterizing the cell-nanomaterial hybrids to assess the stability of a surface-directed conjugation method.

This work has laid the foundation for cell-mediated delivery to the central nervous system. It has also demonstrated the importance to characterize qualitatively as well as quantitatively the localization of nanoparticles on the surface of a cell carrier. There are however many open questions that remain to be answered from this proof of concept study. Whether varying the conjugation approach may lead to more effective transport across the BBB is very attractive and will need to be further investigated. Future work based on this study will also encompass the use of an actual delivery system such as biodegradable polymer-based nanoparticles or nanovesicles (also named polymersomes) as therapeutic nanomaterials for the T cells modification as well as the control released of a therapeutic compound from the nanocarriers. More generally, this approach will also need to be investigated in biodistribution studies to better understand the real impact of using a brain seeking T cell vehicle as compared to free or targeted nanoparticles, and in that regard using very simple and straightforward conjugation chemistry such as that described in **Chapter 3** may be a simple starting point. Finally *in vivo* studies will be undertaken to observe and confirm the results of this initial work in a more clinically relevant set up for the delivery of a CNS active compound.

MAXIME AYER

Avenue de Sévelin 13 C, 1004 Lausanne
+41 79 797 63 74
maxime.ayer@gmail.com
Skype ID: maxime.ayer



Education

Ecole polytechnique fédérale de Lausanne (EPFL)

PhD in Materials Science (2012 – Present)

Eidgenössische Technische Hochschule Zürich (ETH Zürich)

Master of Science in Chemistry (2009 – 2011)

Ecole polytechnique fédérale de Lausanne (EPFL)

Bachelor of Science in Chemistry and Chemical Engineering (2005 – 2009)

Collège Sainte-Croix, Fribourg

Baccalauréat (2005)

Core experience

Polymers Laboratory (EPFL)

PhD thesis work in cell-mediated drug delivery across the blood-brain barrier

PhD thesis supervisor: Prof. Dr. Harm-Anton Klok

- Preparation of nanoparticles for live cell surface decoration and evaluation of nanoparticle-functionalized T cells as carrier across *in vitro* blood-brain barrier models. This delivery strategy is unique and represents the first report for this technology in the context of brain delivery.
- Project carried out in a multidisciplinary environment with the Theodor Kocher institute (University of Bern) for neuroimmunobiology (Group Prof. Dr. B. Engelhardt).
- In charge of the HPLC-MS platform at the Polymers Laboratory and was involved in the evaluation process and purchase of this system.

Laboratorium für Organische Chemie (ETH Zürich)

Master thesis work in Organic Synthesis (2010)

MS thesis supervisors: Prof. Dr. François Diederich, Prof. Dr. Yoko Yamakoshi

- Synthesis of shape persistent molecules and development of a novel NMR characterization approach to determine their 3D-conformations.

Institut für Pharmazeutische Wissenschaften (ETH Zürich)

Drug Formulation & Delivery internship (4 months, 2010)

Group of Prof. Dr. Jean-Christophe Leroux

- Preparation of protein-polymer conjugates as protein therapeutic delivery model systems

Additional experience

Commonwealth Scientific and Industrial Research Organisation, Australia

Australia's national research agency internship, Melbourne (Jan-Sep 2009)

- Preparation of solution processable polyaromatic compounds for the development of novel polymer-based flexible photovoltaics.

Vifor Pharma - Vifor SA, Villars-sur-Glâne, Switzerland

Supply chain, purchase division internship (Summer 2008)

- Packaging and raw material purchasing / purchase forecasting.

Languages

English: fluent spoken and written (C2)

German: fluent spoken (C2) and intermediate written (C1)

French: native language

Technical Skills

Life sciences skills

Cell culture • Viability assay • Proliferation assay • Binding assay • Transmigration assay • Flow cytometry • Confocal microscopy • Time-lapse live cell imaging.

Synthetic skills

Nanoparticle / liposome preparation and formulation • Bioconjugate chemistry • Antibody / Protein modification and purification • Organic synthesis and polymer chemistry • Solid phase peptide synthesis • High pressure liquid chromatography (HPLC) • Size exclusion chromatography (SEC) • Tangential flow filtration (TFF) • Mass Spectrometry (MS) • Nuclear magnetic resonance (NMR) • Dynamic light scattering (DLS) • UV-Vis • Fourier transform infrared spectroscopy (FTIR).

IT skills

ChemDraw Bio • MestReNova • OriginPro • ImageJ • Adobe InDesign • CorelDRAW • Endnote • MS Office: XP-W10; PC & MAC.

Scientific Publications

- Ayer M.; Gruber I.; Blatti, C.; Engelhardt, B.; Klok, H.-A. *Polymer nanoparticle-decorated T cells for blood-brain barrier transport*. in preparation
- Ayer M.; Klok, H.-A. *Biotin-NeutrAvidin mediated immobilization of polymer nanoparticles on T lymphocytes*. in preparation
- Ayer M.; Klok H.-A.; *Cell-mediated delivery of Synthetic Nano- and Microparticles*. J. Control. Release. **2017**, <http://dx.doi.org/10.1016/j.jconrel.2017.01.048>
- Royappa, AR.; Ayer, M.; Fracassi, A.; Ebert, MO; Aroua, S.; Yamakoshi Y. *Conformationally Selective Synthesis of Mononitrocalix[4]arene in Cone or Partial Cone*. Helv. Chim. Acta. **2017**, <http://dx.doi.org/10.1002/hlca.201600391>
- Aroua, S.; Tiu, E. G.; Ayer, M.; Ishikawa, T.; Yamakoshi, Y. *RAFT synthesis of poly(vinylpyrrolidone) amine and preparation of a water-soluble C60-PVP conjugate*. Polym. Chem. **2015**, 6, 2616-2619.
- Gauthier, M. A.; Ayer, M.; Kowal, J.; Wurm, F. R.; Klok, H.-A. *Arginine-specific protein modification using α -oxo-aldehyde functional polymers prepared by atom transfer radical polymerization*. Polym. Chem. **2011**, 2, 1490-1498.

